UNIVERSITY OF SALERNO

DEPARTMENT OF CHEMISTRY AND BIOLOGY "A. Zambelli"

Ph. D. Course in Chemical, Biological and Environmental Sciences

XXXVII Cycle

Ph. D. Thesis in Molecular Biology

BIO/11

USING EPIDRUGS TO INVESTIGATE GENE ACTIVATION MECHANISMS: *Tbx1* GENE MODEL.

Tutor:
Prof. Elizabeth ILLINGWORTH

Elizabeth Illingworth

Ph. D. Student:
Mariangela Cavallaro
8803300030

Ph. D. Program Coordinator:
Prof. Carmine Gaeta

Prof. Carmine Gaeta

ACADEMIC YEAR 2024/2025

INDEX

ABSTRACT **3**

1. INTRODUCTION **4**

1.1 T-BOX GENE FAMILY **4**

1.1.1. *TBX* GENES AND PROTEINS STRUCTURE AND FUNCTION 5

1.1.2. **TBX1**: MOLECULAR AND DEVELOPMENTAL FUNCTIONS 8

1.1.3. 22Q11.2 DELETION SYNDROME: A DISEASE OF *TBX1* HAPLOINSUFFICIENCY 12

1.2. EPIGENETIC REGULATION OF TRANSCRIPTION **13**

1.3. EPIDRUGS AS TOOLS TO STUDY TBX1 REGULATION **15**

1.3.1. HISTONE DEACETYLASE INHIBITORS (HDIS): SAHA 16

1.3.2. LYSINE DEMETHYLASE INHIBITORS: GSKLSD1 AND GSK2879552 19

1.3.3. POLYCOMB INHIBITORS: GSK126 20

2. AIMS OF THE PROJECT **23**

2.1 REASONS FOR THE STUDY / INVESTIGATION 23

2.2 GOALS OF THE PROJECT 23

2.3 CHOICE OF THE EXPERIMENTAL SYSTEMS AND METHODS 24

3. MATERIALS AND METHODS **26**

3.1 MAINTENANCE OF C2C12 CELL LINE IN CULTURE **26**

3.2 DRUG TREATMENT OF C2C12 CELLS **27**

3.3 CELL PROLIFERATION ASSAYS **27**

3.4 RNA EXTRACTION AND PURIFICATION FROM C2C12 CELLS **28**

3.4.1. ASSESSMENT OF RNA QUALITY AND QUANTITY 29

3.5 REVERSE TRANSCRIPTION OF RNA **29**

3.6 RT-PCR **29**

3.7 REAL TIME QPCR **31**

3.8 BIOINFORMATIC ANALYSIS **32**

DATASET FOR EPIGENETIC DATA ACQUISITION 32

DATASET FOR GENE EXPRESSION DATA ACQUISITION ACROSS DIFFERENT TISSUES AND EMBRYONIC STAGES 32
BIOINFORMATIC WORKFLOW 32
3.9 MAINTENANCE OF THE MURINE EMBRYONIC STEM CELL LINE E14TG2A 33
3.10.1. DIFFERENTIATION PROTOCOL 35
3.11 EMBRYO COLLECTION AND INTRACARDIAC INK INJECTION 35

4 RESULTS 37
4.1 EPIDRUG ASSAYS IN C2C12 CELLS 37
4.1.1. OPTIMIZATION OF C2C12 CELL CULTURE CONDITIONS 37
4.1.2.1. The major classes of epidrugs 39
4.1.2.2. SAHA 40
4.1.2.3. GSKLSD1 45
4.1.2.6. CCK8 ASSAYS 47
4.2 A BIOINFORMATICS APPROACH TO IDENTIFY HISTONE MODIFICATIONS AT THE *TBX1* LOCUS 48
4.3 COMBINED EPIDRUG TREATMENTS IN C2C12 CELLS 53
4.4 COMBINED EPIDRUG TREATMENT IN MOUSE EMBRYONIC STEM CELLS 54
4.4.1 E14TG2A CELL CULTURES AND INDUCTION OF MESODERM DIFFERENTIATION 55
4.4.2 EPIDRUG TREATMENT OF DIFFERENTIATING E14 MESC 56
4.5. TESTING THE THERAPEUTIC POTENTIAL OF *TBX1*-ACTIVATING EPIDRUGS USING PHENOTYPIC RESCUE IN *TBX1* MUTANT MICE 57

5. DISCUSSION 59

6. CONCLUSION 62

FIGURE AND TABLE INDEX 63

BIBLIOGRAPHY 65

ABSTRACT

The discovery of the contribution of alterations in the epigenome to genetic diseases has driven research into epidrugs that target such alterations. 22q11.2 deletion syndrome, also called DiGeorge syndrome, is a rare genetic disease that is primarily a disease of *TBX1* haploinsufficiency. Studies conducted in animal models of 22q11.2DS, and especially in *Tbx1* mutant mice, suggest that epigenetic changes at the *Tbx1* locus might contribute to disease pathogenesis. Therefore, epidrugs capable of modulating *TBX1* expression are of particular interest because of their potential to increase our understanding of the mechanisms by which *Tbx1* is regulated during embryogenesis, which are largely unknown. They may also have therapeutic value for treating some of the signs and symptoms of 22q11.2DS, although many of these are congenital anomalies and therefore not amenable to pharmacological intervention.

The major goal of this research project was to identify epigenetic changes in the form of histone modifications that are *Tbx1*-activating in cell cultures and in embryonic tissues. For this, I used two different approaches; the first was a candidate drug approach for which I selected epidrugs that target histone modifications that are generally associated with gene activation. I then tested the ability of single and combined epidrug treatments to increase *Tbx1* expression in two cell culture systems. The second was a bioinformatics-based approach, in which a newly developed algorithm was applied to extract information about histone modifications across the mouse genome from large datasets of gene expression and chromatin organization deposited in public databases and integrate it with the sequence of newly identified putative *Tbx1* enhancers. This novel approach allowed me to identify the most highly represented histone modifications associated with activation of the *Tbx1* locus.

The goals of the project were largely met, as each approach identified two putative *Tbx1*-activating histone modifications. In addition, I identified a combination of epidrug treatment that targets these modifications and increases *Tbx1* expression in cells. In future experiments, the combined epidrug treatment regime will be used to determine the *in vivo* relevance of these *Tbx1*-activating histone modifications through phenotypic rescue experiments in *Tbx1* mutant mice.

1. INTRODUCTION

1.1 T-BOX GENE FAMILY

The T-box gene family comprises transcription factors involved in morphogenesis and organogenesis in early vertebrate development. The first gene of this family to be identified, Brachyury (T), was cloned from the mouse no tail mutant in 1990 (Herrmann et al., 1990), and the subsequent identification of orthologues in different species led to the formation of the family known as the "T-box" family (Bollag et al., 1994). The members of this family are characterized by the presence of a highly conserved sequence of about 200 amino acids, known as the "T domain", which binds specific DNA sequences to regulate gene transcription, in particular transcription factors that are essential for normal embryogenesis.

In humans, 17 T-box genes involved in embryonic development have been identified. The majority of mutations identified in T-box genes are missense mutations, deletions, insertions, and splice site copy number variations. Few mutations have been identified in the regulatory regions, therefore little is known about the transcriptional regulation of many T-box genes. Mutations in T-box genes commonly disrupt the morphological processes that are critical for early embryonic development, leading to congenital anatomical anomalies (Fig.1). (Ghosh et al., 2017)

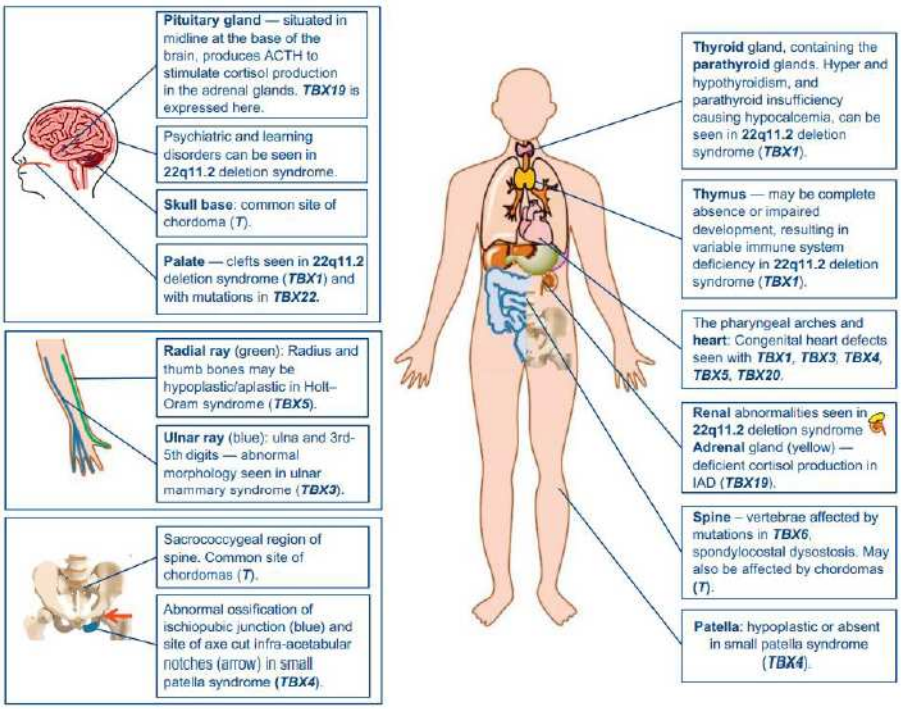


Figure 1. Clinical features associated with disorders related to mutations in TBX genes.
The figure highlights various organs and tissues that exhibit anomalies or dysfunction, including the brain, endocrine glands (thyroid and adrenal glands), heart, upper limbs, palate and spine. Specific examples of pathological conditions are shown, such as congenital heart defects, hypoplasia of radial and ulnar bones and abnormalities in the immune and renal systems. These conditions are often associated with chromosomal deletion syndromes, such as TBX1 deletion is associated with Di George syndrome (22q11.2 deletion syndrome). Figure modified from Ghosh et al., 2017.

1.1.1. *TBX* GENES AND PROTEINS STRUCTURE AND FUNCTION

The T-BOX transcription factor family has ancient origins, with its various members involved in many fundamental processes related to growth and development (Naiche et al., 2005). The first member of this family to be identified, named Brachyury (from the Greek "short tail"), was described in 1927 following observations of a mouse with a mutation that reduced tail length and affected embryonic development (Dobrovolskaia-Zavadskaia, 1927). Brachyury, also known as T or TBXT, was rapidly recognized as a classical developmental gene due to its critical role in the formation of the notochord and posterior mesoderm. Homozygous mutations in TBXT are lethal, while heterozygous mutations result in a truncated tail (Papaioannou, 2001). T-BOX genes are transcriptional activators or repressors. They exhibit a high degree of evolutionary conservation and share a characteristic protein motif with TBXT, known as the T-domain, comprising 180-200 amino acid residues, which enables specific DNA binding (Bollag et al., 1994). In humans, 17 transcription factors belonging to this family have been identified. The relationships among T-BOX genes are reflected in the homology of their DNA-binding domains, based on which they are classified into five subfamilies: T subfamily (TBXT and TBX19), TBX1 subfamily (TBX1, TBX10, TBX15, TBX18, TBX20, and TBX22), TBX2 subfamily (TBX2, TBX3, TBX4, and TBX5), TBX6 subfamily (TBX6 and MGA), and TBR1 subfamily (TBR1, EOMES, and T-BET) (Naiche et al., 2005; Papaioannou and Goldin, 2008) (Figure 2).

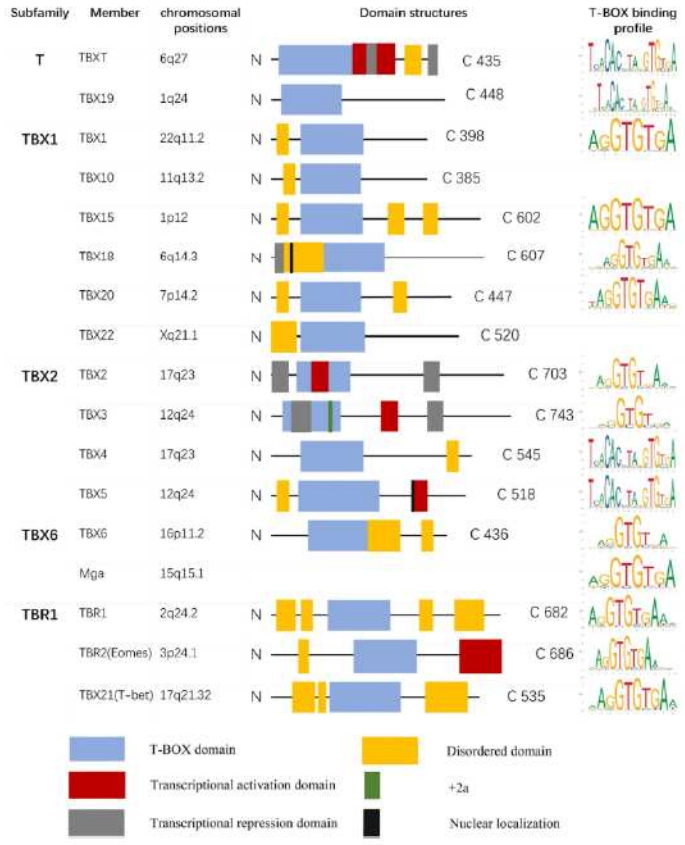


Figure 2. Domain structure and binding profile of human T-BOX transcription factors.
T-BOX family members are classified into five subfamilies that have a similar T-BOX domain sequence, which is an evolutionarily conserved DNA-binding motif and a representative signature of the T-BOX family. In addition

to the shared T-BOX domain, T-BOX members have specific structural domains that result in functional differences. The diagram shows the DNA-binding domain (T-BOX, blue box), inhibitory domains (grey box), activation domain (red box), +2a splicing variant (green box), and nuclear localization sequence (black box). The chromosomal positions and the domain structures of T-BOX family members have been ascertained. The predicted T-BOX binding profiles were obtained from the JASPAR public database. Figure modified from Li et al., 2024.

Thanks to their structural characteristics, which combine common and specific elements, T-BOX factors play a crucial role in multiple aspects of embryonic development. The proteins encoded by these genes have two functional domains: a DNA-binding domain, called the T-domain or T-box, which binds to a specific DNA region known as the T-box Binding Element (TBE) (Figure 3), and a transcriptional activation or repression domain located in the C-terminal region of the protein (Wilson and Conlon, 2002).

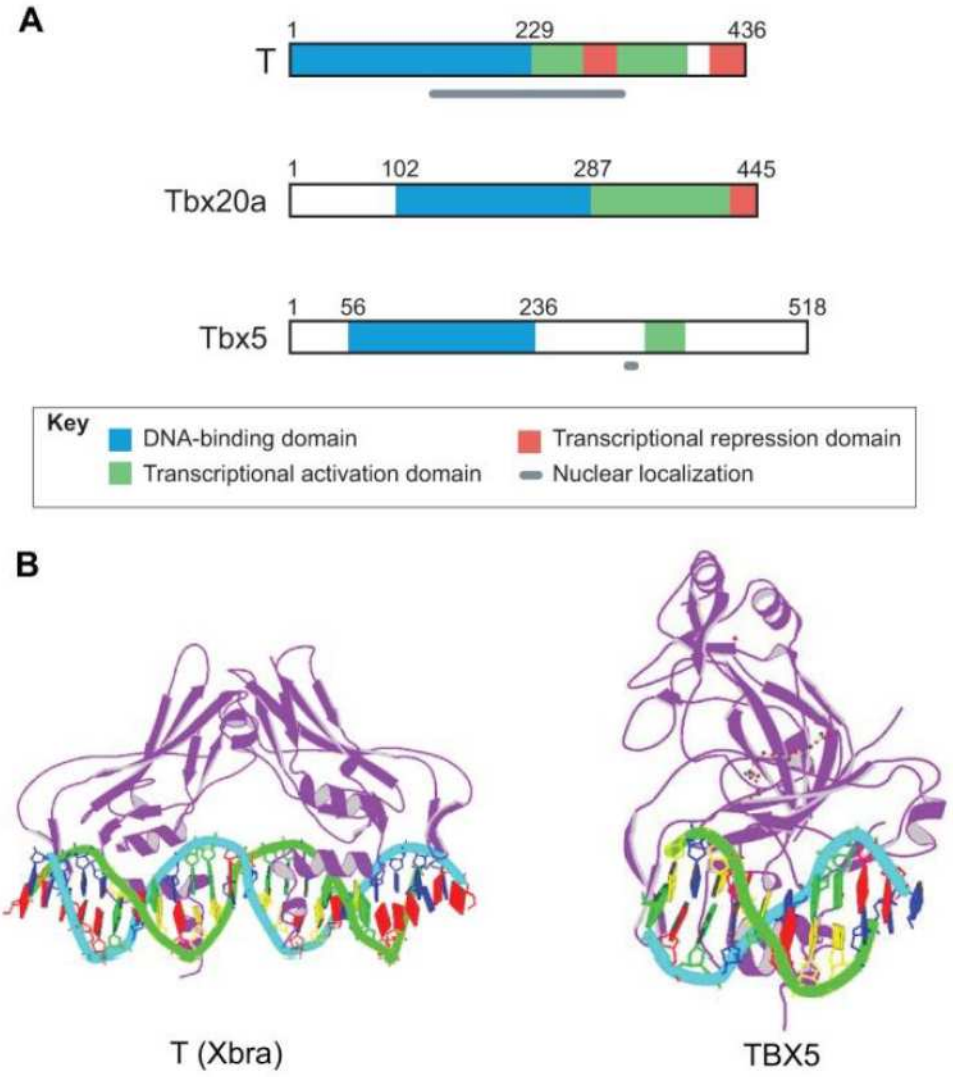


Figure 3. Domain structure of T-box proteins and crystal structure of T-domains bound to DNA.
(A) The domain structure of three T-box proteins [T (Kispert et al., 1995), Tbx20a (Stennard et al., 2005) and Tbx5 (Zaragoza et al., 2004)] illustrating the location of the DNA-binding domain in the N-terminal portion and either a transcriptional activation domain or activation and repression domains in the C-terminal region. The domain involved in nuclear localization has not yet been determined for Tbx20. (B) Crystal structure of T-domains

from *Xenopus laevis* T (Xbra) bound to a palindromic T-box binding element derived from the *in vitro* selected consensus sequence (Müller and Herrmann, 1997) and from human TBX5 bound to a natural T-box binding site from the ANF promoter (Stirnimann et al., 2010). Images are from the RCSB Protein Data Bank (www.rcsb.org): ID numbers 1XBR (Xbra) and 2X6V (TBX5).

Crystallographic studies have identified the TBE sequence bound by various T-BOX proteins. Although the DNA-binding domain is highly conserved, the different effects of activators or repressors may depend on the TBE sequence with which they interact and the manner in which they bind DNA (Conlon et al., 2001). For example, Brachyury (TBXT) binds the palindromic sequence TCACACCTAGGTGTGA, whereas Eomesodermin (Eomes) binds two direct repeats of the central motif separated by four nucleotides (Kispert and Herrmann, 1993).

In model organisms, including mouse, fish and ascidians, T-BOX genes play essential roles in embryonic development, cellular differentiation, and the regulation of numerous physiological processes (**the roles attributed to *TBX1* are described in section 1.1.2**). Most T-BOX genes are expressed early in embryonic development and regulate the development of the posterior mesoderm and primitive streak, as in the case of TBXT. In mice, the absence of TBXT results in severe abnormalities in the notochord, allantois, and primitive streak formation (Beddington et al., 1992; Naiche et al., 2005; Wehn et al., 2020). Similarly, TBX4 is crucial for allantois development, and its loss causes impaired differentiation and disrupted umbilical cord connections, leading to embryonic lethality (Naiche et al., 2011; Naiche and Papaioannou, 2003). TBX6 is involved in somite formation, while TBX18 regulates somatic compartmentalization through Mesp2 and Delta/Notch signalling (Bussen et al., 2004; Naiche et al., 2011). EOMES, on the other hand, is critical for trophoblast growth and differentiation (Russ et al., 2000). Many members of the T-BOX family are critical for heart development and mutations or variants are associated with congenital heart defects. For example, TBXT, TBX1, TBX2, TBX3, TBX5, TBX6, TBX18, and TBX20 are implicated in the development of the ventricular chambers of the heart, valves, septa, outflow tract and the cardiac conduction system (Papaioannou, 2014). TBX2, for example, interacts with other transcription factors, such as Nkx2.5, to inhibit ANF gene expression in the atrioventricular canal during cardiac chamber formation (Habets et al., 2002). TBX5 haploinsufficiency causes conduction abnormalities, while TBX20 mutations are linked to dilated cardiomyopathy and arrhythmias through alterations in Kv11.1 ion channels and ventricular repolarization (Bosada et al., 2023; Caballero et al., 2017; Cai et al., 2013; Chen et al., 2021; van Ouwerkerk et al., 2022; Zhu et al., 2008). T-BOX genes are also essential for limb and craniofacial development. They regulate somatic region development during limb budding and maintain active expression until late developmental stages (Papaioannou, 2014). Mutations in TBX4 and LMX1B, part of the PITX1/TBX4 cascade, cause small patella syndrome, characterized by anomalies of the pelvis, patella and foot (Bongers et al., 2004; Kerstjens-Frederikse et al., 2013). TBX1 regulates pharyngeal growth factors and contributes to craniofacial muscle development (Baldini, 2003; Liao et al., 2004). TBX2 and TBX3 are essential for correct formation of the palate, and their mutation causes cleft palate, as do mutations in TBX22 (Braybrook et al., 2001; Zirzow et al., 2009). Beyond their role in development, T-BOX factors are involved in critical cellular processes. TBX3, for instance, maintains embryonic stem cell pluripotency by promoting self-renewal, and inhibits differentiation (Dong et al., 2019) and can activate genes essential for

mesodermal and extraembryonic differentiation, such as Eomes, T, Sox17, and Gata6 (Lu et al., 2011; Weidgang et al., 2013). Simultaneously, TBX3 acts as a transcriptional repressor of genes such as p14ARF, p21WAF1, and E-cadherin, influencing cell proliferation and cell migration (Willmer et al., 2016). TBX2, as a transcriptional repressor, suppresses p21 and contributes to bypassing cellular senescence, with implications in tumorigenesis (Prince et al., 2004). TBX4 is crucial for lung morphogenesis, while TBX5 is involved in the development of the visual system by regulating vertical image stability (Al-Khindi et al., 2022; Prapa et al., 2022). In the urinary system, TBX18 is necessary for kidney development, and its absence causes anomalies such as hydro ureter and hydro nephrosis (Airik et al., 2006; Xu et al., 2014). Finally, TBR1 regulates neuronal migration and axonal connection formation, with mutations associated with neurological disorders (Co et al., 2022; Papaioannou, 2014). Recent single cell sequencing studies have revealed additional roles for T-BOX factors, such as the spatial heterogeneity of TBX3 expression during the transition between different trophoblast cell lines (S. Li et al., 2024).

1.1.2. **TBX1**: MOLECULAR AND DEVELOPMENTAL FUNCTIONS

1.1.2.1 *TBX1 gene structure*: The human *TBX1* gene has three potential isoforms, composed of 9 or 10 exons, generated through alternative splicing. These isoforms differ in the position of the stop codon. The T-box domain is conserved across all isoforms and spans exons 3 to 7 (Figure 4) (Conti et al., 2003; Ogata et al., 2014; Yagi et al., 2003). The gene is located on the proximal long arm of human chromosome 22 (22q11.2), while its murine homolog is found on chromosome 16 (Chieffo et al., 1997; Gao et al., 2013). Due to the sequence identity of approximately 93% to 98% between the murine *Tbx1* gene and its human counterpart, the mouse has been used as a model organism to study the potential effects of mutations in the human gene (Garg et al., 2001).

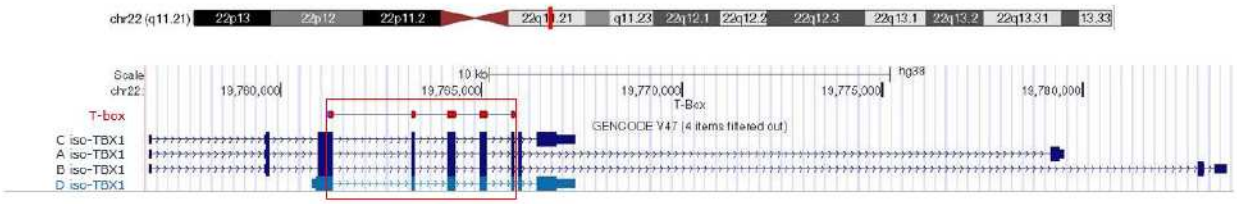


Figure 4. TBX1 isoforms visualized using the UCSC Genome Browser.
The isoforms A, B, and C are shown in blue, while an in silico-derived isoform D is represented in light blue. The T-box domain, which is conserved across all isoforms, is depicted in red. The UCSC Genome Browser platform allows visualisation of introns (lines with arrows), exons (thick segments), and non-coding regions (narrower segments). Arrows indicates the transcriptional orientation of the gene. At the top of the figure, the chromosomal ideogram is displayed. http://genome.ucsc.edu Assembly: Human (GRCh38/hg38)

Comparative studies of human and murine genomic sequences revealed that the terminal exons of isoforms TBX1A (exon 9A) and TBX1B (exons 9B and 10) are not

conserved, suggesting that the C isoform is the functional isoform. A conserved 1 kb region located 400 bp downstream of exon 8 with 67% identity to the murine sequence has been identified. This region has been proposed as a new exon, designated as 9C, which defines the TBX1C isoform (Gong et al., 2001). Expression analysis via RT-PCR confirmed the presence of TBX1C in adult skeletal muscle, adult testis and fetal lung, tissues already known to express TBX1. Moreover, comparison between the transcription levels of the TBX1A, TBX1B, and TBX1C demonstrated that TBX1C is the predominant isoform.

1.1.2.2 *DNA-binding properties of TBX1*: The linear domain structure and crystallographic structure of the TBX1 protein are shown in Figures 2 and 5 respectively. T-BOX proteins bind a highly conserved consensus sequence, termed the T-half site, corresponding to the sequence 5'-AGGTGTGAAATT-3' (Kispert and Herrmann, 1993). The optimal consensus binding sequence for TBX1 has been determined as AGGTGT[G/T][A/T] (Fulcoli et al., 2016). Comparative crystallographic studies among family members revealed that, like TBX3, TBX1 binds DNA as two monomers, each monomer binding to a single half-site (Figure 5). Additionally, as observed with other T-BOX family members (Xbra, TBX3, and TBX5), the two monomers are stabilized in position through interaction with the major and minor grooves of the DNA (El Omari et al., 2012). Only a few amino acid residues directly contact the DNA. Specifically, in the major groove, arginine 137 (R137), and in the minor groove tyrosine 176 (Y176), asparagine 289 (N289) and phenylalanine 291 and 295 (F291, F295).

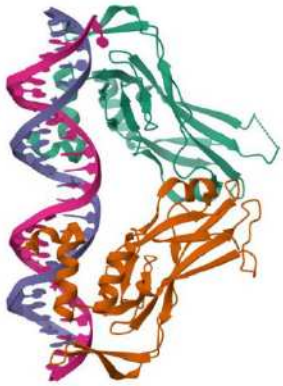


Figure 5. Structure of the DNA-bound T-box domain of human TBX1 protein
Cartoon of the TBX1-DNA complex. The TBX1 protein monomers (green and amber) bind DNA (red and blue) in the major and minor grooves. Image from the RCSB PDB (RCSB.org) of PDB ID 4A04 (El Omari et al., 2012)

1.1.2.3. Protein and chromatin interactions: TBX1 function does not depend exclusively on DNA binding; it has been shown to bind SMAD1 in a DNA-independent manner, which indirectly disrupts BMP-signalling (Fulcoli et al., 2009), and also SRF (Chen et al., 2009). However, most other known interactions are related to transcriptional functions, and in particular with histone modifiers and chromatin remodelling complexes (CRC). For example, it interacts with methyltransferases Setd7 and Ash2l. The latter is required for the methylation of histone lysine residues (Fulcoli et al., 2016; Stoller et al., 2010), and it co-localizes with the lysine demethylase LSD1/KDM1A. Through the interactions TBX1 has been shown to regulate

(promote) H3K4 mono-methylation of target genes (Fulcoli, 2016), thereby activating their expression. TBX1 also interacts with Smarcd1, a subunit of the SWI-SNF CRC, which it recruits to chromatin (Chen et al., 2012). These data provide evidence that TBX1 regulates transcription of targets genes through epigenetic mechanisms. More recently, studies of TBX1 expression and binding across the genome support the notion that TBX1 functions to prime (prepare) target enhancers and thereby render them accessible to other transcription factors, which may be activators or repressors (Cirino et al., 2020; Fulcoli et al., 2016).

1.1.2.4 *Developmental role of TBX1:* The phenotypic consequences of *Tbx1* loss of function in the mouse are broad but they primarily affect the embryonic pharyngeal apparatus (PA) and the structures that derive from it, namely the cardiac outflow tract (OFT), thymus, parathyroid glands and some skeletal muscles and bones of the lower face. Additional, structures affected are the ear, lymphatic vasculature, brain cortex and brain vasculature. As will be described in the following section (1.1.2.5) the structures affected largely reflect where the gene is expressed in mid-term mouse embryos.

Due to the high incidence of congenital heart defects in 22q11.2DS patients, the heart and great arteries are the most well studied structures in *Tbx1* mutant mice and fish. *Tbx1* expression defines a region within the PA known as the second heart field (SHF) from which the cardiac OFT, right ventricle (RV) and parts of the great arteries derive (Huynh et al., 2007; Kelly, 2012) (Figure 6).

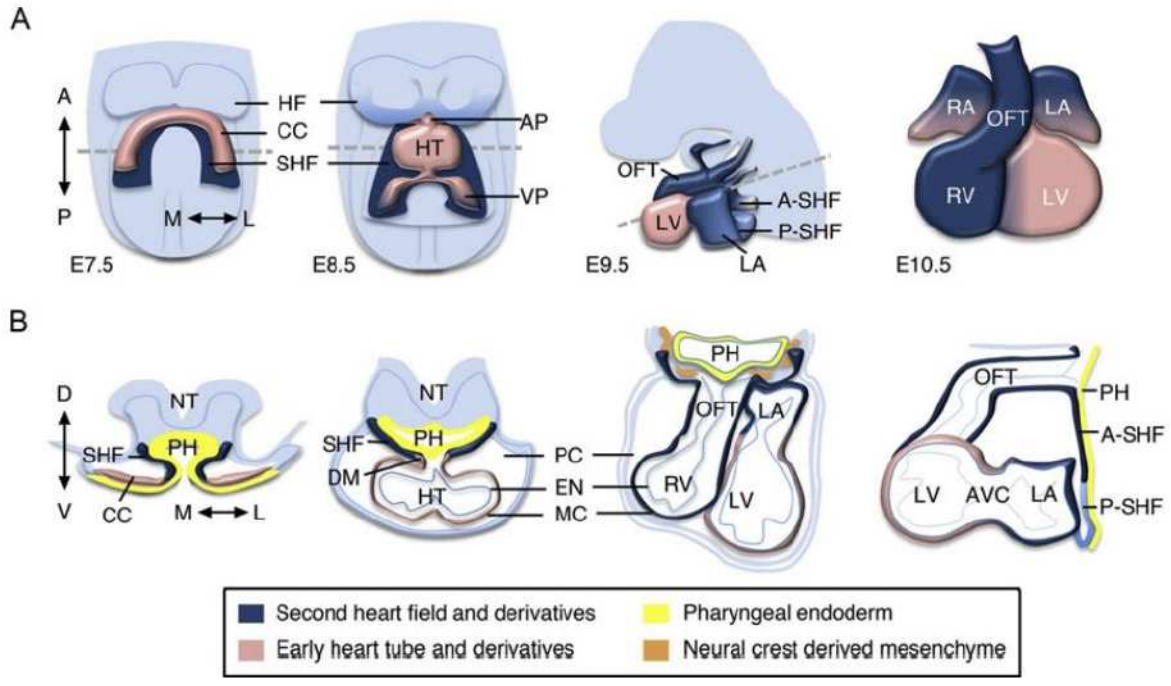


Figure 6. Topography of the second heart field.
(A) Cartoons showing the stages of mouse heart development during which second heart field progenitors are added to the heart. From left to right: embryonic day (E) 7.5 (cardiac crescent, ventral view), E8.5 (early heart tube, ventral view), E9.5 (looped heart, left lateral view), and E10.5 (ventral view). Second heart field progenitor cells and their contribution to the heart are shown in dark blue and the early heart tube-giving rise to the left ventricle in pink. Anterior (A) posterior (P) and medial (M) lateral (L) embryonic axes are indicated. (B) Schematized histological sections showing the location of second heart field cells and their myocardial derivatives

(dark blue) at the stages shown in (A) relative to pharyngeal endoderm (yellow), myocytes derived from the early heart tube (pink), and neural crest-derived mesenchyme (orange). The first three panels show transverse sections at the levels indicated by the dotted lines in (A). The right-hand panel shows a mid-sagittal E9.5 section. Dorsal (D) ventral (V) and medial (M) lateral (L) embryonic axes are indicated. CC, cardiac crescent; SHF, second heart field; HF, head fold; HT, heart tube, AP, arterial pole; VP, venous pole; OFT, outflow tract; LV, left ventricle; LA, left atrium; RV, right ventricle; RA, right atrium; A-SHF, anterior component of the second heart field; P-SHF, posterior component of the second heart field; NT, neural tube; PH, pharynx; PC, pericardial cavity; DM, dorsal mesocardium; EN, endocardium; MC, myocardium. Figure modified from Kelly et al., 2012.

As embryogenesis progresses, *Tbx1*-expressing cardiac progenitors within the SHF are deployed towards the OFT and pharyngeal arch arteries (PAA), where they are required for their formation and growth. *Tbx1* is thought to be required to maintain SHF progenitors in a proliferative state and to prevent their premature differentiation. Thus, in its' absence, an insufficient number of SHF-derived cells reaches its' destination leading to the observed hypoplasia or absence of the aforementioned structures (Chen et al., 2009; Rana et al., 2014; Xu et al., 2005). Although TBX1 is primarily a transcriptional activator, inhibition of differentiation involves suppressive interactions with cardiac transcription factors such as *Gata4, Mef2C, Smad1* and *Srf* (Chen et al., 2009; Fulcoli et al., 2016; Liao et al., 2008; Pane et al., 2012).

In the PA, TBX1 is also expressed the surface ectoderm, pharyngeal endoderm, and pharyngeal mesoderm. Tissue-specific inactivation of TBX1 has revealed distinct developmental roles in different tissues, as well as cell autonomous and non-autonomous roles (Arnold et al., 2006; Flore et al., 2017; Lania et al., 2009; Xu et al., 2005; 2007; Zhang et al., 2005).

However, while the regulation exerted by this gene is well characterized, the mechanisms governing its regulation remain poorly understood. Literature studies have identified a potential gene regulation mechanism for *Tbx1* in cancer cells that depends on the activation of the *Wnt/β*-catenin pathway (Verdelli et al., 2017). Furthermore, a potential cis-regulatory element upstream of the Tbx1 gene has been identified. This element is recognized by transcription factors of the forkhead box (Fox) family, including FOXA2, FOXC1, and FOXC2, and is essential for the regulation of Tbx1 in the pharyngeal endoderm and head mesenchyme (Yamagishi et al., 2003). Recent findings have demonstrated that a chromatin modifier, the zinc finger protein of monocytic leukemia (MOZ/MYST3/KAT6A), regulates acetylation on lysine 9 residues of histone H3 (H3K9ac), leading to transcriptional activation of the *Tbx1* locus. This activation plays a role in the development of structures such as the cardiac aortic arch, thymus, and palate (Vanyai et al., 2015; Voss et al., 2012). A study conducted in 2023 by Zhao et al., using whole-genome sequence (WGS), confirmed a possible epigenetic regulation mediated by protein complexes of the MYST family, such as the MOZ acetyltransferase complex and the NuA4 histone acetyltransferase complex (NuA4)(Zhao et al., 2023).

1.1.2.5 *TBX1 expression in the mouse*: Studies conducted during various stages of mouse embryonic development have revealed expression in the following tissues; pharyngeal apparatus, including the second heart field, cardiac outflow tract, jugular lymph sacs,

pulmonary epithelium, otic vesicle, and in some brain blood vessels (Chapman et al., 1996; Chen et al., 2010, 2009; Lindsay et al., 2001; Xu et al., 2007, 2004; Zhang et al., 2006). TBX1 is activated at embryonic day (E) 7.5 in the anterior mesoderm, after which it is rapidly activated in the aforementioned tissues. From E13.5 onwards its' expression is downregulated, and postnatally it is limited to the hair follicles, including the vibrissae, the tongue and some brain blood vessels. Reactivation of TBX1 has been reported after injury. In particular, ligation-induced myocardial infarction induced its' expression in endothelial cells of newly formed lymphatic vessels (Wang et al., 2023).

Engineered mutation of *Tbx1* in the mouse has revealed its' critical function in most of the tissues and organs that express the gene during mouse embryogenesis. In particular. heterozygous mutation impairs development of the 4th pharyngeal arch artery (Jerome and Papaioannou, 2001; Lindsay et al., 2001; Merscher et al., 2001) and mild abnormalities in the embryonic brain cortex (Flore et al., 2017) and cerebellum (Eom et al., 2024), while homozygous mutation is associated with severe congenital heart defects, a failure of ear development (Jerome and Papaioannou, 2001; Lindsay et al., 2001; Merscher et al., 2001) and the loss of most lymphatic vessels (Chen et al., 2010). As *Tbx1* loss of function is lethal postnatally its' role, if any, in the adult mouse is largely unknown.

1.1.3. 22q11.2 DELETION SYNDROME: A disease of *TBX1* haploinsufficiency

TBX1 is the major gene involved in 22q11.2 deletion syndrome (22q11.2DS), also known as DiGeorge syndrome and velocardiofacial syndrome. This condition is the most common chromosome microdeletion syndrome, with an estimated incidence of 1 in 2,500 live births (McDonald-McGinn et al., 2015; Ryan et al., 1997). Phenotypic variability is a hallmark of this syndrome, with clinical manifestations ranging from cardiovascular anomalies and immune defects to neurological developmental disorders and facial dysmorphism (Cillo et al., 2024). The clinical severity, which is characterized by incomplete penetrance, is probably attributable at least in part to the genetic complexity of the affected region. Among the most significant clinical anomalies observed in patients, facial dysmorphism and congenital heart defects (CHD) are the most frequent, with a penetrance of 100% and 75% respectively. CHD include interrupted aortic arch type-B, tetralogy of Fallot and persistent truncus arteriosus, reflecting abnormal formation of the pharyngeal arches and arch arteries during fetal development (Merscher et al., 2001; Ryan et al., 1997). Other abnormalities include thymic hypoplasia, and parathyroid aplasia, which lead to T cell-related immunodeficiency and hypoparathyroidism, respectively and imbalance of calcium homeostasis (Morsheimer et al., 2017). Developmental biology studies have shown that many of these anomalies likely arise from the anomalous deployment of neural crest cells, which play a crucial role in cardiovascular and craniofacial morphogenesis (reviewed in Baldini et al., 2017 and Scambler et al., 2000). Children and adults affected by 22q11.2DS also suffer from learning and memory deficits, anxiety-related behavioural anomalies and they have a greatly increased risk for developing psychiatric diseases, including schizophrenia.

The common 22q11.2 deletion, which occurs in >90% of cases, spans a region of approximately 3 Mb of DNA and encompasses approximately sixty genes, including *TBX1*.

However, substantial evidence suggests that *TBX1* plays a central role in the pathogenesis of the syndrome. This is because individuals who carry rare *TBX1* point mutations manifest the same clinical signs and symptoms as those with the chromosomal microdeletion (Ogata et al., 2014; Paylor et al., 2006; Torres-Juan et al., 2007; Yagi et al., 2003). In addition, prior to these human studies, the development of genetically modified murine models had demonstrated that mutation of *Tbx1* replicated many of the physical defects observed in 22q11.2DS patients, including cardiovascular anomalies and pharyngeal arch and arch artery defects (Jerome and Papaioannou, 2001; Lindsay et al., 2001; Merscher et al., 2001). Less than 10% of patients carries a smaller deletion spanning approximately 1.5 Mb of DNA that includes TBX1. The clinical phenotype observed in these patients is not distinguishable from those with the 3 Mb microdeletion. Patients with 22q11.2 microdeletion syndrome are at an increased risk of developing neuropsychiatric disorders, such as schizophrenia, anxiety, Autism Spectrum Disorder, ADHD (Bassett and Chow, 1999; Biswas and Furniss, 2016; Campbell et al., 2015; Caterino et al., 2025; McDonald-McGinn et al., 2015; Murphy et al., 1999; Niarchou et al., 2015; Niklasson et al., 2001; Schneider et al., 2014; Vangkilde et al., 2016; Vorstman et al., 2015).

Beyond the direct contribution of *TBX1* heterozygosity to the clinical manifestations of 22q11.2DS, studies have suggested that epigenetic regulation of the remaining functional allele might also contribute. Modifications such as DNA methylation, histone acetylation, and interactions with non-coding RNA may significantly influence TBX1 activity, contributing to the phenotypic variability observed in patients (Bassett et al., 2011; McDonald-McGinn et al., 2015).

In conclusion, the evidence that TBX1 represents a central node in the pathogenesis of 22q11.2DS, combined with the growing understanding of the epigenetic mechanisms modulating *TBX1* gene expression, emphasises the need for further studies in this area. A greater understanding of the epigenetic mechanisms underlying *TBX1* regulation could not only clarify the biological basis of the phenotypic variability of 22q11.2DS but also pave the way for targeted therapeutic interventions, with significant implications for the clinical management of the syndrome.

1.2. EPIGENETIC REGULATION OF TRANSCRIPTION

The term epigenetics was coined in 1942 by Conrad Waddington, a British scientist, who defined it as the basis of changes in phenotype without underlying genotypic changes (Waddington, 1942). Now, we know that epigenetics is one of the main mechanisms of gene regulation through which the heritable phenotype is modified without altering the structure of the DNA (Allis, 2016). Epigenetic mechanisms work together with the DNA template to modify gene expression programs and, consequently, the identity of the cell type (Allis and Jenuwein, 2016). Over time, it has been recognized that they are involved in a wide range of biological processes as growing evidence suggests that epigenetic changes can occur independently of alterations in somatic cells and their state of differentiation (Bird, 2007).

Gene regulation is directly correlated to DNA structure and different mechanisms can regulate gene expression through chemical modifications of DNA bases and changes to

chromatin in which DNA is packaged. In eukaryotic cells, the DNA wraps approximately 1.5 times around an octamer of four core histones (H2A, H2B, H3, H4), thus forming the nucleosome (Quina et al., 2006). The portion of DNA that is in contact with the histones is sterically inaccessible. Furthermore, the N-terminal tail of histone H4, which extends from the nucleosome core, interacts with a specific acidic zone of the histone group of the adjacent nucleosome, stabilizing interactions between nucleosomes and promoting local chromatin condensation. The binding between nucleosomes is further stabilized by the linker histone, H1, which binds to DNA entry and exit points on the nucleosome and limits the action of nucleosome remodels (Pepenella et al., 2014; Ramachandran et al., 2003). To date, numerous epigenetic regulatory mechanisms have been identified, such as DNA/RNA methylation, histone modifications, nucleosome localization, non-coding RNA (ncRNA) expression and 3D chromatin structure, all of which are involved in cell growth, development and differentiation (Allis and Jenuwein, 2016).

DNA methylation, which is the most extensively studied epigenetic mechanism, is catalysed by DNA methyltransferase enzymes and involves the addition of a methyl group to a cytosine nucleotide within a cytosine-guanine sequence (CpG). These dinucleotides are often clustered into CpG islands (CpGIs) that represent a principal target for DNA methylation and are preferentially located at the 5' promoter region in more than 50% of human genes (Saxonov et al., 2006). CpG dinucleotides are dispersed across the genome and most are heavily methylated. In contrast, CpGIs remain largely unmethylated, especially in promoter regions (Lin et al., 2020). Methylated cytosines within promoters recruit gene suppressor proteins and inhibit interactions between DNA and transcription factors (Moore et al., 2013). Additionally, cytosine methylation promotes heterochromatin formation, resulting in nucleosome compaction that prevents the transcriptional machinery from accessing DNA (McMahon et al., 2017). DNA methylation plays a central role in embryonic development, chromosome X inactivation, genomic imprinting, in the establishment of cell identity and lineage specification (Gopalakrishnan et al., 2008; Jin et al., 2008; Robertson, 2005).

Three major DNA methyltransferases (DNMTs), DNMT1, DNMT3a and DNMT3b, have been identified as being involved in DNA methylation. DNMT1 is the main one due to its major catalytic activity in favouring the methylation of hemi-methylated DNA during replication and in favouring the maintenance of the methylation state (Goyal et al., 2006; Pradhan et al., 1997). On the contrary, DNMT3a and DNMT3b are the main "de novo" methyltransferases, able to structure the precise methylation state of DNA starting from unmethylated residues independently of the cellular replication process (Liang et al., 2002). Conversely, DNA demethylation reverses the effects of DNMTs, restoring the expression of silenced genes. A family of Ten-eleven translocation methyl cytosine dioxygenases, including TET1, TET2, and TET3, mediates this process. These enzymes facilitate the conversion of 5-methylcytosine (5mC) to 5-hydroxymethylcytosine (5-hmC), which can then be further oxidized to 5-formylcytosine (5-fC) and 5-carboxylcytosine (5-caC) (Scourzic et al., 2015). The balance between DNA methylation and demethylation operates as a dynamic regulatory mechanism that governs gene expression in many cell types.

The second major epigenetic mechanism involves post-translational modifications of histones, including acetylation, methylation, phosphorylation, and ubiquitylation. Histone acetylation typically occurs at lysine residues, reducing DNA-histone interactions, thereby

loosening chromatin structure and promoting transcription (Bannister and Kouzarides, 2011). Histone methylation is more complex, involving the addition of one to three methyl groups to lysine residues, or one to two methyl groups to arginine residues (Bannister and Kouzarides, 2011). Methylation of lysine 4 on histone H3 (H3K4me) is associated with transcriptional activation, while trimethylation of lysines 9 and 27 (H3K9me3 and H3K27me3) is linked to transcriptional repression (Esteller Manel, 2008).

Histone phosphorylation, which is less well understood, involves adding phosphate groups to histone tails. Phosphorylation of histone H2A(X) is implicated in the DNA damage response and repair processes (Rossetto et al., 2012). Ubiquitylation, involving the attachment of a ubiquitin molecule to lysine residues, has diverse effects. For example, H2AK119ub is associated with gene silencing, while H2BK123ub facilitates transcription (Bannister and Kouzarides, 2011). Though histone acetylation directly influences gene expression, the effects of other modifications are complex and highly context-dependent. The most recently characterised epigenetic mechanism is ncRNA-associated gene silencing. NcRNAs are small RNA molecules that do not code for protein and include microRNAs (miRNAs) and small interfering RNAs (siRNAs), which are fewer than 30 nucleotides in length, and long non-coding RNAs (lncRNAs), exceeding 200 nucleotides. While the full scope of their epigenetic roles remains under investigation, ncRNAs have been shown to mediate DNA methylation, histone modifications, and gene silencing (Wei et al., 2017). For example, both siRNAs and lncRNAs contribute to heterochromatin formation and subsequent gene expression regulation (Chisholm et al., 2012).

1.3. EPIDRUGS AS TOOLS TO STUDY TBX1 REGULATION

The increasing knowledge of epigenetic mechanisms and their role in disease pathogenesis has favoured the development of therapies aimed at modulating epigenetic regulatory processes. Due to the chemical reversibility of DNA methylation and post-translational modifications of histones, epigenetic proteins are attractive drug targets. In particular, small molecule enzyme inhibitors have been developed to restore aberrant epigenetic mechanisms and potentially reverse pathological epigenetic signatures (Ganesan et al., 2019). Epigenetic drugs (epidrugs) are molecules that act at the level of DNA and histones mainly by acting on enzymes responsible for the creation and maintenance of the epigenetic modification, thereby modifying gene expression. For example, by reactivating silenced genes involved in cellular repair and homeostasis, epidrugs demonstrate their therapeutic potential in various pathological conditions (Salarinia et al., 2016). The United States Food and Drug Administration (FDA) has approved several epigenetic therapies, paving the way for their expanded use in the management of non-oncological diseases (Berdasco and Esteller, 2019; Hailu et al., 2017). This evolving field underscores the potential of epigenetic therapy to address unmet medical needs by targeting fundamental regulatory mechanisms of gene expression.

In the case of 22q11.2DS, which is primarily a disease of *Tbx1* haploinsufficiency, epidrugs are of interest because of the possibility of increasing expression from the remaining healthy *Tbx1* allele. However, for my Ph.D project, my primary goal was to use them to gain insights

into the epigenetic regulation of TBX1. Of course, having identified epidrugs that fulfil this role they could, indeed should, be tested for therapeutic efficacy.

Historically, it was found that molecules designed to act at the epigenetic level not only reduced the targeted enzymatic activity, but frequently caused indirect (and undesirable) transcriptional changes in multiple genes (Nebbioso et al., 2012). The search for epigenetic inhibitors led to the development of the first generation of epidrugs, which were characterized by a low degree of selectivity (Cartron et al., 2019). In this category were various DNA methyltransferase inhibitors (DNMTis) and histone deacetylase inhibitors (HDACis), some of which have been approved for the treatment of different cancers (Bennett and Licht, 2018). First generation of DNMTis, such as pyrimidine analogues, are incorporated into DNA during replication, activating DNA damage response pathways and inducing apoptosis of cancerous cells. However, this was associated with significant cytotoxic effects on normal cells (Kelly et al., 2010; Morel et al., 2020). In contrast, first-generation HDACis inhibit Zn^{2+}-dependent histone deacetylases (HDACs), with the exception of sirtuin inhibitors, which specifically target a class of NAD^{+}-dependent histone deacetylases (HDACs) (Morel et al., 2020). Both inhibitors exhibited numerous unfavourable pharmacokinetic properties and poor target selectivity, necessitating the development of second-generation epidrugs (Morel et al., 2020).

Second-generation epidrugs, including DNMTis such as zebularine and guadecitabine, and HDACis such as hydroxamic acids, belinostat, panobinostat, tucidinostat, and valproic acid, were developed with improved pharmacological properties (Morel et al., 2020). These drugs were the result of intensive academic research and industrial drug discovery efforts aimed at designing molecules with greater inhibitory potency and fewer side effects. One significant challenge with the first-generation compounds was their poor pharmacokinetics, characterised by low bioavailability, activity limited to non-physiological pH ranges, and susceptibility to cellular deaminases, leading to short half-lives.

The third generation of epidrugs emerged from a deeper understanding of the role of epigenetic factors in reading, writing and erasing epigenetic marks within the context of protein complexes. Consequently, designing highly selective epidrugs required a comprehensive analysis of the epigenetic protein interactome (Cartron et al., 2019). These epidrugs include inhibitors of histone methyltransferases (HMTs), histone demethylases (HDMs), and bromodomain and extra-terminal domain inhibitors (BETis) (Morel et al., 2020). These advances reflect the increasing precision in identifying molecules especially from the classes of histone acetylases and methylases increasingly targeted to hit specific epigenetic regulators, minimizing unwanted side-effects and expanding their functions in the medical field.

The following section presents essential information about the epidrugs that I used in my project. Each was selected as representative of one of the major classes of epidrugs, given that my objective was not to evaluate their potential therapeutic efficacy, but rather as tools to identify histone marks that are potentially relevant for activating or increasing *TBX1* expression.

1.3.1. Histone Deacetylase Inhibitors (HDIs): SAHA

Two classes of enzymes, histone acetyltransferases (HATs) and histone deacetylases

(HDACs), regulate the reversible addition or removal of acetyl groups on the amino acid residues of histone tails (Figure 7) (Selvi and Kundu, 2009). Following the addition or removal of acetyl groups, the enzymatic activity of HATs and HDACs is associated with gene activation and silencing respectively (Keppler and Archer, 2008a, 2008b).

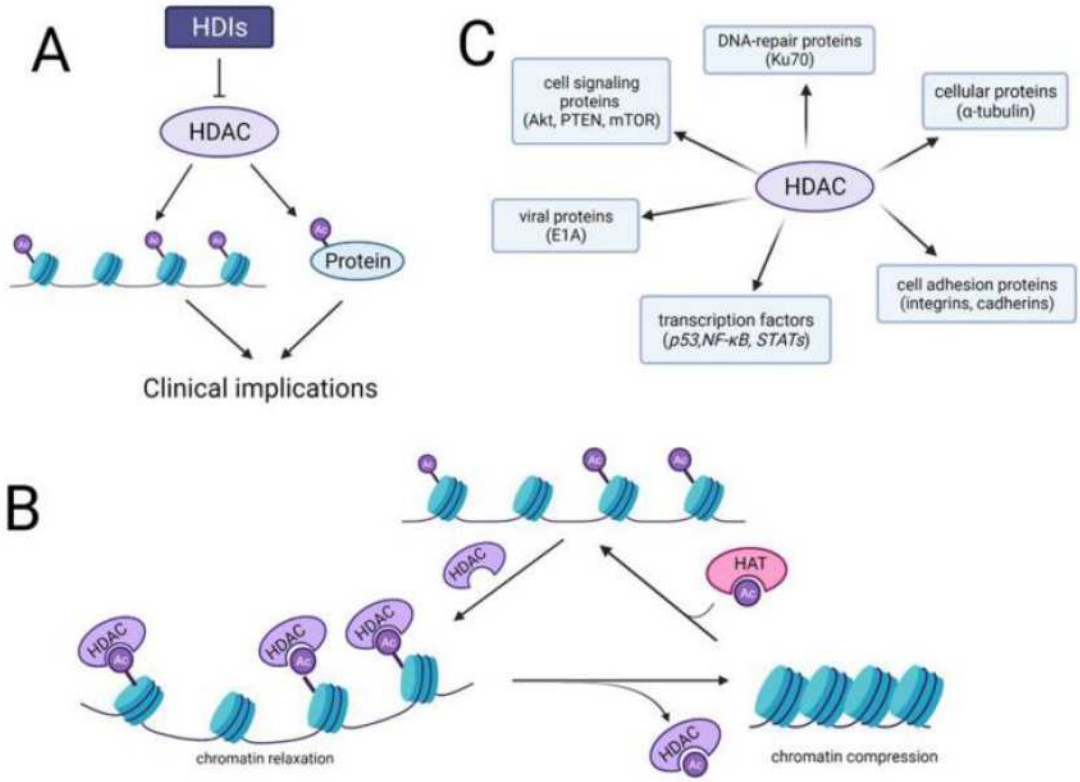


Figure 7. Reversible posttranslational lysine residues acetylation of histones is maintained by HATs and HDACs.
Removal of acetyl group by HDACs leads to condensation of chromatin and its inactivation. Figure modified from (Wawruszak et al., 2021).

HDACs function as transcriptional repressors by facilitating chromatin condensation through histone deacetylation, a process that reduces DNA accessibility to transcription factors. HDAC inhibitors (HDIs) are therefore of interest to me because blocking the removal of acetyl groups from lysine residues on histones H2A, H2B, H3, and H4 (Turner, 2000) could, potentially, increase *TBX1* expression. In general terms, HDIs exert their effects by selectively altering the structure of the enzyme involved in the epigenetic modification, thus influencing the dynamics of epigenetic regulation (Eckschlager et al., 2017; Takai et al., 2004b, 2004a). For this reason, specific HDAC inhibitors (HDACi) are under investigation for their therapeutic potential in the contest of neurodegenerative and cardiac diseases due to their ability to enhance the transcription of genes involved in these diseases (Guan et al., 2009; Webster et al., 2013).

The HDAC family consists of 18 members divided into four classes, based on their evolutionary characteristics (homology with yeast proteins) and functional properties (mechanisms and catalytic requirements). The first class shares homology with yeast RPD3 and includes four members: HDAC1, HDAC2, HDAC3, and HDAC8. The second class is further

classified into two subclasses: IIa, based on homology with yeast HDA1, comprising HDAC4, HDAC5, HDAC7, and HDAC9; and IIb, which includes HDAC6 and HDAC10, characterized by members with two catalytic sites. The third class, known as the sirtuin family, consists of seven members (SIRT1-SIRT7) and shares homology with yeast Sir2. Finally, the fourth class includes a single member, HDAC11, which has conserved residues in its catalytic centre shared by both class I and class II deacetylases (Bolden et al., 2006; Marks et al., 2001; Seto and Yoshida, 2014). The HDACs of class I and II differ in their activity. For example, class I HDACs are primarily nuclear in localization and ubiquitous. Class II HDAC expression is more tissue restricted; these HDACs shuttle between the nucleus and the cytoplasm, and some are primarily cytoplasmic proteins. Class I HDACs play a role in cell proliferation and death, whereas class II HDACs appear to have tissue-specific developmental activity (Marks and Breslow, 2007). All the aforementioned HDACs depend on the presence of a zinc ion in their catalytic site for their activity, except for the sirtuin group. Unlike other members of the HDAC family, sirtuins require nicotinamide adenine dinucleotide (NAD^+) as a cofactor for their catalytic activity (Hai et al., 2021).

In 2006, the FDA approved Vorinostat, also known as SAHA, as the first HDI for the treatment of cutaneous T-cell lymphoma (CTCL) (Mann et al., 2007). Among the HDAC inhibitors currently in clinical trials, this epidrug has been tested for its therapeutic potential in the context of genetic disorders, like Fragile X syndrome (FXS) (Ding et al., 2022) Suberoylanilide hydroxamic acid (Vorinostat, SAHA; $C_{14}H_{20}N_2O_3$) is a dicarboxylic diamide composed of suberic acid (octanedioic acid) coupled with aniline and hydroxylamine (Figure 8).

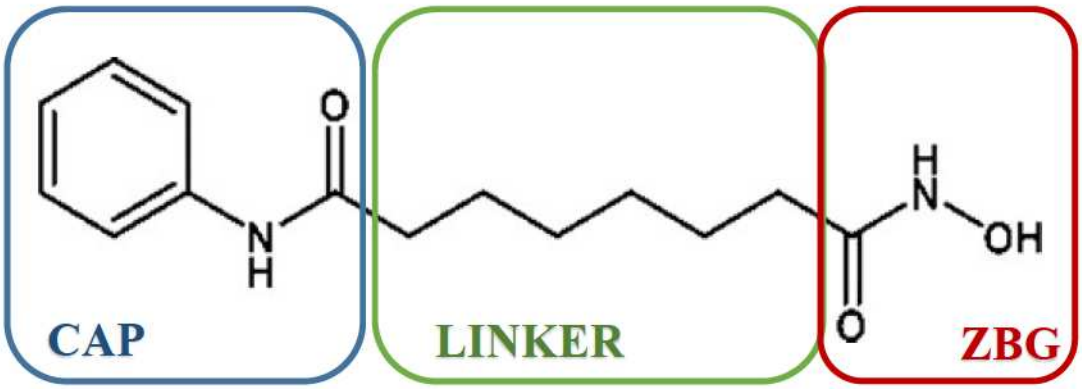


Figure 8. Structure of vorinostat (suberoylanilide hydroxamic acid, SAHA).
Image from PubChem. Like other HADACi we can recognize in SAHA a zinc-binding group (ZBG), a linker domain and a hydrophobic cap group (CAP). The CAP group interacts with the rim of the enzyme binding pocket; the linker group connects the CAP and the ZBG; the ZBG chelates the zn++ in the active site. The cap, linker and the Zn^{2+} binding group are represented in blue, green and red, respectively.

SAHA is a first-generation pan-inhibitor of HDACs, belonging to the class of histone deacetylase inhibitors (HDIs) based on hydroxamic acids (Bubna, 2015). The mechanism of action of SAHA involves the inhibition of the catalytic activity of class I and II HDACs (Antoniou and Easton, 2006; Sung et al., 2021) through direct binding to the zinc ion in the enzyme's catalytic site (Ataollahi et al., 2015; De Souza and Chatterji, 2015; Eckschlager et al., 2017). Specifically, its structure is characterized by three domains: the cap region (CAP), the linker domain, and the zinc-binding group (ZBG) (Sangwan et al., 2018). The CAP and linker domains interact with residues within the HDAC active site, promoting ligand-receptor

interactions and modulating selectivity toward specific HDACs. The inhibitory activity of the compound is mediated by the ZBG, which establishes bonds with the zinc ion in the active site and surrounding residues, thereby facilitating HDAC inhibition (Manal et al., 2016) (Figure 9).

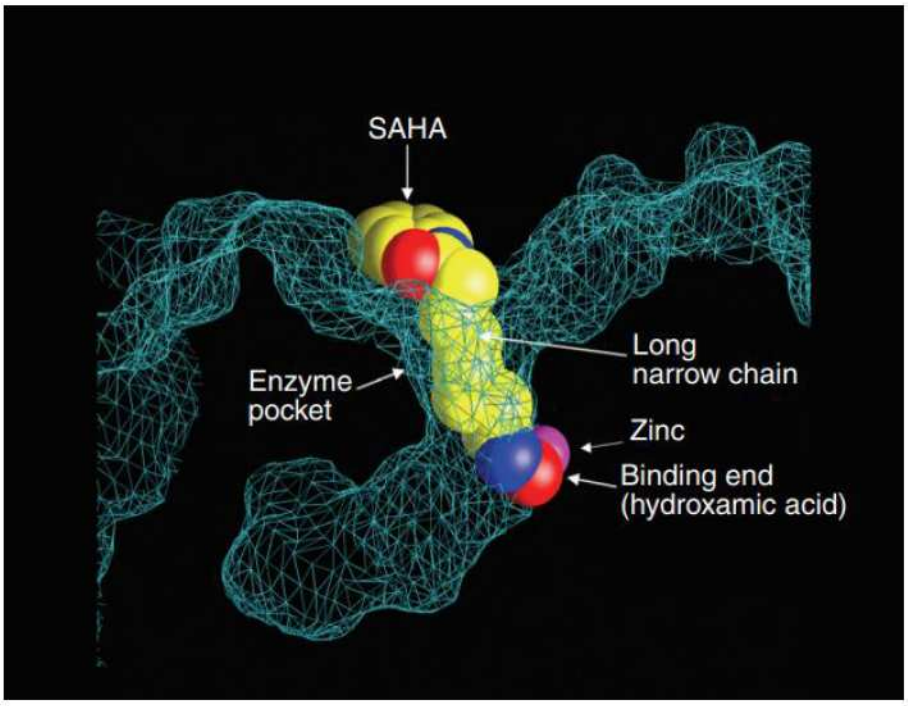


Figure 9. 3D structure of the enzyme with the SAHA compound bound in the active pocket to highlight the interaction mechanism between the inhibitor (SAHA) and the target enzyme (HDAC).
The image shows the enzyme pocket: The enzyme pocket (in light blue) represents the active site of the enzyme, where SAHA stably binds. The SAHA: Chemical Structure Model (Space-Filling) shown in yellow and red, represents the inhibitor compound with a conformation suitable for the active site. Linker domain and CAP: The long narrow chain of SAHA and the CAP at the end allows interaction with the enzyme pocket, optimizing binding. ZBE (hydroxamic acid): The end of the SAHA containing the hydroxamic group (in red and blue) is critical for coordination with the zinc ion in the active site. Zinc: The zinc ion (in violet) is an essential cofactor for the activity of the enzyme. Its interaction with the hydroxamic group contributes to the inhibition of the enzyme. Figure modified from Marks and Breslow, 2007.

1.3.2. Lysine Demethylase Inhibitors: GSKLSD1 and GSK2879552

Unlike DNA methylation, which silences gene expression, the methylation of certain H3 and H4 lysine residues is an activating histone mark, for example, mono-, di- and trimethylation of H3K4. Therefore, lysine demethylase inhibitors that target such residues are of interest to me because blocking demethylation could, potentially, increase *TBX1* expression.

Since the 2000s, the study of lysine methylation has garnered increasing interest (Hayward and Cole, 2016). Lysine methylation can occur as mono-, di-, or trimethylation. Before the discovery of the LSD1 (Lysine-Specific Demethylase 1) enzyme in 2004, the reversibility of lysine methylation was debated. This uncertainty was resolved with the work of

Shi et al. (2004), which demonstrated LSD1's ability to demethylate lysine residues. Currently, 18 lysine demethylases are recognized, which can be divided into 2 main families; the LSD family, which includes two flavin-dependent enzymes, LSD1 (KDM1A) and LSD2 (KDM1B), and the JmjC domain-containing family (JmjC-KDM), which rely on non-heme iron and α-ketoglutarate for their catalytic activity (Culhane and Cole, 2007; Thinnes et al., 2014). LSD1/KDM1A and LSD2/KDM1B feature N-terminal SWIRM domains (Swi3p, Rsc8p, Moira), a flavin adenine dinucleotide (FAD)-binding motif, and a C-terminal amine oxidase domain responsible for FAD-dependent activity (Maiques-Diaz and Somervaille, 2016). These enzymes catalyse the N-demethylation of mono- or demethylated lysine residues on H3K4, primarily acting as transcriptional corepressors (Hoffmann et al., 2012; Shi et al., 2007; Kaniskan, 2017). However, LSD1 acts as a co-activator of the androgen receptor by demethylating H3K9me1/me2 (Metzger et al., 2005). Since H3K4 methylation is associated with gene activation, LSD1 activity is generally linked to gene silencing (Shi et al., 2004).

The discovery of the reversible nature of histone methylation paved the way for the study of drugs targeting this epigenetic modification (Zhang et al., 2021). The identification of tranylcypromine (TCP) as an LSD1 inhibitor spurred the development of new irreversible and more selective inhibitors, including GSK2879552, used in this study. Mechanistically, TCP-based inhibitors inactivate LSD1 through a single-electron reduction reaction and subsequent cyclopropyl ring cleavage, generating covalent complexes between FAD and the inhibitor compound (Forneris et al., 2006). However, they also inactivate monoamine oxidase (MAO) enzymes, which are structurally similar. GSK2879552 was identified through a screening of 2.5 million compounds and demonstrated high selectivity for LSD1 (Mohammad et al., 2015), irreversibly inactivating LSD1 without disturbing MAO activity (Tan et al., 2019). Despite its selectivity, GSK2879552 exhibited reversible toxicity in preclinical studies, including thrombocytopenia and neutropenia (Hou at al., 2015).

1.3.3. Polycomb Inhibitors: GSK126

HMTs are categorized into three families: SET-domain-containing enzymes and Dot1-like proteins that act on lysines (KMTs) (Black et al., 2012), and protein arginine N-methyltransferases (PRMTs), which methylate arginine residues (Bedford and Clarke, 2009; Yang and Bedford, 2013). Methylation predominantly occurs at lysine residues K4, K9, K27, K36, and K79 of histone H3 and K20 of histone H4 (Hon et al., 2009). Generally, methylation at H3K9, H3K27, and H4K20 is associated with transcriptional repression, while methylation at H3K4, H3K36, and H3K79 is associated with gene activation (Vermeulen et al., 2010). H3K9me2/me3, H3K27me2/me3, and H4K20me3 are typically found in heterochromatin regions, where genes are transcriptionally silent (Vermeulen et al., 2010). Unlike histone acetylation, the effect of histone methylation depends on the specific residues targeted. For instance, methylation of H3K4/36/79 contributes to active transcriptional states, whereas H3K9/27 and H4K20 methylation are predominantly associated with repressive epigenetic marks (Barski et al., 2007; Bernstein et al., 2006; Wiles and Selker, 2017). Trimethylation of histone H3 at lysine 27 (H3K27me3) is particularly associated with gene silencing (Cao et al., 2002)., in particular of genes critical for embryonic development (Bernstein, 2006), stem cell self-renewal (Kamminga et al., 2006), and cancer progression (Wilson et al., 2016). The

Polycomb repressive complex 2 (PRC2) is an essential chromatin modifier that specifically catalyses H3K27 methylation through its catalytic subunit enhancer of zeste homolog 2 (EZH2) (O'Meara and Simon, 2012). Additionally, previous studies have shown that EZH2 is involved in regulating *TBX1* expression in human embryonic stem cells (Caprio et al., 2021; Collinson et al., 2016).

GSK126 (Fig. 10), a potent inhibitor of EZH2, exhibits Ki values (the equilibrium constant for the binding of an inhibitor to an enzyme, reflecting the inhibitor's potency; lower Ki values indicate stronger binding affinity) ranging from 0.5 to 3 nM for both wild-type and mutant forms of EZH2, demonstrating its efficacy irrespective of the substrate utilized.

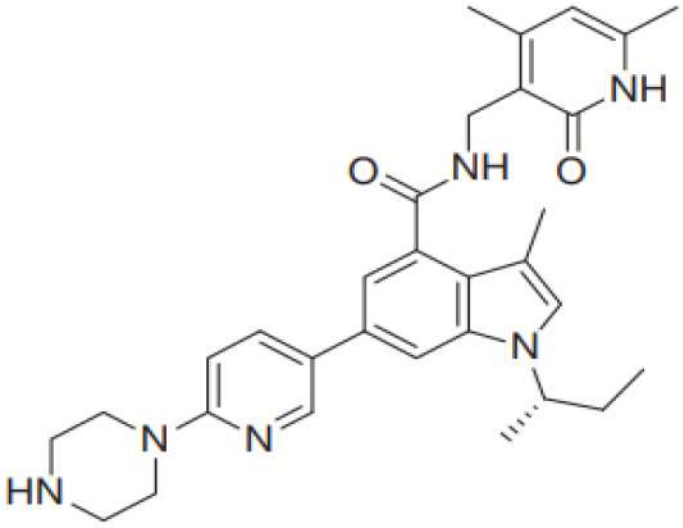


Figure 10. GSK126 structure

Mechanistically, GSK126 functions as a competitive inhibitor for S-adenosylmethionine (SAM) while remaining non-competitive with peptide substrates. The compound shows high specificity, being over 1,000-fold more selective for EZH2 compared to 20 other human methyltransferases, including those with and without the SET domain. Notably, EZH1, which shares 96% sequence identity with EZH2 within the SET domain, is inhibited with significantly lower potency of Ki 89 nM (McCabe et al., 2012). Structural docking analyses indicate that GSK126 binds within the SAM-binding pocket, where it establishes extensive interactions with the post-SET domain. This unique interaction profile likely contributes to its exceptional selectivity for EZH2 over EZH1. In functional assays, GSK126 effectively diminishes H3K27me3 levels, achieving the most pronounced reduction at H3K27me3, followed by H3K27me2. However, its effect on H3K27me1 is minimal, even at the highest tested concentrations of the inhibitor. This differential impact on histone methylation states underscores GSK126's potential as a precise epigenetic modulator (McCabe et al., 2012).

Table 1 provides a summary of the major epigenetic modifications of histones and their potential biological effects.

Modification	Regions	Activity Level	Epidrugs
H3K4me3	promoters	active, poised	
H3K4me2	promoters, enhancers	active, poised	GSKLSD1, GSK2879552 (LSD1i)
H3K4me1	enhancers	active, poised	GSKLSD1, GSK2879552 (LSD1i)
H3K27ac	promoters, enhancers	active	SAHA (HDACi)
H3K9ac	promoters, enhancers	active	SAHA (HDACi)
H3K36me3	exons	active	
H3K27me3	introns, intergenic	repressed	GSK126 (EZH2i)
H3K9me3	heterochromatin	repressed	

Table 1. Table of Epigenetic Modifications and Their Potential Effects in Different Genomic Regions.
In the table, the first column lists the epigenetic markers. The second column indicates the genomic regions that can be affected by these modifications. The third column classifies the modifications as either activating or repressive marks. The last column includes the epidrugs used in this study.

2. AIMS OF THE PROJECT

2.1 Reasons for the study / investigation

As a classical transcription factor, TBX1 activates target genes that are involved in the development of diverse embryonic tissues, including the pharyngeal apparatus, ear and vascular systems (introduction section 1.1.2.4). TBX1 has also been hypothesized to act as a pioneer transcription factor (Cirino et al., 2020; Fulcoli et al., 2016), i.e., one that is able to bind chromatin in a closed (condensed) conformation and prime enhancers which are then activated by tissue-specific transcription factors. In both cases, most research attention has focused on the genes and /or biological processes that are activated as a result of TBX1 binding, whereas almost nothing is known about the genes and proteins that regulate *Tbx1* gene expression (section 1.1.2.4). The latter is the only known epigenetic regulator of *Tbx1*. It is likely that other histone modifications are associated with the activation of *Tbx1* expression, but this is not known. This project seeks to address this issue using experimental (wet lab) and bioinformatic approaches.

2.2 Goals of the project

The main objective of my project is to gain insights into the histone modifications that promote *Tbx1* gene expression and to determine whether epidrugs that target these modifications have therapeutic potential in mouse models of DiGeorge syndrome. I propose three specific aims to achieve this objective.

Aim 1. To identify histone modifications that increase Tbx1 gene expression in cultured cells

Rationale: Epigenetic regulation of gene expression is commonly a combinatorial process, i.e., involving more than a single histone modification, and it can involve increasing activating histone marks while at the same time reducing repressive ones. As we do not know *a priori* which histone modifications activate *Tbx1* expression, I will take a pharmacological approach to investigate this. By using epidrugs that target specific candidate histone modifications I expect to discover those that alone or in combination increase *Tbx1* gene expression.

Aim 2. To test a novel bioinformatic approach for identifying Tbx1-activating histone modifications

Rationale: Public databases such as ENCODE and the UCSC Genome Browser house a wealth of genomics data relating to gene expression and chromatin organization in diverse organisms and cell lines. In this Aim, I will use a bioinformatics approach to integrate such data with our current knowledge of *Tbx1* enhancers (murine) in order to identify histone modifications

present at 14 newly identified putative enhancers. Through this approach I expect to obtain information about the epigenetic profile associated with *Tbx1* activation and, potentially, gain insights into the most effective combinatorial epidrug treatments that could be used to increase *Tbx1* expression in cases of *Tbx1* insufficiency, as a result of *Tbx1* mutation.

Aim 3. To investigate the therapeutic potential of Tbx1-activating epidrugs using phenotypic rescue in Tbx1 mutant mice.

Rationale: DiGeorge syndrome (DGS) is primarily a *TBX1* haploinsufficiency disorder. In the mouse, gene haploinsufficiency is less common, and in the case of mouse models of DGS, cardiovascular development seems to be the only morphogenetic process that requires two functional copies of the *Tbx1* gene. In particular, >90% of $Tbx1^{+/-}$ embryos have hypoplasia or absence of the 4th pharyngeal arch artery, 4PAA (Lindsay et al., 2001). Thus, this phenotype is suitable for phenotypic rescue experiments in treated versus non-treated animals. In this Aim, I will test the most promising epidrug treatments identified in Aim 1 in *Tbx1* mutant embryos. The readout of these experiments will be the ability of the epidrug/s to rescue (normalize) 4PAA development in $Tbx1^{+/-}$ embryos.

2.3 Choice of the experimental systems and methods

Aim 1.

As I might need to test many epidrugs and/or combinations of epidrugs, it is important to select a simple cell-based system for initial drug testing. An additional consideration influencing the selection is that *Tbx1* expression is undetectable in many of the available murine cell lines. Two cell lines that have been used in Prof. Illingworth's lab for gene expression studies are C2C12 cells and mouse embryonic stem cells (mESC). C2C12 cells are undifferentiated mouse myoblasts that express low levels of *Tbx1*, thus they are suitable for studies that aim to increase *Tbx1* expression. They also have developmental relevance because in mouse embryos, *Tbx1*-expressing progenitors in anterior mesoderm differentiate into muscle cells, as well as other cell lineages (Lescroart , et al., 2014) (Diogo, et al., 2015). Mouse ESC cells on the other hand do not express *Tbx1*, but it's expression can be activated by inducing cell differentiation (Chen et al., 2009). This has particular relevance for my project because the induced differentiation activates *Tbx1* expression for the first time, which is a different biological context compared to increasing *Tbx1* expression in cells that already express the gene. Whether the epigenetic regulation of *Tbx1* in these two contexts is the same or different is not known. As mESC are not a very homogeneous cell population, and the growth factors required to induce their differentiation are costly, I envisage using them to validate key results obtained in C2C12 cells.

Aim 2.

The identification of enhancer sequences and histone modifications associated with

activation of the *Tbx1* gene is a challenging task because the epigenetic mechanisms promoting *Tbx1* expression are not yet fully characterized. The primary goal here is to integrate genomic data obtained from largescale sequencing studies of gene expression and chromatin organization that are deposited in public databases with data (sequences) on putative TBX1 enhancers. The latter were identified by extraction of the genomic coordinates derived from a single-cell multi-omic dataset that included ATAC-seq and RNA-seq integrated data. Through a collaboration with Dr. Olga Lanzetta and Prof. Antonio Baldini, I will apply an algorithm that leverages the extensive genomic data available in the UCSC Genome Browser and ENCODE databases, to identify epigenetic profiles associated with *Tbx1* activation. This tool relies on the cross-analysis of ChIP-seq datasets to identify histone modifications at the putative *Tbx1* enhancers and RNA-seq datasets that report *Tbx1* expression levels across different tissues and embryonic stages. The algorithm is designed to correlate the putative enhancers with their characteristic epigenetic modifications and *Tbx1* expression levels in tissues expressing high *vs* low levels of *Tbx1*. This will enable us to identify the histone modifications associated with active *Tbx1* enhancers and provide a bioinformatic model to guide validation experiments. Furthermore, the model will serve to identify potentially effective epidrugs, or combinations of epidrugs, that modulate *Tbx1* expression, thereby contributing to a deeper understanding of the epigenetic regulation of this gene.

Aim 3:

Phenotypic rescue experiments are commonly used in studies involving animal models of human diseases as a way to demonstrate the potential efficacy of drug treatments for correcting specific abnormalities. I have selected this approach because of its' proven efficiency and because it is a frequently used approach in Prof. Illingworth's lab. Thus, I will have the necessary technical support for my experimental work. In the mouse, the approach can be applied postnatally by direct administration of the drug of interest to pups or adult animals. It can also be applied to the analysis of embryonic phenotypes by administering the drug to pregnant dams, with subsequent sacrifice of the dams and collection of treated and untreated embryos at the appropriate embryonic stage(s). The phenotype to be evaluated here is the formation of the 4th pharyngeal arch artery (4PAA). In *Tbx1*$^{+/-}$ embryos, hypoplasia o absence of the 4PAA is highly penetrant (>90%) in midterm embryos (E10.5) and as it occurs in a heterozygous animal, it is likely to be more amenable to correction than phenotypes found in *Tbx1* homozygotes. That is, even a small increase in *Tbx1* expression might be sufficient to normalize 4PPA formation. For some murine embryonic structures, the precise dosage of TBX1 necessary for their development is known (Xu et al., 2005).

I will perform dose-response experiments based on published data on the specific epidrug to be tested in mice, if available. Epidrug- and vehicle- (control) treated embryos will be collected at E10.5 and intracardiac ink injection will be performed immediately after collection as described by Lindsay et al., 1999.

3. MATERIALS AND METHODS

3.1 MAINTENANCE OF C2C12 CELL LINE IN CULTURE

The C2C12 cell line originates from a subclone of the C2 line isolated by Yaffe and Saxel (1977) from satellite cells of thigh muscle derived from a 2-month-old female C3H mouse donor, 70 hours after a crush injury. Subsequently, in the laboratories of Blau, Chiu, and Webster (1983), the C2C12 cells were cloned and subjected to karyotypic characterization. Therefore, this cell line is not a tumour-derived line but rather an immortalized cell line.

Culture Medium

C2C12 cells were maintained in a growth medium composed of Dulbecco's Modified Eagle Medium (DMEM) supplemented with 10% fetal bovine serum (FBS), 1% penicillin-streptomycin (P/S), and 1% L-glutamine. The medium was prepared under sterile conditions and pre-warmed to 37°C prior to each use.

Thawing

Frozen cells were retrieved from liquid nitrogen and rapidly thawed in a 37°C water bath for 2-3 minutes. The vial contents were transferred into a 15 mL conical tube containing 8 mL of pre-warmed growth medium. After centrifugation at 1000 rpm for 5 minutes, the supernatant was discarded, and the cell pellet was resuspended in 1 mL of fresh medium. Cells were then seeded into a P100 plate containing 9 mL of growth medium and incubated at 37°C with 95% humidity and 5% CO_2.

Cell Passage

Cell passaging was performed regularly upon reaching 70-80% confluence to ensure continuous proliferation and optimal growth conditions. After removing the culture medium, cells were washed twice with 2 mL of 1X PBS to eliminate serum residues and dead cells. Trypsin/EDTA (0.25%) was then added and incubated at 37°C for 3-5 minutes to facilitate the detachment of adherent cells. The resulting cell suspension was neutralized with 4 mL of growth medium and transferred into a 15 mL conical tube, followed by centrifugation at 1000 rpm for 5 minutes. The supernatant was discarded, and the cell pellet was resuspended in fresh medium. An appropriate fraction of the cell suspension was seeded into new P100 plates containing 10 mL of growth medium to continue the culture. Plates were incubated at 37°C with 95% humidity and 5% CO_2.

Freezing

Cells were cryopreserved at the end of the active growth phase. Following medium removal, cells were washed with 1X PBS and detached using trypsin/EDTA (0,25%). The cell suspension was centrifuged at 1000 rpm for 5 minutes, and the pellet was resuspended in cryopreservation medium consisting of DMEM supplemented with 10% FBS and 10% dimethyl sulfoxide (DMSO). Aliquots of 1 mL of the suspension were transferred into 2 mL cryovials and gradually frozen at -80°C for 24 hours before being stored in liquid nitrogen at -196°C for long-term preservation.

3.2 DRUG TREATMENT OF C2C12 CELLS

After at least two passages following thawing, C2C12 cells were detached from the parent plate upon reaching 70-80% confluence. Following the removal of the culture medium, cells were treated with trypsin/EDTA (0.25%) to facilitate detachment and neutralized with fresh culture medium containing DMEM, 10% fetal bovine serum (FBS), 1% penicillin-streptomycin (P/S), and 1% L-glutamine. The cell suspension was centrifuged at 1000 rpm for 5 minutes, the pellet resuspended in fresh medium, and the cells were counted using a Bürker chamber. A total of 7.5×10^4 cells was seeded into each well of a 6-well plate, with 2 mL of culture medium per well.

After 24 hours of incubation, the culture medium was replaced with 3 mL of fresh medium containing the appropriate concentration of the epigenetic drug (epidrug) for each specific treatment. The concentrations and types of epidrugs used were determined according to the experimental objectives.

At the end of the defined incubation period for each treatment, cells were processed for RNA extraction.

The epidrugs were dissolved in DMSO to prepare a stock solution at the concentration of 50 mM (for SAHA, GSK2879552, GSK LSD1), 10 mM (for GSK126). Next, serial dilutions of the stock solution in DMSO were prepared to generate intermediate stock solutions at desired concentrations. For all experimental conditions, the same volume of each stock intermediate solution was added to the culture medium to obtain the final concentrations of the drug to be tested. The final concentration of DMSO was maintained constant under all conditions, including controls treated with the vehicle alone, and did not exceed 0.1% (v/v). The control samples were treated with an equivalent volume of DMSO (vehicle only) to account for any solvent-related effects. The final concentration of DMSO in the treatment medium was maintained at 0.1% (v/v) for SAHA and GSK126, 0.05% (v/v) for GSKLSD1, 0.02% (v/v) for GSK2879552.

3.3 CELL PROLIFERATION ASSAYS

Cell proliferation in C2C12 cells was evaluated using the Enhanced Cell Counting Kit 8 (WST-8/CCK-8, Elabscience, Cat. No: E-CK-A362) following the manufacturer's instructions. Cells were seeded in 96-well plates with 100 µL of cell suspension containing approximately 1,500 cells per well. After an incubation period of approximately 24 hours to allow cell adhesion and proliferation, treatment with various epidrugs was performed according to the specified parameters. At the end of the treatment period (18 hours), 10 µL of CCK-8 reagent was added to each well. Samples were then incubated at 37 °C for approximately 1.5 hours, ensuring no bubbles formed. Following incubation, absorbance was measured at 450 nm using a microplate reader. Absorbance values were corrected by subtracting the reading obtained from wells containing only culture medium. The percentage of cell viability was calculated using the following formula:

$$\text{Cell Survival Rate (\%)} = \frac{OD_{sample} - OD_{blank}}{OD_{control} - OD_{blank}} \times 100\%$$

$$\text{Inhibition Rate} = \frac{OD_{control} - OD_{sample}}{OD_{control} - OD_{blank}} \times 100\%$$

All samples were analysed in triplicate.

3.4 RNA EXTRACTION AND PURIFICATION FROM C2C12 CELLS

Total RNA extraction was performed using TRIzol™ reagent (Thermo Fisher Scientific). For adherent cultures (C2C12), the cell culture medium was removed and the cells washed with PBS. Subsequently, 1 mL of TRIzol™ was added directly to each well of a 6-well plate. The lysis was completed by repeatedly pipetting the lysate, followed by scraping to ensure uniform homogenization. For suspension cultures (mESC E14), cells were harvested by centrifugation at 1,500 × g for 5 minutes, the supernatant discarded, and the cell pellet washed twice with PBS before being treated with 0.75 mL of TRIzol™ per cell quantity collected from a single P60 plate. The lysate was homogenized thoroughly by pipetting. Phase separation was carried out by adding 0.2 mL of chloroform for each 1 mL of TRIzol™ used. After vigorous manual shaking and a 3-minute incubation at room temperature (RT), samples were centrifuged at 12,000 × g for 15 minutes at 4°C. This process yielded three distinct phases:

- An upper clear aqueous phase containing RNA,
- A white proteine interphase,
- A pink organic phase rich in DNA and lipids.

The aqueous phase was carefully collected to avoid contamination with the interphase or organic phase. RNA precipitation from the aqueous phase was achieved by adding 0.5 mL of isopropanol per 1 mL of TRIzol™ used, followed by a 10-minute incubation at RT and overnight precipitation at -20°C. After centrifugation at 12,000 × g for 10 minutes at 4°C, the resulting RNA pellet appeared as a white gel-like deposit. The pellet was washed with 1 mL of 75% ethanol (prepared with RNase-free or DEPC-treated water) per 1 mL of TRIzol™ used and centrifuged again at 7,500 × g for 5 minutes at 4°C. To optimize the sample, the pellet was air-dried for 5–10 minutes, ensuring it did not over-dry to preserve solubility. The RNA was then resuspended in 50 µL of RNase-free water and incubated at 55°C for 10 minutes to facilitate dissolution. To further purify the RNA, an additional overnight precipitation step was performed at -20°C by adding 1/10 volume of 3M sodium acetate (pH 5.2) and 2.5 volumes of cold 100% ethanol. After centrifugation at 13,000 rpm for 10 minutes, the pellet was washed with 0.5 mL of 70% cold ethanol, followed by centrifugation at 7,500 × g for 10 minutes. The RNA pellet was air-dried and resuspended in approximately 30 µL of RNase-free water. RNA purity and concentration were assessed spectrophotometrically using the NanoDrop 2000c (Thermo Fisher Scientific).

3.4.1. ASSESSMENT OF RNA QUALITY AND QUANTITY

The quantification of total extracted RNA was determined using a NanoDrop 2000c UV-Vis microvolume spectrophotometer. The NanoDrop software is then accessed, and the "Nucleic Acid" option is selected, followed by "RNA". A blank reading was performed by applying 2 µL of deionised H_2O onto the lower optical surface and closing the lever arm. Subsequently, the sample of interest was measured by placing 2 µL of the extracted RNA onto the same surface. For the quantification of multiple samples, the device was cleaned with 2 µL of deionised H_2O after each measurement. The software automatically calculates the sample concentration in ng/µL and provides the characteristic absorption spectrum with a peak at 260 nm. Additionally, the software generates specific ratios, such as A260/A280 and A260/A230, to evaluate the quality of the sample and detect any potential contaminants.

3.5 REVERSE TRANSCRIPTION OF RNA

Total RNA extracted from the cells was retrotranscribed using the QuantiTect® Reverse Transcription Kit (QIAGEN, cat. no.: 205310) according to the manufacturer's instructions. In this kit genomic DNA is removed using a reaction mix (Wipeout buffer) containing DNAse1: 14 µL of reaction mix, including 2 µL gDNA Wipeout Buffer (7x), RNA (up to 1 µg), and nuclease-free water, were incubated at 42°C for 2 minutes, then cooled immediately on ice. Next, a reverse transcription master mix was prepared, containing 1 µl Quantiscript reverse transcriptase, 4 µl Quantiscript RT buffer (5x), and 1 µl RT primer mix for each reaction. The genomic DNA knockout mix (14 µl) was added to the master mix (6 µl) to a final volume of 20 µl. The reaction was incubated at 42°C for 15 minutes to allow first-strand cDNA synthesis, followed by treatment at 95°C for 3 minutes to inactivate Quantiscript reverse transcriptase. cDNA samples were stored at −20°C until use in RT-PCR or quantitative real-time PCR reactions.

3.6 RT-PCR

PCR was performed using a BioRad ”Thermal Cycler T100” thermocycler. The protocol varies and is specific to the gene being amplified. The process begins by preparing the reaction mix on ice, following the specific protocol guidelines. The mix is then aliquoted into pre-numbered Eppendorf tubes containing 19 µl of the reaction mix and 1 µl of cDNA. The samples are placed in the thermocycler, and the program set according to the protocol instructions. Upon completion, the program is stopped, and the samples are placed on ice for subsequent use or stored at -20°C. PCR products were analysed by gel electrophoresis.

PCR conditions for *Tbx1,* GAPDH and other genes

PCR Reaction Mix for 1 Sample (Invitrogen Taq DNA Polymerase Kit)

REAGENTS [Ci]	FINAL CONCENTRATION	QUANTITY Vol=20µL
MgCl2 [50mM]	[1.5mM]	0.6 µl
Buffer [10X]	[1X]	2µL
Reverse primer [10 µM]	[0.5 µM]	1 µl
Forward primer [10 µM]	[0.5m µM]	1 µl
Mixed dNTPs [20mM]	[0.2 mM]	0.2 µl
Taq DNA Pol. [1000-5 U/10 µl]	[0.075 U/10 µl]	0.3 µl

Make up to volume with 12.9 µl of deionized and autoclaved H_2O.

Add 2 µl of DNA [5ng/µl] to be amplified

Primer sequences

Gene	Forward primer	Reverse primer	bp
Pecam1	TGGTTGTCATTGGAGTGGTC	TTCTCGCTGTTGGAGTTCAG	136bp
Kdr/Vegfr2	GTCGACATAGCCTCCACTGTTT	GTGATGTACACGATGCCATGCT	95bp
VE-Cadh.	TCATCAAACCCACGAAGTCC	GGTCTGTGGCCTCAATGTAGA	72bp
CD-34	CTGCCTGGAACTAAGTGAAGC	AGCCTCCTCCTTTTCACACA	94bp
Mesp1	GCGACATGCTGGCTCTTCTA	TGGTATCACTGCCGCCTCTTCC	175bp
Mef2c	AGATACCCACAACACACCACGCGCC	ATCCTTCAGAGAGTCGCATGCGCTT	196bp
Gata4	CTGTCATCTCACTATGGGCA	CCAAGTCCGAGCAGGAATTT	259bp
Isl1	GCCTCAGTCCCAGAGTCATC	AGAGCCTGGTCCTCCTTCTG	308bp
Tbx1	TTTGTGCCCGTAGATGACAA	AATCGGGGCTGATATCTGTG	239bp
GAPDH	TGCACCACCAACTGCTTAGC	TCTTCTGGGTGGCAGTGATG	106bp
Oct3/4	TCAGCTTGGGCTAGAGAAGG	TGACGGGAACAGAGGGAAAG	254bp
Pdgfrα	CTGGTGCCTGCCTCCTATGAC	CACGATCGTTTCTCCTGCCTTAT	198bp
Nanog	AAGTACCTCAGCCTCCAGCA	GTGCTGAGCCCTTCTGAATC	163bp
cTnt2	GAAGTTCGACCTGCAGGAAA	TTCCCACGAGTTTTGGAGAC	102bp
Eng	GTGTTCCTGGTCCTCGTTTC	TCTTGGCTGTCCTTGGAAGA	114bp

Amplification conditions for Tbx1 and other genes

94°C 10 min

94°C 30 sec
60°C 30 sec
72°C 30 sec
} x 30 cycles

72°C 10min

Amplification conditions for GAPDH

94°C 5 min

94°C 45 sec
60°C 30 sec
72°C 1 min e 30 sec
} x 26 cycles

72°C 10min

3.7 REAL TIME qPCR

This technique allows the relative quantification of transcripts of interest to be determined. Gene expression is normalized compared to that of a ubiquitously expressed control gene, such as GAPDH (Glyceraldehyde-3-phosphate dehydrogenase).

Real Time qPCR was performed using the iTaq Universal SYBR Green Supermix (Biorad) which contains iTaq DNA polymerase, dNTPs, MgCl2, SYBR Green I dye, enhancers, stabilizers and a mixture of reference dyes (ROX and fluorescein). To evaluate the expression level of *Tbx1* and other genes compared to GAPDH, I prepare two different reaction mixes, each containing the two primers (forward and reverse) specific for the gene of interest. The reaction mix was prepared based on the number of samples to be amplified (in triplicate). For each sample, 16 µl of reaction mix was prepared with the following reagents:

- iTaq Universal SYBR Green Supermix 2X 10 µl
- Forward primer [10 µM] 0.3 µl
- Reverse primer [10 µM] 0.3 µl
- H_2O (deionized and autoclaved) 5.4 µl

The following primers were used for *Tbx1*:

- *Tbx1*_F: 5′-GGACGACAACGGCCACAT-3′
- *Tbx1*_R: 5′-CGGCATATTTCTCGCTATCTTTG-3′

The following primers were used for *GAPDH*:

- GAPDH_F: 5′-TGCACCACCAACTGCTTAGC-3′
- GAPDH_R: 5′-TCTTCTGGGTGGCAGTGATG-3′

Results were download in Excel format which reports the Ct (Cycle threshold) for each sample, i.e. the point on the curve in which the quantity of fluorescence (SYBR Green) begins to increase exponentially. *Tbx1* expression was normalized with respect to *GAPDH*. In experiments using epidrugs, samples were also normalized compared to a DMSO control (drug solvent). Changes in gene expression are reported as fold change (using the $2^{-\Delta\Delta Ct}$ method).

3.8 BIOINFORMATIC ANALYSIS

DATASET FOR EPIGENETIC DATA ACQUISITION

The bioinformatics analysis was conducted using publicly available data from the ENCODE (Encyclopedia of DNA Elements) database, version v134.0-patch08d7deb [ENCODE portal (arxiv; PMID: 31713622; PMCID: PMC7061942]. ChIP-seq data for 8 histone modifications from 12 embryonic mouse tissues at 8 different developmental stages were downloaded. These tracks, uploaded to the portal, result from a comprehensive study of chromatin states during embryonic development from E10.5 to P0, based on 1,128 ChIP-seq analyses of 8 histone modifications across 12 tissues, performed by Bing Ren's laboratory as part of the ENCODE consortium.

We selected to use data from a single source and operational protocol to reduce heterogeneity.

The histone modifications analyzed include:

- Activating modifications: H3K4me1, H3K4me2, H3K4me3, H3K9ac, H3K27ac, H3K36me3
- Repressive modifications: H3K27me3, H3K9me3

ChIP-seq data were retrieved using the UCSC Genome Browser platform (http://genome.ucsc.edu). Specifically, using an R-based algorithm, 563 BigBed files were downloaded and analyzed. The BigBed file format is an efficient, compact binary file used for genome-wide datasets and includes the genomic coordinates of each statistically confirmed ChIP-seq peaks.

DATASET FOR GENE EXPRESSION DATA ACQUISITION ACROSS DIFFERENT TISSUES AND EMBRYONIC STAGES

Tbx1 gene expression RNA-seq data were retrieved from the ENCODE database (Lab: Barbara Wold, Caltech, CA), using a bulk polyA RNA-seq dataset. We downloaded a total of 72 tabulated files listing genes and their expression values indicated in transcript per million mapped reads (TPM). Tissues encompassing multiple developmental stages were classified into two groups based on expression levels

- Low *Tbx1* expression (n=53, TPM $\leq$ 3)
- High *Tbx1* expression (n=19, TPM > 3)

Data normalization was performed relative to the *Gapdh* gene, used as an endogenous control.

BIOINFORMATIC WORKFLOW

Bioinformatics analyses were conducted using using Rstudio and R version 4.2.0 (https://www.r-project.org/).

The analyses was further refined using unpublished data generated by Prof. Antonio Baldini and Dr. Olga Lanzetta at IGB-CNR, Naples. Through the combined analysis of ATAC-seq and scRNA-seq data, a machine learning algorithm based on L1-penalized logistic regression was employed to identify significant scores associated with 14 potential enhancers of the *Tbx1* gene. Differentiated mESCs were harvested at d2 and d4 to extract RNA or DNA used for RNA-seq

and ATAC-seq techniques, respectively. The machine-learning procedure applied to enhancer identification has been previously reported (Aurigemma et al., 2024).

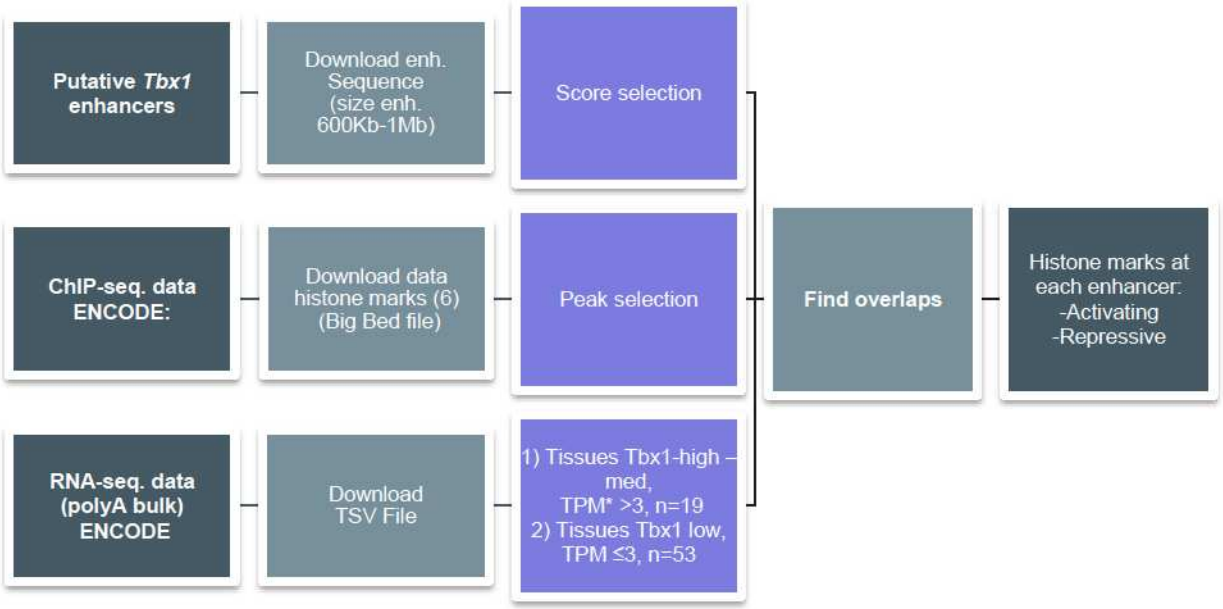
RNA-seq data covering the entire transcriptome were analyzed, and *Tbx1* expression levels were extracted for all tissues and developmental stages. Based on TPM values, these data were subsequently categorized into two groups: Low *Tbx1* expression levels and Medium-high *Tbx1* expression levels.

The genomic locations of the 14 putative enhancers was intersected with the ChIP-seq data from the downloaded datasets (subdivided according to Tbx1 gene expression). To this end, we used the Findoverlaps function from the GenomicRanges R package (v1.52.0) (https://bioconductor.org/packages/release/bioc/html/GenomicRanges.html), with the command:

```
o <- findOverlaps(tbx1_gr, bb, type='any', maxgap = 100)
```

The algorithm developed by Dr. Lanzetta generated an Excel matrix, where a value of "1" was assigned to regions where an overlap occurred and "0" where it did not. This matrix, comprising 372 observations, was used to extract histone modifications occurrence and frequency for each putative *Tbx1* enhancer.

Histone modifications H3K36me3 and H3K9me3 were excluded from the analysis because they returned very few overlaps with the 14 putative enhancers.



Summary of the workflow followed for the bioinformatics analysis.

3.9 MAINTENANCE OF THE MURINE EMBRYONIC STEM CELL LINE E14TG2a

Culture Medium

Murine embryonic stem cells (E14TG2a) were maintained in culture using a specific medium to preserve their pluripotent characteristics. The medium was prepared by mixing 161.6 mL of

GMEM supplemented with 15% fetal bovine serum (FBS for ES, 30 mL), 1% L-glutamine (2 mL), 1% penicillin-streptomycin (P/S, 2 mL), 1% sodium pyruvate (NaP, 2 mL), 1% non-essential amino acids (NeAA, 2 mL), and 400 µL of β-mercaptoethanol. Before use, leukemia inhibitory factor (LIF) was added at a concentration of 5 µL per 50 mL of medium to maintain the cells in an undifferentiated state. The medium was prepared and stored under sterile conditions and pre-warmed to 37°C prior to use to ensure optimal cell growth.
Cells were plated on dishes pre-treated with 0.1% gelatine, applied evenly to each well and aspirated just before adding fresh medium and cells. The medium was replaced daily, and passaging was performed approximately every two days.

Gelatine Coating for Multiwell Plates

Multiwell plates used for the maintenance of E14 embryonic stem cells were pretreated with 0.1% gelatine, prepared by diluting 2% gelatine in sterile PBS. To prepare 2% gelatine, 4 g of gelatine were dissolved in 200 mL of PBS under a biological safety hood using a designated pipette. The solution was sterilized by autoclaving, cooled to room temperature, and stored at 4°C. Before use, the 2% gelatine solution was warmed in a water bath and diluted in sterile PBS to a final concentration of 0.1%. The diluted gelatine solution was filtered through a sterile filtration system. For coating, 3 mL of 0.1% gelatine were applied to each well of a 6-well plate, ensuring even coverage of the entire surface. Plates were briefly incubated to facilitate cell adhesion and subsequently prepared for use with the specific culture medium.

Thawing

Cells were retrieved from liquid nitrogen and rapidly thawed in a 37°C water bath for 2–3 minutes. The cryovial contents were transferred into a 15-mL tube containing 8 mL of pre-warmed ES medium supplemented with LIF. Following centrifugation at 800 rpm for 5 minutes, the supernatant was discarded, and the cell pellet was resuspended in 2 mL of ES medium. Cells were then plated on pre-gelatinized dishes and incubated at 37°C with 95% humidity and 5% CO_2.

Cell Passage

Cell passaging was performed upon reaching 70–80% confluence. After removing the culture medium, cells were washed twice with 2 mL of 1X PBS to remove serum residues and dead cells. A volume of 300 µL of 0.25% Trypsin-EDTA (diluted 1:5) was added and incubated at 37°C for up to 1 minute to detach the cells. Trypsin activity was neutralized by adding 2 mL of ES medium supplemented with LIF. The cell suspension was transferred into a 15-mL Falcon tube and centrifuged at 800 rpm for 5 minutes. After discarding the supernatant, the cell pellet was resuspended in 1 mL of ES+LIF medium, and an appropriate volume of cells was plated in 2 mL of fresh ES+LIF medium in new gelatinized dishes to continue the culture.

Freezing

At the end of the growth phase, cells were prepared for freezing. Following cell passaging, the cells were counted, and the suspension was diluted in a freezing medium consisting of 40% ES medium, 40% FBS for ES, and 20% DMSO. A total of 1×10^6 cells per vial was aliquoted into 2-mL cryovials. The cryovials were gradually frozen at -80°C for 24 hours before being transferred to liquid nitrogen at -196°C for long-term storage.

3.10 DIFFERENTIATION OF MURINE EMBRYONIC STEM CELL LINE E14TG2a

Serum-Free Defined medium (SFD medium)

The SFD Medium used throughout the protocol was prepared by mixing 178.7 mL of IMDM, 62.5 mL of HamF12, 1.25 mL of 10% BSA, 1.9 mL of glutamine, and 1.9 mL of penicillin-streptomycin. The mixture was filtered and supplemented with 2.5 mL of B27 supplement and 1.25 mL of N2 supplement. The medium was used fresh and pre-warmed to 37°C for each phase of the protocol.

3.10.1. Differentiation Protocol

The differentiation of the murine embryonic stem cell line E14TG2a was conducted following Andersen's protocol, which is structured into multiple temporal phases. On day 0 (D0), the standard culture medium was removed from the E14TG2a cells, and the cells were washed once with 1X PBS. Subsequently, 300 µL of trypsin diluted 1:5 was added, and the cells were incubated for up to 1 minute at 37°C. The reaction was neutralized by adding 2 mL of complete embryonic stem (ES) medium supplemented with leukemia inhibitory factor (LIF). The cell suspension was transferred into a 15-mL Falcon tube, centrifuged at 800 rpm for 5 minutes, and washed twice with IMDM. The cells were then resuspended in SFD Medium, counted, and plated at a density of 100,000 cells/mL in Petri dishes containing SFD Medium supplemented with ascorbic acid (100 µL of a 5 mg/mL stock) and MTG (30 µL of a 1:100 dilution in IMDM).

On day 2 (D2), embryoid bodies (EBs) were collected from the Petri dishes and washed thoroughly with IMDM, allowing them to settle by gravity for 4–5 minutes between washes. After two washes, the EBs were resuspended and replated in SFD Medium supplemented with ascorbic acid (100 µL), MTG (30 µL), Activin A (1 ng/mL), and BMP4 (1 ng/mL).

On day 4 (D4), the EBs were collected again and subjected to a cycle of washes in IMDM, following the same procedure as on day 2. After washing, the EBs were resuspended and plated in SFD Medium supplemented with the same factors as on day 2.
On day 6 (D6) and day 8 (D8), the EBs were manually detached from the bottom of the Petri dishes to ensure all cells remained in suspension.
On day 8 (D8), the differentiation process was concluded.
For each key time point (D0, D2, D4, D6, D8), one Petri dish of cells was harvested for RNA extraction to be used in subsequent analyses.

3.11. EMBRYO COLLECTION AND INTRACARDIAC INK INJECTION

These experiments will be conducted in the laboratory of our collaborator Prof. Antonio Baldini at the IGB-CNR, Naples and with the technical assistance of the staff of the mouse facility. Embryos from the intercross Tbx1+/- x wild type will be collected at E10.5. Freshly

isolated embryos will be injected intracardially with India ink (approximately 100 □l) in order to visualize the pharyngeal arch arteries. Injected embryos will be fixed in 70% ethanol immediately after injection in order to prevent diffusion of ink away from the heart and arch arteries. After 24 hr in 70% ethanol embryos will be clarified in 50:50 methyl salicylate : benzyl benzoate. PAAs will be examined at a stereomicroscope and the phenotype of the bilateral 4th PAA scored manually (normal, hypoplastic or aplastic). At the time of embryo collection, the yolk sac of individual embryos will be collected for DNA preparation and, subsequently, genotyping of the embryos.

4 RESULTS

My project initially focused on the development of a cellular system that would be suitable for evaluating changes in *Tbx1* expression, and the optimization of the experimental conditions to evaluate the efficacy of epigenetic drugs (epidrugs) in modulating *Tbx1* expression. Subsequently, I took a bioinformatics approach to identify the histone modifications associated with high and low levels of *Tbx1* expression, which I then used to prioritize the selection of epidrugs of greatest potential interest to my study. The findings were tested in two cellular models, namely immortalized murine myoblasts (C2C12) and murine embryonic stem cells (mESC).

4.1 EPIDRUG ASSAYS IN C2C12 CELLS

4.1.1. OPTIMIZATION OF C2C12 CELL CULTURE CONDITIONS

To achieve the first experimental objective of my project, which was to identify histone modifications that increase *Tbx1* gene expression, it was first necessary to optimize the cell culture conditions for maintaining C2C12 cells in an undifferentiated state (Fig 10, panel C-D), so as to preserve their cellular properties and to avoid gene expression changes associated with differentiation (Diokmetzidou et al., 2016). In particular, it is known that conditions that facilitate differentiation into myotubes (Fig 11, panel E-P) reduce or eliminate *Tbx1* expression (Diokmetzidou et al., 2016).

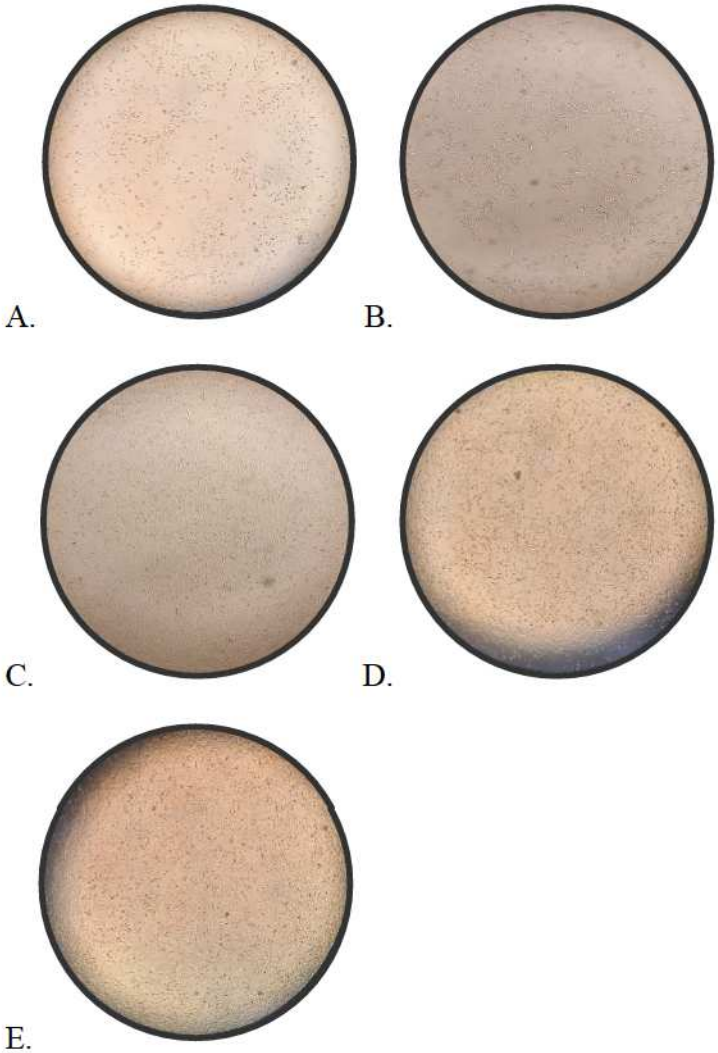
I first tested different plating densities and culture times (Table 2) in order to identify the conditions that prevented the cells from reaching confluence, a condition that can trigger spontaneous differentiation into myotubes , associated with a morphological change with cells resembling long pins in some cases multinucleated (Fig 11, panel I-P). This was first determined in P100 plates and subsequently in 6-well plates; the latter were used for epidrugs assays in order to contain the costs of media and drugs.

In P100 plates, the ideal seeding density for this cell line was determined to be 1.2×10^5 cells per 55 cm^2, with re-plating approximately every three days.

In 6-well plates, I tested the following cell densities: 1.2×10^4, 7.5×10^4, and 5×10^5 cells per well. I determined that a density of 7.5×10^4 cells/9.40 cm^2 was the optimal density for maintaining the cells in a proliferative state without inducing differentiation. Optimizing the culture conditions proved to be crucial for ensuring the reproducibility of subsequent experiments.

Density (cells/cm²)	Cell State	Differentiation observed after 48/72 hours
1.2×10^4	Proliferative	No
7.5×10^4	Proliferative	No
5×10^5	Confluent	Yes

Table 2. Effect of cell density on the growth of C2C12 cells in 6-well plates
The table summarizes the behaviour of C2C12 cells as a function of their initial seeding density. 48 hours after seeding. Proliferating cells had sufficient space and resources for growth while maintaining an undifferentiated phenotype. In contrast, confluent or near-confluent cells showed a differentiated phenotype (morphological changes in some cells, see panels I - P in Figure 11) and cell mortality (panel G-H in Figure 11).



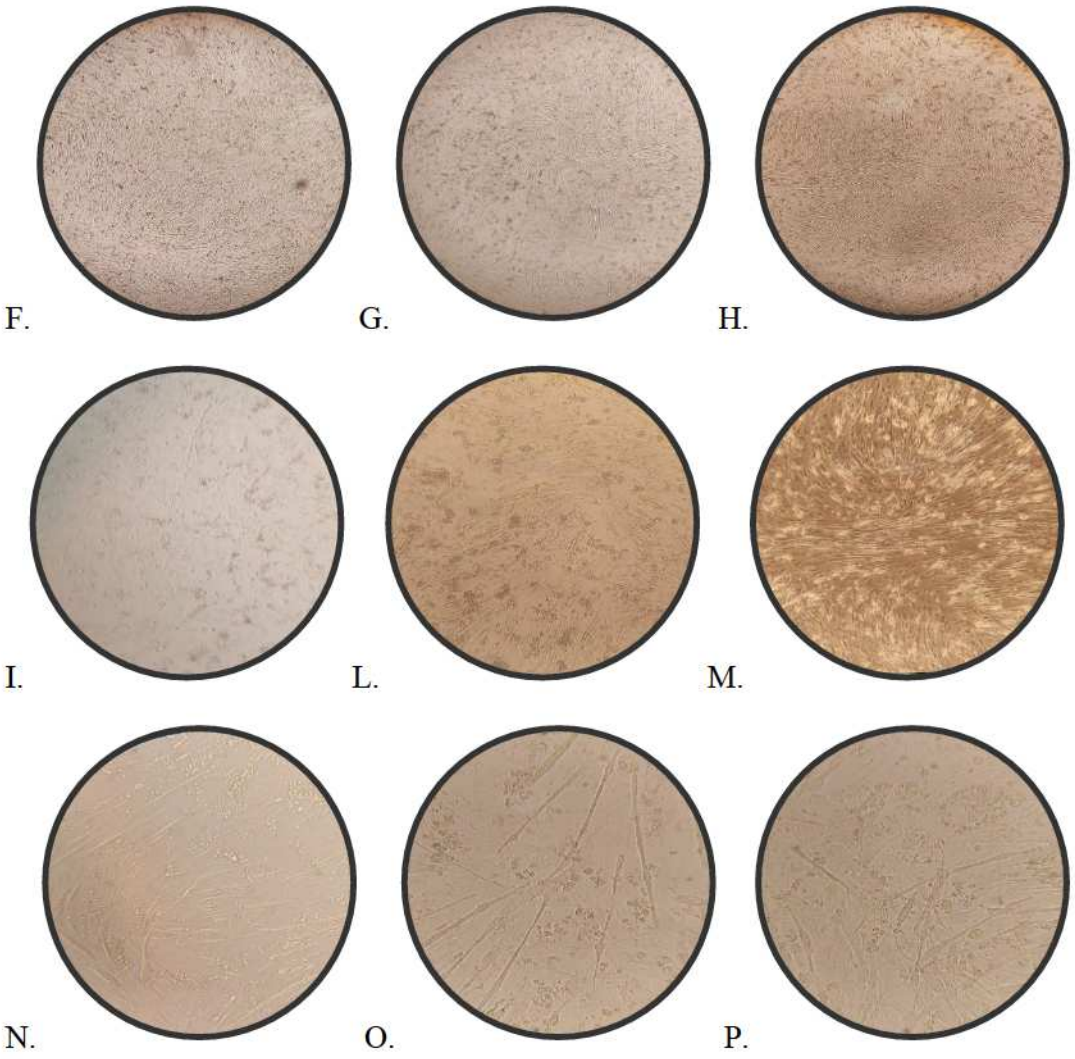


Figure 11. Images of C2C12 cells in culture at various seeding densities observed at 48 hours post-seeding (A-E) and after 48 hours (F-P).
In 6 well plates Panels A and B show low-confluence cells in a proliferative state. Panels C and D depict cells at optimal confluence, still proliferative and suitable for collection. Panel E shows cells at near confluence, showing early signs of differentiation in the areas of the plate with higher cell density. Panels A, B, C, D, and E were observed under the "Motic AE20" optical microscope at 4X magnification. Panels F, G, and H display cells seeded at high densities after 48 hours, showing signs of differentiation into spindle-like shapes; cells observed at 4X magnification. Panels I, L, and M show differentiated cells observed at 10X magnification. Panels N, O, and P provide a close-up of differentiated cells observed at 20X magnification.

4.1.2. EPIDRUGS AND EPIDRUG ASSAYS

4.1.2.1. The major classes of epidrugs

Among the various classes of epidrugs known to date (see Introduction 1.3), this study focused on molecules that act by modulating the methylation or acetylation of lysine residues on histone tails (H3 and H4). Specifically, the selected classes were histone deacetylase inhibitors (HDACis), histone demethylase inhibitors (HDMis), and histone methyltransferase inhibitors (HMTis). For the HDACis class, suberoylanilide hydroxamic acid (SAHA) was selected. This molecule interacts with the HDAC enzyme, inhibiting the deacetylation of lysine residues

on histones H2A, H2B, H3, and H4 (Turner, 2000). By maintaining a non-condensed chromatin state, SAHA facilitates active gene transcription. For the HDMis class, two compounds were selected: GSKLSD1 and GSK2879552. Both compounds inhibit the activity of LSD1, preventing the demethylation of lysine 4 on histone H3 (H3K4). The maintenance of the methylated state is associated with gene activation mechanisms. For the HMTis class, GSK126 was chosen. This epidrug inhibits the activity of EZH2, a member of the Polycomb Repressive Complex 2 (PRC2). By blocking the trimethylation of lysine 27 on histone H3 (H3K27me3) carried out by EZH2, GSK126 promotes gene transcription activation.

I collaborated with EPI-C Epigenetic Compounds (EPI-C s.r.l.) to obtain epidrugs from each major class. Additionally, EPI-C provided guidance on the selection of specific compounds within each class.

4.1.2.2. SAHA

I performed my first experiments using SAHA. Cell-based studies indicate that SAHA inhibits class I and II HDACs at a dose of approximately 50 nM (Butler et al., 2002; Gui et al., 2004; O. Moradei et al., 2005; Richon et al., 2000). Additionally, it arrests the growth of a wide variety of transformed cells in culture at doses ranging from 2.5 to 5.0 μM (Marks and Breslow, 2007; Ungerstedt et al., 2005). Based on these observations, I selected doses of 1, 2, 3, and 5 μM, which have been used in clinical studies and shown to affect transcription (Marks and Breslow, 2007; Ungerstedt et al., 2005) in line with its' HDAC inhibitor activity.

To evaluate the effect of these drug concentrations on *Tbx1* expression, I conducted biological triplicate experiments by plating C2C12 cells in 6-well plates. Twenty-four hours after plating, SAHA at the selected concentrations was added in fresh media to the different wells, while cells in one well were treated with DMSO (dimethyl sulfoxide) as a control, as the drug is resuspended in this solvent at this concentration. (Fig. 12). In this case, for all the treatments shown, in 3 ml of fresh growth medium per well, 0.1% of treatment was added on the total volume.

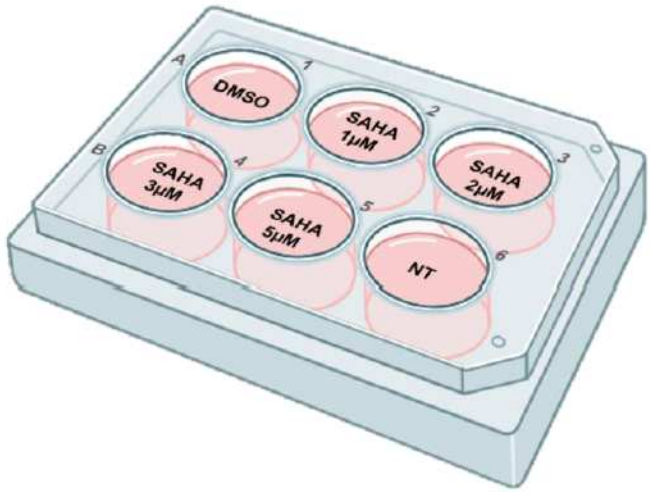


Figure 12. Schematic representation of the SAHA treatment experiment conducted in 6-well plates.

Twenty-four and forty-eight hours after the initiation of treatment, I lysed the cells in TRIzol and extracted, purified and quantified the total RNA. RNA extraction and purification were performed using a protocol that included cell lysis with TRIzol reagent followed by phase separation with chloroform and precipitation with isopropanol (materials and methods 3.4). The quality and quantity of the RNA samples was assessed using a NanoDrop spectrophotometer. This allowed me to measure the RNA yield for each sample and assess the quality through purity ratios. Specifically:

- A260/280 ratio: Optimal values are between 1.8 and 2.0. Values outside this range indicate the presence of protein contamination.
- A260/230 ratio: Optimal values are ~2.0. Values above or below 2.0 are indicative of carbohydrate or solvent (phenol) contamination.

Subsequently, expression of *Tbx1* was evaluated by quantitative real-time PCR (qPCR, Materials & Methods, 3.7). For this, RNA samples (1 µg) of good quality were retro-transcribed using the QuantiTect Reverse Transcription Kit (Materials & Methods, 3.5). 40 ng of cDNA was used for each reaction and experiments were performed in triplicate. *Tbx1* expression in each sample was normalized relative to the ubiquitously expressed control gene, GAPDH (Glyceraldehyde-3-phosphate dehydrogenase). Relative expression levels were calculated as the Fold Change between samples treated with various concentrations of SAHA compared to control samples treated with DMSO.

The results obtained from three experiments revealed a reduction in *Tbx1* expression at all of the tested doses of SAHA compared to DMSO-treated controls, and at both 24 hours and 48 hours of treatment (Fig. 13). This finding suggests that SAHA could exert a dose-dependent suppressive effect on the expression of *Tbx1* in the shorter treatment conditions initially tested. This result is the opposite to that expected, given that SAHA inhibits histone deacetylation.

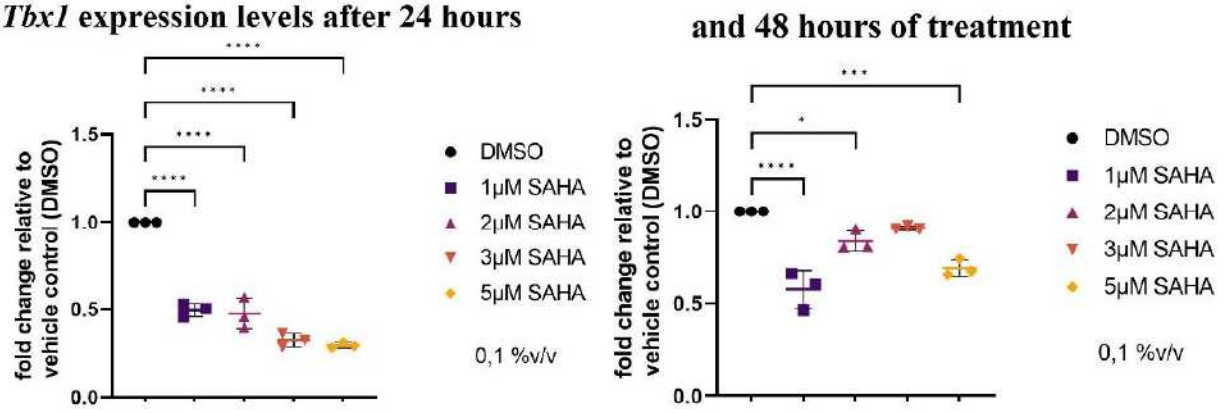


Figure 13. Tbx1 expression in C2C12 myoblasts treated with SAHA at different concentrations (RTqPCR)
The 24-hour treatment shows a significant reduction in Tbx1 expression for all concentrations. B) The 48-hour treatment shows a reduction in Tbx1 expression for three out of four concentrations (1, 2, 5 µM). The experiments were conducted at 0.1% v/v (drug/vehicle in the treatment solution). Control cells were treated with DMSO at the same final concentration used in drug treatments. Results are the mean of three experiments. Statistical analysis was performed using the one-way ANOVA method with multiple comparison tests.

Given the unexpected results, I considered several potential technical problems that might have caused these effects:

1. Treatment timing
2. Toxicity of DMSO (the drug solvent)
3. Cytotoxic effects of SAHA

To address these concerns, I evaluated each possibility in separate experiments.

1. Treatment Timing;

To test whether reduced expression of *Tbx1* was due to inappropriate treatment timing, I selected the highest dose (2 µM) of SAHA that, according to clinical studies, does not induce cell death (Ungerstedt et al., 2005) and then varied the treatment times (8, 13, 18, 24, 30, and 48 hours), while repeating the same experimental conditions described above, for three replicates. This ensured that any observed under-expression of *Tbx1* could not be attributed to cytotoxic effects of the drug. The results confirmed a reduction in *Tbx1* expression across all time points analysed (Fig. 14). This outcome suggests that treatment timing is not a contributing factor to the observed reduction in *Tbx1* expression.

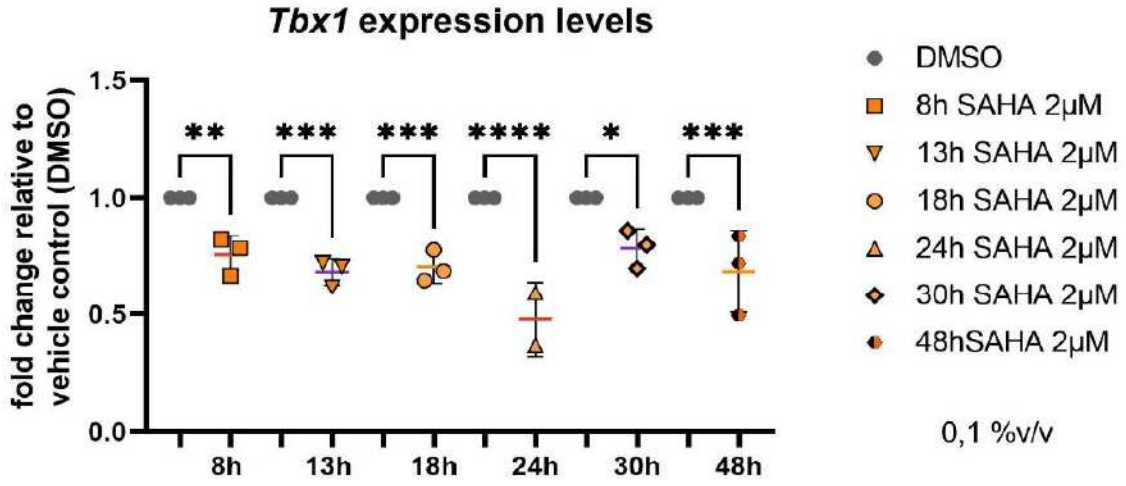


Figure 14. Effect of SAHA (2uM) on Tbx1 expression at different treatment times.
The results confirmed decreased Tbx1 expression at all treatment times. Results are the mean of three experiments. Statistical analysis was performed using the one-way ANOVA method with multiple comparison tests. The experiments were conducted at 0.1% v/v (drug/vehicle in the treatment solution). Control cells were treated with DMSO at the same final concentration used in drug treatments.

2. Toxicity of DMSO (the drug solvent)

Dimethyl sulfoxide (DMSO) is a polar aprotic organic compound commonly used as a solvent for hydrophobic small molecules due to its amphipathic nature (Szmant, 1975). For this reason, it is widely used as a control in both *in vivo* and *in vitro* studies that use compounds dissolved in this solvent (F. R. Li et al., 2024; Sankpal et al., 2012). However, numerous studies have highlighted the toxic nature of DMSO (Julien et al., 2012). *In vitro* toxicity has been reported at concentrations above 10% (de Ménorval et al., 2012; Galvao et al., 2014; Notman et al., 2006) while *in vivo* toxicity has been reported at concentrations as low as 0.1% v/v (Galvao et al., 2014).

To test whether the concentration of DMSO used in my original experiments (0.1%) had a negative impact on *Tbx1* expression, I compared untreated C2C12 cells (media only) with SAHA-treated cells with DMSO at concentrations of 0.1% and 0.02% v/v. Results showed that *Tbx1* expression was reduced in SAHA-treated cell samples, even with the lower DMSO concentration (Fig. 15) This suggests that DMSO toxicity was not responsible for the reduction in *Tbx1* expression in SAHA-treated cells.

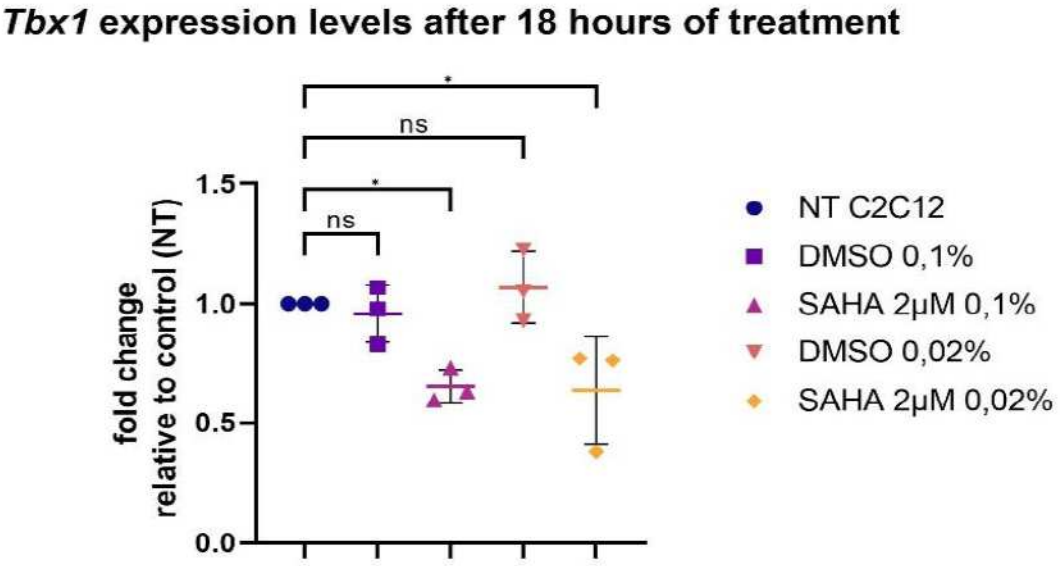


Figure 15. Lowering DMSO concentration did not improve Tbx1 expression in C2C12 cells treated with SAHA.
C2C12 cells were treated with SAHA using a standard concentration of diluent (DMSO 0.1%). SAHA treatment with standard and low conc. DMSO (0.02%) both led to reduced Tbx1 expression. NT, not treated. Results are the mean of three experiments Statistical analysis was performed using the one-way ANOVA method with multiple comparison tests.

The experiments in this project were conducted using varying %v/v volumes of drug or vehicle (DMSO, in which the drugs were dissolved in the total treatment volume, selecting the lowest possible %v/v. This variability depended on the different initial concentrations of the drugs (SAHA 50 mM, GSK126 10 mM, GSKLSD1 50 mM, GSK2879552 50 mM) and the specific final concentrations selected for each treatment.

3. Cytotoxic effects of SAHA

To evaluate potential cytotoxic effect of SAHA, I used the CCK-8 kit (Enhanced Cell Counting Kit 8 (WST-8/CCK8), (E-CK-A362), a colorimetric kit designed to assess cell viability and cell proliferation (Materials & Methods 3.3). The kit uses a water-soluble tetrazolium salt, WST-8, which is reduced by dehydrogenase enzymes present in living cells to produce a stained compound, formazan. The intensity of the resulting orange colour, which is measured by absorbance at 450 nm, is proportional to the number of viable cells that have metabolized the reagent. Compared to other tetrazolium-based assays such as MTT, XTT, or MTS, CCK-8 offers higher sensitivity in detecting viable cells. Moreover, the low cytotoxicity of the reagent allows for extended incubations (up to 48 hours), enabling the monitoring of long-term effects of cell manipulations.

In brief, I adapted the kit's protocol to my cell line by testing different cell seeding densities (5×10^3, 2.5×10^3, 1.5×10^3) and selected the most suitable density for C2C12 cells. Specifically, I prepared a cell suspension, and 1,500 cells (1.5×10^3) were plated into the wells of 96-well plates and, after 24 hours, the cells were treated with various concentrations of SAHA (1µM – 5µM) for 18 hours. Finally, the absorbance was measured at 450 nm using a microplate reader.

Results showed no reduction in cell survival across the range of SAHA doses tested (Fig. 16)

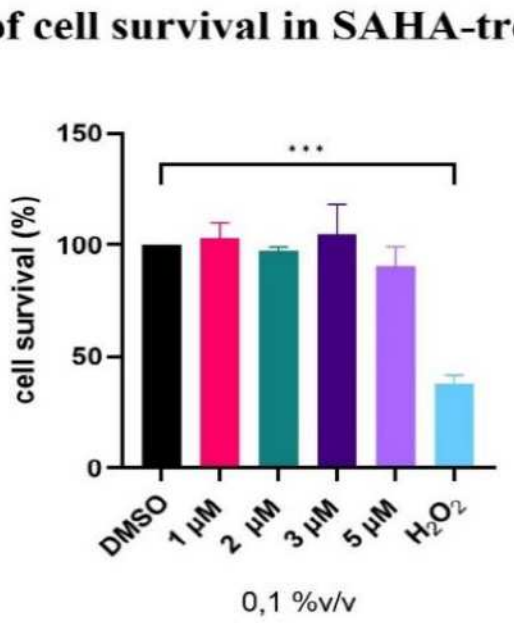


Figure 16. SAHA treatment (1uM- 5uM) did not induce cytotoxicity in C2C12 cells.
Potential cytotoxic effects of SAHA were evaluated in the CCK8 assay in C2C12 cells treated with different epidrug concentrations. The experiments were conducted at 0.1% v/v (drug/vehicle in the treatment solution). Control cells were treated with DMSO at the same final concentration used in drug treatments. Results are the mean of two experiments. Statistical analysis was performed using the one-way ANOVA method with multiple comparison tests.

With these studies, I excluded that reduced *Tbx1* expression in SAHA-treated C2C12 cells was caused by technical problems rather than a specific effect of the epidrug. Previous studies, conducted *in vivo* on gastric carcinoma cells and on primary murine tumor cells derived from satellite cells and myoblasts, have observed a repressive effect of SAHA on genes including *MYB, APOC1, CBX5*, *PLA2G2A* and *Pax3:Foxo1*(Abraham et al., 2014; Claerhout et al., 2011)), suggesting that the unexpected result may be associated with complex transcriptional regulatory mechanisms. Both authors describe a SAHA-dependent repressive effect that varies according to the cell line (Abraham et al., 2014; Claerhout et al., 2011). Specifically, in the study on alveolar rhabdomyosarcoma, repression at the *Pax3:Foxo1* locus is linked to epigenetic modifications that regulate the potential conversion of tumor cells into a less aggressive phenotype (Abraham et al., 2014). In gastric carcinoma, on the other hand, the reduction in oncogene expression is accompanied by different cellular responses, including the activation of autophagy, which may influence the therapeutic efficacy of the treatment

(Claerhout et al., 2011). Further studies would be necessary to elucidate the molecular mechanisms underlying these differential responses.

4.1.2.3. GSKLSD1

I next tested the LSD1-specific histone demethylase inhibitor GSKLSD1.

LSD1 is involved in multiple regulatory cellular processes, and studies have evaluated the effects of LSD1 inhibition in different cell types, demonstrating only minimal effects on cell viability (Jingjing et al., 2021). A 2023 study demonstrated that inhibition of LSD1 in certain tumour cell subtypes using GSK-LSD1 at a dose of 10 µM for four days, increased the levels of H3K4me2 and H3K9me2 (He et al., 2023), which as activating histone marks might increase gene expression. Therefore, I tested the following concentrations 2, 5, 10, and 20 µM of GSK-LSD1. C2C12 cells were treated for 18 hours and experiments were conducted in triplicate. Results showed a modest reduction in *Tbx1* gene expression at concentrations of 10µM and 20µM (Fig. 17). Thus, also in this case, the result obtained was the opposite to that expected given the pharmacological effect of this epidrug (increases activating histone marks H3K4me2 and H3K9me2).

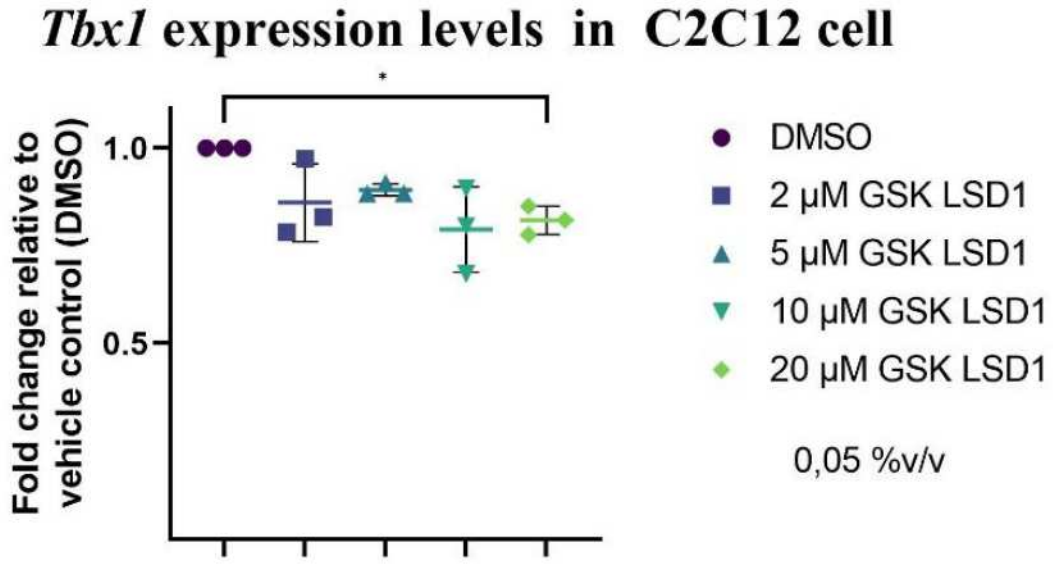


Figure 17. Treatment of C2C12 cells with GSK LSD1 reduces Tbx1 expression at high concentrations. After 18 hours of treatment, a reduction in ***Tbx1*** expression was observed at higher concentrations tested across all three biological replicates. These experiments were conducted using 0.05% as the %v/v of drug/vehicle volume in the total treatment medium. Control cells were treated with DMSO at the same final concentration used in drug treatments. Statistical analysis was performed using the one-way ANOVA method with multiple comparison tests.

4.1.2.4. GSK2879552

GSK2879552 has been described as a specific and relatively potent inhibitor of LSD1 (Mohammad et al., 2015). Numerous studies have investigated the use of this drug, revealing alterations in cell viability at concentrations above 10 µM administered for 72 hours (Lillico et

al., 2018), with an EC50, defined as the concentration at which 50% of the maximum biological effect is observed, of 137 ± 30 nM observed across 20 cell lines (Smitheman et al., 2019) and increased cell mortality reported at concentrations above 100 nM (Sacilotto et al., 2021). Based on these findings, I selected concentrations of 5, 10, 20, 50, and 100 nM and conducted experiments following the same experimental conditions as described for GSKLSD1. In this case, as well, no increase in *Tbx1* expression was observed (Fig. 18).

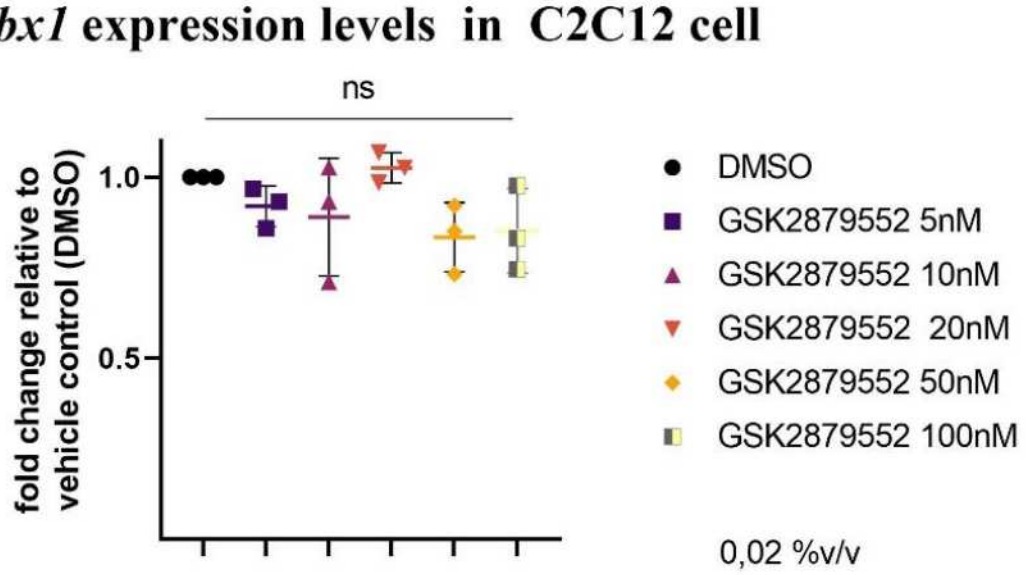


Figure 18. Treatment with GSK2879552 did not increase Tbx1 expression
After 18-hours of treatment, C2C12 cells showed a significant reduction in Tbx1 expression especially at higher concentrations across all three biological replicates. These experiments were conducted using 0.02% as the %v/v of drug/vehicle volume in the total treatment medium. Control cells were treated with DMSO at the same final concentration used in drug treatments. Statistical analysis was performed using the one-way ANOVA method with multiple comparison tests.

4.1.2.5. GSK126

EZH2 is a subunit of the Polycomb PRC2 complex, a repressive complex that is associated with the silencing of many genes. GSK126, a competitive inhibitor of S-adenosylmethionine (SAM), is a highly selective inhibitor of this EZH2 (McCabe et al., 2012). A 2013 study reported reduced cell proliferation at doses above 8 µM and variable sensitivity to inhibition, depending on the cell line tested, at doses between 0.5 and 2 µM (Sato et al., 2013). In a 2017 study evaluating cell viability across six multiple myeloma (MM) cell lines exposed to increasing concentrations of GSK126 for 72 hours, it was shown that GSK126 strongly inhibited the cell growth, with IC50 values, defined as the concentration required to inhibit 50% of the maximum biological activity, ranging between 12.6 µM and 17.4 µM (Zeng et al., 2016). Based on these findings, I selected concentrations of 0.5, 1.5, and 5 µM and evaluated their effects on *Tbx1* expression following the same experimental procedures as described for GSKLSD1 and GSK2879552. Results obtained from three biological replicates showed no increase in *Tbx1* expression compared to controls (DMSO alone) (Fig. 19).

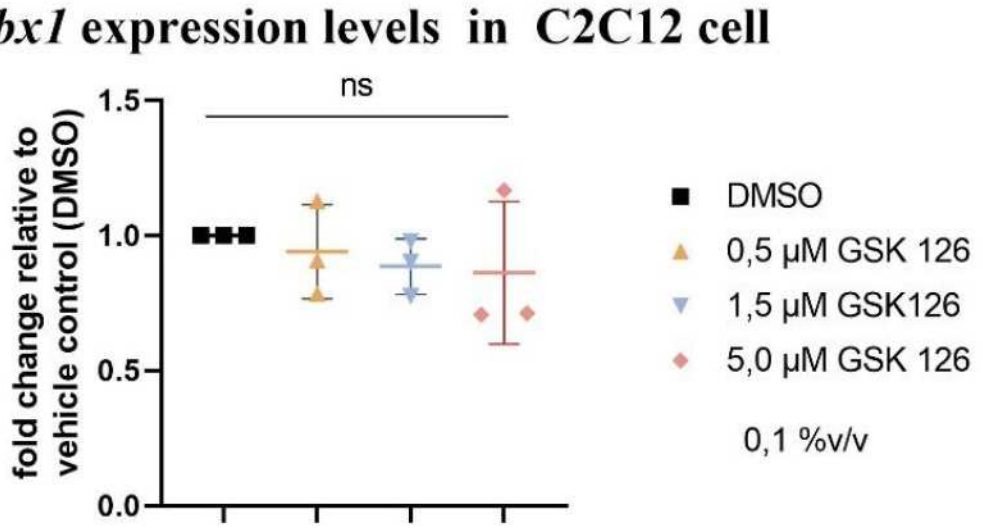


Figure 19. Treatment with GSK126 did not increase *Tbx1* expression.
After 18-hours of treatment with this epigenetic drug, there was no significant increase in ***Tbx1*** expression across three biological replicates. These experiments were conducted using 0.1% as the %v/v of drug/vehicle volume in the total treatment medium. Control cells were treated with DMSO at the same final concentration used in drug treatments. *Statistical analysis was performed using the one-way ANOVA method with multiple comparison tests.*

4.1.2.6. CCK8 ASSAYS

At this point, I had only tested SAHA for cytotoxic effects on C2C12 cells. I therefore performed CCK8 cell counting assays for the other compounds. As described in Section 4.1.2.1, cells were seeded at a density of 1.5×10^3 cells per well in 96-well plates and cultured for 24 hours. Subsequently, the cells were treated for 18 hours with the selected concentrations of the epi-drugs. At the end of the treatment, the absorbance was measured at 450 nm using a microplate reader. For all epidrugs, experiments were performed on two biological replicates. Results showed, for all of the epi-drugs tested, there were no cytotoxic effects at any of the concentrations that had been used in experiments that evaluated the effects of treatment on *Tbx1* expression (Fig. 20).

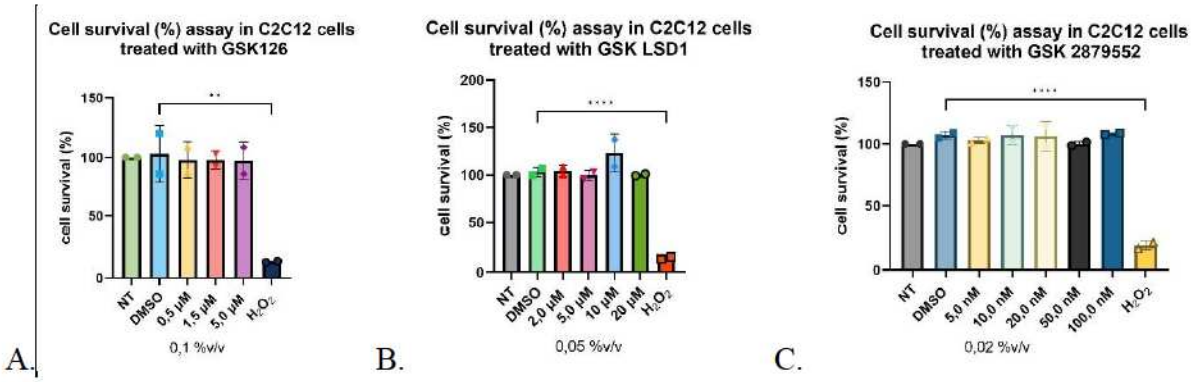


Figure 20. Evaluation of cytotoxicity in C2C12 cells treated with epidrugs.
Cytotoxicity was tested for GSK126 (A), GSK LSD1 (B), and GSK2879552 (C) at the concentrations used in previous experiments. Statistical analysis was performed using the one-way ANOVA method with multiple comparison tests.

4.2 A BIOINFORMATICS APPROACH TO IDENTIFY HISTONE MODIFICATIONS AT THE *TBX1* LOCUS

The goal of this part of my project was to identify histone modifications associated with *Tbx1* activation. For this study, I collaborated with Dr. Olga Lanzetta and Prof. Antonio Baldini, IGB-CNR, Naples. Dr. Lanzetta is a bioinformatician who has experience with the analysis of large genomic datasets, and the development of algorithms for handling and integrating big data. Together with Prof. Baldini, Dr. Lanzetta has identified 14 putative enhancer sequences in the *Tbx1* locus (unpublished data) through the integration of scRNAseq and ATACseq datasets derived from experiments performed on differentiating E14TG2a mouse embryonic stem cells (mESC), Figure 21.

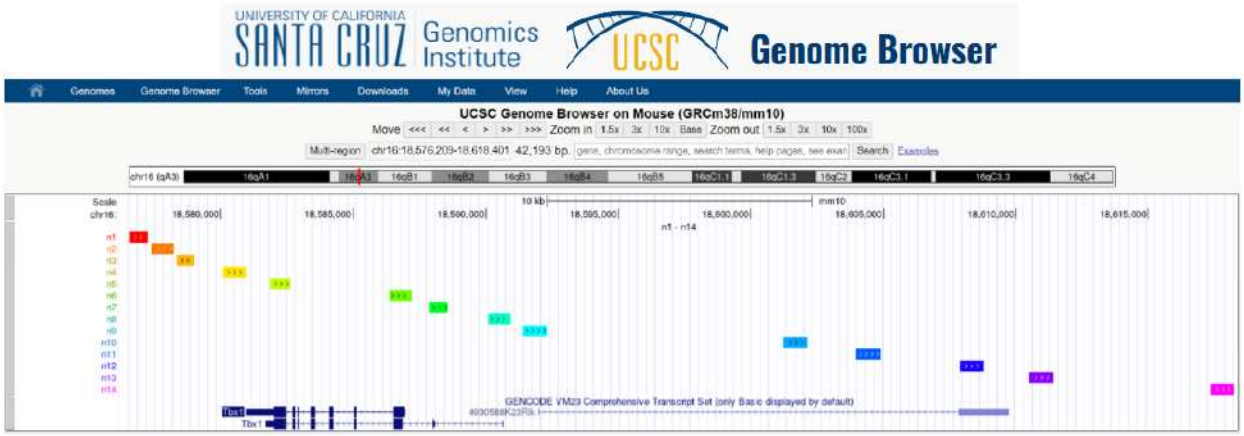


Figure 21. Track of 14 putative enhancers at the Tbx1 locus.
The UCSC Genome Browser shows the putative enhancers in rainbow colours. The track of the *Tbx1* gene is shown in dark blue.

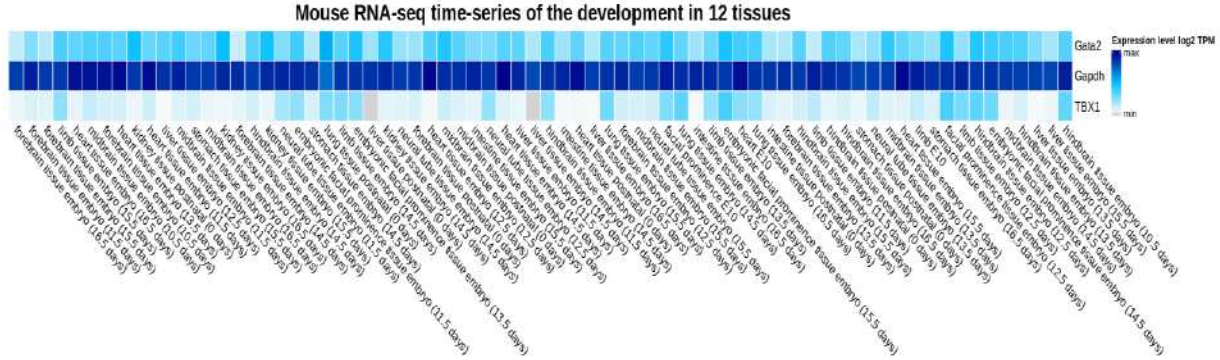
We first downloaded histone modifications (marks) in embryonic tissue (8 marks, 12 tissues, 8 embryonic stages) from ChIP-seq data by ENCODE 3 (UCSD/Ren) (http://genome.ucsc.edu) to identify the histone modifications that overlap the sequences of the 14 putative enhancers (Table 3).

	HISTONE MODIFICATIONS								
	H3K4me3	**H3K4me2**	**H3K4me1**	**H3K27ac**	**H3K9ac**	H3K36me3	**H3K27me3**	H3K9me3	
TISSUE	**Forebrain**				E10.5 - P0				**EMBRYONIC STAGES**
	Midbrain				E10.5 - P0				
	Hindbrain				E10.5 - P0				
	Neural tube				E11.5 - E15.5				
	Facial prominence				E10.5 - E15.5				
	Limb				E10.5 - E15.5				
	Heart				E10.5 - E14.5, P0				
	Kidney				E14.5 - E.16.5, P0				
	Lung				E14.5 - E.16.5, P0				
	Liver				E11.5 - E14.5, P0				
	Stomach				E14.5 - E.16.5, P0				
	Intestine				E14.5 - E.16.5, P0				

Table 3. Histone modifications in embryonic tissues.
The data comprise 8 histone marks, 12 tissues, 8 embryonic stages from ChIP-seq by ENCODE 3 (UCSD/Ren). P0, postnatal day zero.

Additionally, we retrieved bulk polyA RNA-seq data from the ENCODE database (Lab: Barbara Wold, Caltech, CA) (https://www.encodeproject.org) , where *Tbx1* expression had been measured in the same tissues and stages as the ChIP-seq data. The expression data were used to classify tissues into two groups: low *Tbx1* expression (nr=53) (TPM ≤ 3) and high *Tbx1* expression (nr=19) (TPM > 3), normalized to Gapdh (Figure 22).

A.



B.

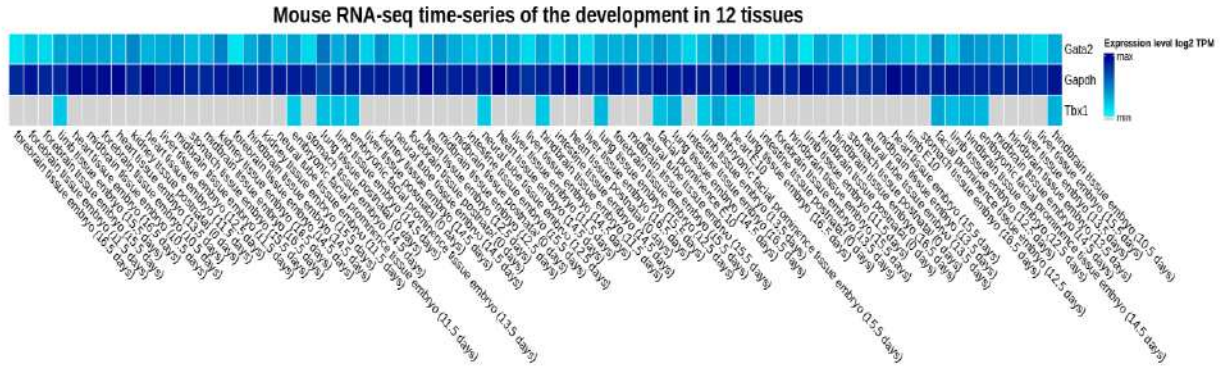


Figure 22. Heatmap of normalized gene expression levels of *Gata2*, *Gapdh,* and *Tbx1* across 12 mouse tissues during different stages of embryonic development.

A. Colours represent expression levels, with light blue indicating minimal expression and dark blue indicating maximum expression.
B. Normalization of the gene expression levels of *Gata2, Gapdh*, and *Tbx1* was performed relative to the 19 tissues exhibiting medium-high levels of *Tbx1* expression, selected for TPM >3

We then performed the analysis of the overlap between the peaks of histone modification tracks and the peaks of the 14 putative enhancer, separately for tissues with low and high *Tbx1* expression. Using an R-based algorithm, we compared ChIP-seq and RNA-seq data to generate a file where a value of 1 was assigned to points where an overlap between the two datasets was detected, and a value of 0 where no overlap was present. The resulting matrix for both groups was reorganized and analyzed to obtain information on the number of overlaps for each histone marker and putative enhancer (Figure 23). In this preliminary analysis, the dataset size (i.e., the number of observations composing the analyzed groups) for individual histone modifications was not taken into account.

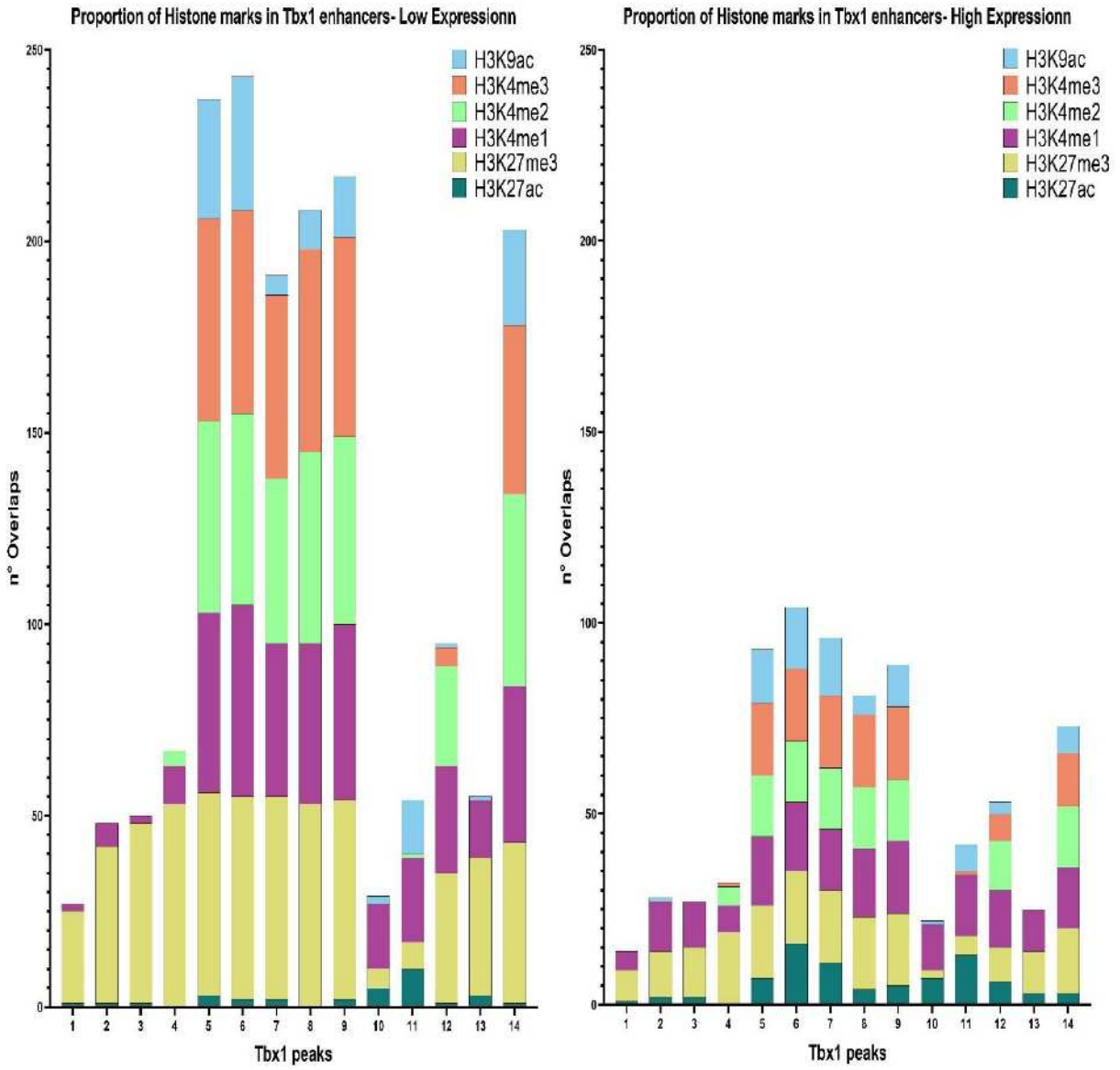


Figure 23. Bar charts showing the number of sequence overlaps obtained for each putative enhancer. Histone modifications at enhancers with low *Tbx1* expression (left) and high *Tbx1* expression (right). The charts display only the number of overlaps for different histone modifications (H3K27ac, H3K27me3, H3K4me1, H3K4me2, H3K4me3, H3K9ac, H3K9me3) at each putative enhancer, indicated in the side legends and represented by distinct colors. Comparing the distribution of histone modifications provides an initial evaluation of the differences in the epigenetic profile of the 14 putative enhancers in tissues with low and high *Tbx1* expression.

The six selected histone modifications were then individually evaluated. For each histone mark, in samples with high *Tbx1* expression, the putative enhancers showing an increased frequency of the histone mark compared to samples with low *Tbx1* expression were identified. In this analysis, for both high-expression and low-expression *Tbx1* samples, the frequency of each histone mark was assessed based on the number of observations (tissue and embryonic stage) in each group (Figure 24). A summary of the interpretation of these data is shown in Table 4.

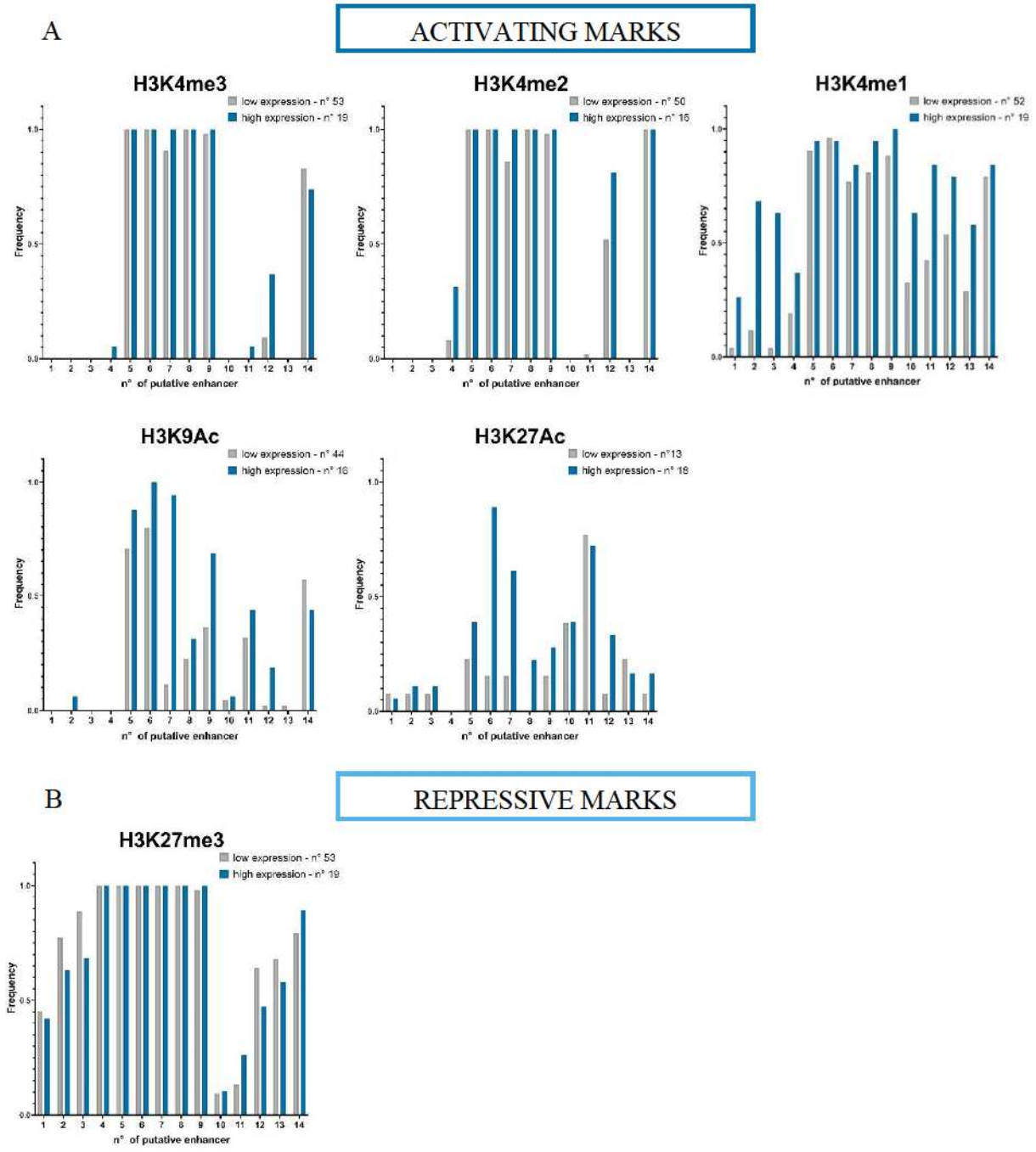


Figure 24. Distribution frequency of individual histone modifications (marks) across the 14 putative *Tbx1* enhancer sequences in tissues with high and low *Tbx1* expression.
The bar charts illustrate the frequency distribution of each histone modification across the 14 putative enhancers in tissues with high and low *Tbx1* expression levels. Data were normalized based on the total number of observations (tissue and embryonic stage) in each group (low or medium-high *Tbx1* expression). Histone modifications are categorized as activating (A) and repressive (B). The bar charts display the frequency of observations (tissues and stages) for the low *Tbx1* expression group in light gray, while the medium-high *Tbx1* expression group is represented in dark blue.

.

Overall, the results showed that in tissues with medium-high levels of *Tbx1* expression, H3K4me1 of the putative *Tbx1* enhancers was frequent (13/14), compared to tissues with low *Tbx1* expression (1/14) (Table 4), a result that is consistent with its' status of an activating

histone mark. Conversely, for H3K27me3, only 9 enhancers in total showed a high frequency of this histone mark. In particular, when the medium and high *Tbx1*-expressing groups were separated, few enhancers in the high *Tbx1*-expressing groups showed this histone mark. Together, these results suggest that high levels of H3K4me1, together with low levels of H3K27me3, are associated with *Tbx1* activation.

Histone Modifications at the putative Tbx1 enhancers

	Histone Modification	Tissue Group	Enhancers (n = 14)	Key Observations
ACTIVATING MARKS	H3K4me1	Low *Tbx1* expression	1/14 (52 obs.)	In tissues with high *Tbx1* expression most of the putative enhancers display this activating histone mark.
		Medium-high *Tbx1* expression	13/14 (19 obs.)	
	H3K9ac	Low *Tbx1* expression	3/14 (44 obs.)	Many enhancers display this activating histone mark in tissues with high levels of *Tbx1* expression.
		Medium-high *Tbx1* expression	8/14 (16 obs.)	
	H3K27ac	Low *Tbx1* expression	3/14 (12 obs.)	Both groups contain few observations; however, in the group comprising tissues with medium-high *Tbx1* expression, a greater number of enhancers exhibit this activating mark compared to the group with low *Tbx1* expression.
		Medium-high *Tbx1* expression	10/14 (18 obs.)	
	H3K4me2	Low *Tbx1* expression	1/14 (50 obs.)	Both activating marks exhibit only a few enhancers with a higher frequency in the group of observations with high *Tbx1* expression.
		Medium-high *Tbx1* expression	4/14 (16 obs.)	
	H3K4me3	Low *Tbx1* expression	1/14 (53 obs.)	
		Medium-high *Tbx1* expression	5/14 (19 obs.)	
REPRESSIVE MARK	H3K27me3	Low *Tbx1* expression	5/14 (53 obs.)	There are few differences between the two tissue groups, but in tissues with high levels of *Tbx1* expression, few enhancers carry this repressive histone mark
		Medium-high *Tbx1* expression	4/14 (19 obs.)	

Table 4. Histone modifications at putative *Tbx1* enhancers.
The table summarizes the interpretation of the data obtained from the bioinformatic analysis. The column "Enhancers (n/14)" reports the number of enhancers that showed an increased frequency of the specific histone mark in the low and medium-high *Tbx1* expression groups. In brackets, the number of observations (tissue and embryonic stage) in the data set is indicated, as shown in Figure 24. The interpretation of the data is indicated in the right column.

In addition, we can deduce from this result that using a combination of epidrugs that target these two specific histone modifications might be more efficacious than the individual drugs for increasing *Tbx1* expression. We tested this hypothesis in C2C12 cells.

4.3 COMBINED EPIDRUG TREATMENTS IN C2C12 CELLS

Several studies have reported the synergistic responses that epigenetic drugs can produce when used in combination (Cameron et al., 1999; Smitheman et al., 2019). This is in line with the observation that chromatin status (condensed - inaccessible or decondensed – accessible) is determined by multiple histone marks. Guided by the results of the bioinformatics analysis of the histone modifications at the putative *Tbx1* enhancers, I performed experiments using a combination of GSK126 and GSK2879552, which, given their mode of action should reduce H3K27me3 and promote H3K4me1 respectively.

- GSK126, an EZH2-specific inhibitor, reduces trimethylation on the K27 residue of histone H3 by inhibiting this methyltransferase complex, thereby reducing gene repression.
- GSK2879552, an LSD1-specific inhibitor, increases monomethylation on the K4 residue of histone H3 by blocking the activity of this demethylase, thereby promoting gene activation.

To set up the combination experiment, I used a fixed-ratio approach, which involves maintaining a constant concentration of one drug while varying the concentration of the other (Tallarida, et al., 1997). I began by evaluating the combined treatment of these two epidrugs after 18 hours, maintaining GSK126 at a constant concentration of 5 µM while varying the concentration of GSK2879552 (10, 20, 50, and 100 nM). Results showed a significant increase in *Tbx1* expression with the combination of 5 µM GSK126 and 20 nM GSK2879552. Interestingly, treatment with 5 µM GSK126 alone increased *Tbx1* expression, which had not been observed in my previous experiment (Fig. 25). Further, experiments will be needed to confirm this result.

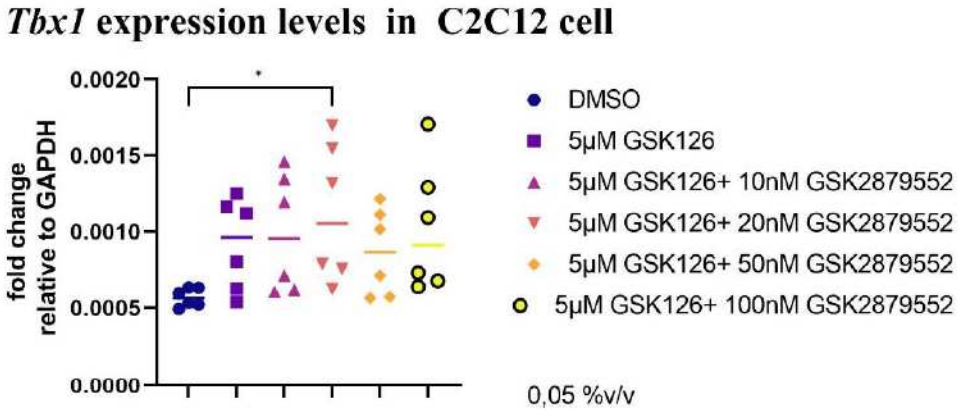


Figure 25. Combined GSK126 – GSK2879552 treatment increases Tbx1 expression in C2C12 cells. The experiment was conducted by maintaining a constant concentration of GSK126 while varying the concentration of GSK2879552 (10–100 nM). A significant increase in *Tbx1* expression is observed with the combination of 5 µM GSK126 and 20 nM GSK2879552. The technical replicates of two separate experiments are shown in the graph. These experiments were conducted using 0.05% as the %v/v of drug/vehicle volume in the

total treatment medium. Control cells were treated with DMSO at the same final concentration used in drug treatments. *Statistical analysis was performed using the one-way ANOVA method with multiple comparison tests.*

Given this promising result, I performed new experiments using the inverse combination, i.e., keeping GSK2879552 fixed at a concentration of 20 nM and varying the concentration of GSK126 (0.5 µM, 1.5 µM, 5 µM). Results confirmed the efficacy of the combination of 20 nM GSK2879552 and 5 µM GSK126, and at the lower dose of 1.5 µM GSK126 (Figure 26). In future experiments, I will test GSK126 doses higher than 5 µM.

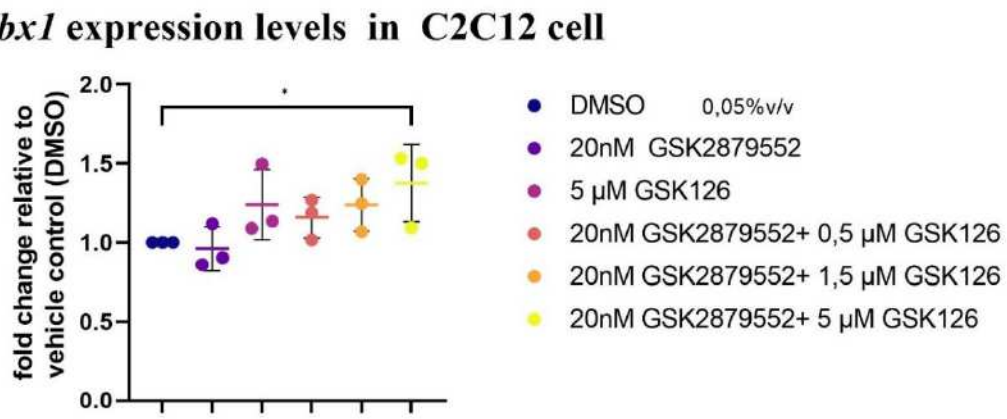


Figure 26. Combined GSK126 – GSK2879552 treatment increases Tbx1 expression in C2C12 cells. The graph illustrates the combined treatment with GSK2879552 and GSK126. The experiment was conducted by maintaining a constant concentration of GSK2879552 (20 nM) while varying the concentration of GSK126 (0.5–5.0 µM). A significant increase in *Tbx1* expression is observed with the combination of 20 nM GSK2879552 and 5 µM GSK126. The data represent the averages of technical replicates from three biological replicates. These experiments were conducted using 0.05% as the %v/v of drug/vehicle volume in the total treatment medium. Control cells were treated with DMSO at the same final concentration used in drug treatments. *Statistical analysis was performed using the one-way ANOVA method with multiple comparison tests.*

4.4 COMBINED EPIDRUG TREATMENT IN MOUSE EMBRYONIC STEM CELLS

The murine embryonic stem cells (mESC) used in this study were of the line E14TG2a (ATCC CRL-1821), hereafter called E14. Murine ESCs constitute a valuable experimental model for studying the initial activation of the *Tbx1* gene, as occurs during mouse embryogenesis, including the epigenetic regulation of its' activation. Unlike C2C12 cells, which express basal levels of *Tbx1*, mESC, including E14, do not express *Tbx1*. However, the induction of differentiation in mESC using specific factors leads to its' activation shortly after (Chen et al., 2009). Thus, while potentially serving as a second cell model in which to validate key results obtained in C2C12 cells, performing similar experiments in E14 mESC has independent relevance and validity, because it is not known whether the initial activation of *Tbx1* during embryogenesis, as opposed to increasing *Tbx1* expression above basal levels are governed by the same histone modifications. Therefore, having identified a combination of epidrugs that increases *Tbx1* expression above basal levels in C2C12 cells, I initiated

experiments in E14 cells in order to test whether they responded in the same way. If so, it would suggest that the same histone marks (high H3K4me1 and low HeK27me3) are involved in the initial activation of *Tbx1*.

4.4.1 E14TG2a cell cultures and induction of mesoderm differentiation

The E14TG2A (E14) cell line was isolated from mouse blastocysts of the 129/Ola strain (Hooper et al., 1987; Incarnato et al., 2014). These cells can be maintained in an undifferentiated state in culture without the use of feeder cells and they can be induced to differentiate into various cell lineages under specific stimuli (Hooper et al., 1987; Murry and Keller, 2008; Seifert et al., 2008). Details of the differentiation procedure used here can be found in the Materials & Methods, 3.9. Briefly, E14 mESCs were cultured on tissue culture plates coated with 0.1% gelatine, using a growth medium containing Glasgow Minimum Essential Medium (GMEM) enriched with fetal bovine serum (FBS), L-glutamine, penicillin-streptomycin (P/S), beta-mercaptoethanol (BME), sodium pyruvate (NaP), non-essential amino acids (nonEAAs), and Leukaemia Inhibitory Factor (LIF) to maintain their pluripotent state (Zhang and Feng, 2022). The culture medium is replaced daily, and cells are passaged every 2–3 days to avoid confluency, which induces spontaneous differentiation.

To induce *Tbx1* expression, 100,000 cells/mL were subjected to a differentiation protocol involving the addition of specific growth factors (Fig. 27, (Andersen et al., 2018) Materials & Methods, 3.9). From day (d) 0 to d4, BMP4, Activin A, ascorbic acid, and monothioglycerol (MTG) were added every two days in a Serum-Free Defined medium (SFD medium) composed of Iscove's Modified Dulbecco's Medium (IMDM), HamF12 (HF12), bovine serum albumin (BSA), glutamine, penicillin-streptomycin (P/S), B27 supplement, and N2 supplement. This protocol is based on the method described by Andersen et al. (2018), which demonstrated the effectiveness of these factors in inducing precardiac organoid formation through Bmp/Wnt signaling.

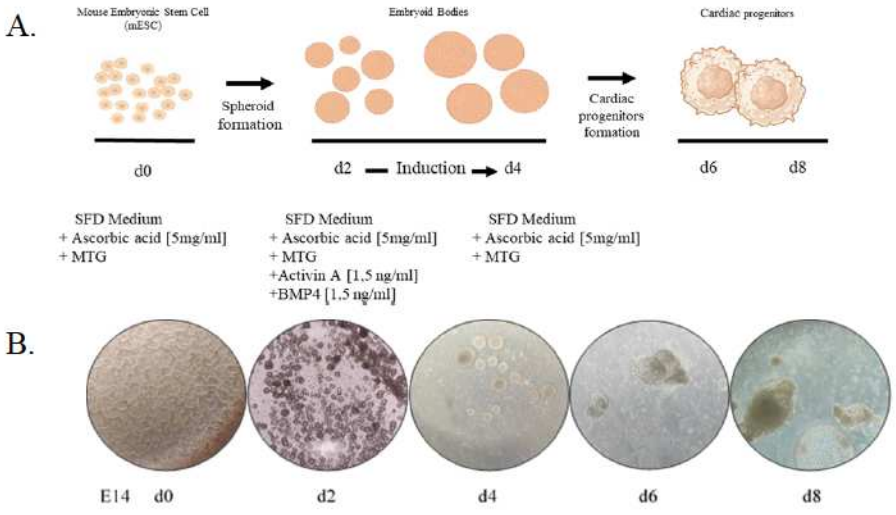


Figure 27. Differentiation of cultured E14 mESCs.
A) Schematic representation of the differentiation procedure. This involves plating 100,000 cells/mL in SFD

medium supplemented with ascorbic acid and MTG on day 0 (d0) and day 4 (d4). The induction phase begins on day 2 (d2) with the addition of Activin A and BMP4. Differentiation continues until day 8 (d8) without further medium changes. B) Images of differentiating E14 cells, captured at an optical microscope at 10X magnification.

Using reverse transcribed PCR (RT-PCR), I monitored the expression of *Tbx1* and of selected markers of differentiation at various time points (d0, d2, d4, d6, and d8). Markers such as *Mef2c, Gata4, Isl1, Ve-cad*, and *Pecam1* were analysed to confirm that differentiation had occurred (Figure 28). Results showed successful induction of *Tbx1* expression at d5, achieving maximum expression at d6-d8.

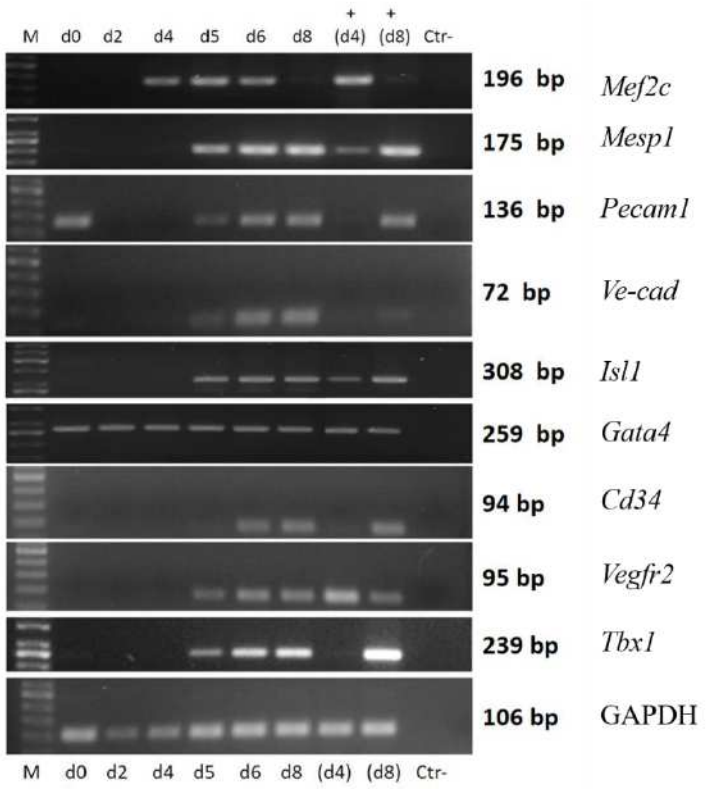


Figure 28. Induction of differentiation in E14 mESC cells activates genes involved in mesodermal and endothelial differentiation.
RT-PCR analysis of E14 cells isolated at different time points shows that *Tbx1* is activated at d5 and expression increases until d8, the latest time point to be analysed. M, 50 bp marker, d0-d8, samples at differentiation day 0 - day 8, (d4) and (d8), positive controls, Ctr- negative (technical blank) control.

4.4.2 EPIDRUG TREATMENT OF DIFFERENTIATING E14 mESC

Based on the successful enhancement of *Tbx1* expression in C2C12 cells treated with GSK126 and GSK2879552, I tested the most promising combination of these two epidrugs, i.e., 5 μM GSK126 and 10, 20, 50, and 100 nM GSK2879552. Using the differentiation procedure shown in Fig. 25, I induced differentiation in the E14 mESCs, then added the drugs directly to the culture medium d5, 24 hours prior to the *Tbx1* expression peak and then

harvested the cells at d6 and d7, i.e., after 24 hours and 48 hours of drug treatment. Subsequently, I analysed *Tbx1* expression by Real-Time qPCR. This permitted a quantitative assessment of the impact of these molecules on *Tbx1* activation during differentiation.

Results obtained in the first experiment showed high variability across the different drug concentrations, which prevented interpretation. A second experiment in progress.

4.5. TESTING THE THERAPEUTIC POTENTIAL OF *TBX1*-ACTIVATING EPIDRUGS USING PHENOTYPIC RESCUE IN *TBX1* MUTANT MICE

The last objective of my project was to test promising epidrug treatments in *Tbx1* mutant embryos. This will allow me to understand whether the *Tbx1*-activating histone marks identified in cell culture have *in vivo* relevance. The readout of these experiments will be the ability of the epidrug/s to rescue (normalize) the development of the 4th pharyngeal arch arteries (4PAA) in *Tbx1*$^{+/-}$ embryos. Aplasia or hypoplasia of one or both arteries is a highly penetrant *Tbx1* haploinsufficiency phenotype that is relatively easy to score at embryonic day (E)10.5 by intracardiac injection of India ink (Lindsay et al., 2001), see Material & Methods, 3.10, Fig 29.

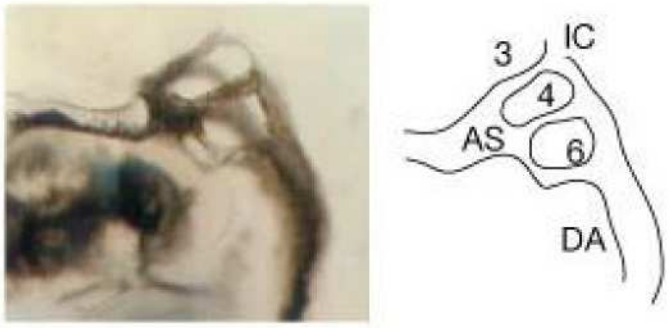


Figure 29. Indian ink Injection.
Typical PAA morphology in a wild-type E10.5 embryo as visualized by intracardiac ink injection. Figure modified from Lindsay et al., 2001.

Due to an outbreak of *Pasteurella* infection in the mouse colony at the IGB-CNR, Naples in November 2023, I have only recently initiated these experiments. The infection necessitated the rederivation of the *Tbx1* mutant mouse line, and it has taken one year to recover. I now have a small group of male *Tbx1*$^{+/-}$ mice that have reached sexual maturity (8 weeks of age) that will be crossed with wild type female mice and embryos will be collected E10.5 and injected intracardially with ink. To date, I have set up a pilot experiment with a small number of timed matings in order to have embryos for practicing ink injection. For this, I have the technical support of two members of Prof. Illingworth's' research group who have experience with this technique.

Once I have achieved the necessary technical expertise, I will perform the experiments

using the combined epidrug treatment with GSK126 and GSK2879552. For this, I will be guided by the scientific literature for establishing the appropriate drug dosage and treatment regimes, considering that treatment is administered to the pregnant dams. I shall collect and inject a sufficient number of embryos to achieve statistically significant data, i.e., approximately 25 embryos per genotype (*Tbx1*$^{+/-}$ *vs* wild type) and per treatment group (epidrug-treated *vs* vehicle (DMSO)-treated. I expect to be in a position to initiate these experiments in February 2025.

5. DISCUSSION

The objective of this study was to identify histone modifications that promote *Tbx1* expression in cell cultures and *in vivo*. Such modifications might contribute to the epigenetic regulation of *Tbx1* during mouse embryogenesis, about which little is known. The novelty of the study lies in the integration our own data with large genomic datasets deposited in public databases containing information about gene expression in different tissues and at different stages of embryonic development, and histone marks genome-wide. Overall, our goals were met, in that we identified two histone modifications that were strongly associated with a set of newly identified putative *Tbx1* enhancers in tissues expressing high levels of *Tbx1*. In addition, treatment of C2C12 cells with epidrugs that target these modifications increased expression of *Tbx1*, thereby providing tools that will allow us to validate the *Tbx1*-activating histone modifications *in vivo*.

Choice of the cell lines

The choice of which cell line to use was limited because of the low level of *TBX1* expression in many commonly available cell lines. TBX1 has critical functions in endothelial cells, and in my lab, several endothelial cell (EC) lines have been used to study the effects of *TBX1* inactivation on transcriptional targets (Chen et al., 2010; Cioffi et al., 2014; Martucciello et al., 2020), these include human umbilical vein ECs (HUVEC), human and mouse lymphatic ECs (LECs) and dermal microvascular ECs (HDMEC). However, these are all primary cell lines, which are slow growing and require defined media and expensive growth factors. Thus, they were deemed unsuitable for my project initially, as we envisaged performing a high throughput screen of epidrugs. Transformed cell lines generally grow more robustly and do not need specific growth factors, but the only transformed EC line available to me was a mouse brain EC line, in which I did not detect *Tbx1* expression. C2C12 myoblasts have been used in my lab to study muscle differentiation (Pane et al., 2018). As they express low levels of *Tbx1,* they were deemed to be suitable for studies that aim to increase *Tbx1* expression pharmacologically. The second cell line selected was the mouse embryonic stem cell (mESC) line E14TG2a. This cell line was initially selected because mESC do not express *Tbx1*, but upon induction of mesoderm differentiation, it is activated. Thus, together, these two cell lines represent the two biological contexts of interest to me; C2C12 cells express basal levels of *Tbx1* that can be modulated pharmacologically, a context that is similar to that envisaged for treating *Tbx1* haploinsufficiency in 22q11.2DS patients, where drugs/epidrugs would be used to increase expression from the healthy *Tbx1* allele. In contrast, E14TG2a mESC do not express *Tbx1* until it is activated by an external cue, namely differentiation, a context that is similar to that which occurs in mouse embryos after gastrulation, when *Tbx1* is activated for the first time in anterior mesoderm (Huynh, 2007). Therefore, these two cellular models would allow me to discriminate between *Tbx1*-activating histone modifications in the two different biological contexts.

The results obtained to date do not allow me to conclude definitively whether combined GSK126-GSK2879552 treatment affects *Tbx1* expression in differentiating E14TG2a mESCs because the results obtained are highly variable. This may be due in part to the non-

homogeneous nature of mESCs. Further experiments are in progress in which the timing of treatment and the dosage of the individual epidrugs are manipulated. Should these experiments fail, it would suggest that these histone modifications do not contribute to the initial activation of TBX1.

Selection of epidrugs

There are at least two different approaches to identify *Tbx1*-activating histone modifications. The first, is to perform a cell-based screen of known epidrugs and select those that increase *Tbx1* expression. The class of the *Tbx1*-inducing epidrug/s should inform upon the histone modifications associated with increased expression. An alternative approach is to analyse the histone modifications in regulatory elements of *Tbx1* in mutant *vs* wild type conditions or in tissues expressing high *vs* low levels of *Tbx1*.

The early phase of my project was dedicated to the first approach through a collaboration with EpiC s.r.l. The objective was to perform a semi-high-throughput screen of epidrugs using a cell line carrying a TBX1-GFP transgene. This approach was abandoned during my first year after a series of pilot experiments showed that it would not be possible to adapt the growing conditions of the cell line (genetically modified mESCs), to the experimental conditions required to treat the cells for 24-48 hrs and then measure gene expression. Therefore, with the help of Prof. Altucci, Director of EpiC s.r.l., I adopted the more modest strategy of testing one or two members of the main classes of epidrugs, giving priority to those that generally promote gene expression, namely H3K4 mono-, di- and tri-methylation, or that inhibit repressive histone marks, namely H3K9 tri-methylation and H3K27 tri-methylation. The results obtained with the first five epidrugs tested showed no significant increase in *Tbx1* expression when used alone and at the doses tested. Interestingly, treatment with SAHA, a modulator of the acetylation state of chromatin, revealed a reduction in *Tbx1* expression in multiple experiments, which is the opposite of that expected. To ensure that this effect was not attributable to cytotoxicity or inadequate treatment timing, I performed cell viability assays and quality analysis of the extracted RNA. These experiments ruled out technical problems, but they did not address the underlying biological question of the repression. This could be addressed in future studies. These should include confirmation of *Tbx1* repression using an epidrug that has similar activity to SAHA, for example Trichostatin A (TSA), Valproic Acid (VPA) or Entinostat (MS-275).

For the second approach to identify *Tbx1*-activating histone modifications, I was greatly assisted by the identification of several putative *Tbx1* enhancers through the integration of single cell RNA-seq and ATAC-seq datasets derived from experiments performed on differentiating E14TG2a mESCs. The group of our collaborator Prof. Antonio Baldini, at the IGB-CNR, Naples, generated these data. These data allowed me to identify histone modifications that were associated with high *Tbx1* expression in a panel of different mouse tissues and, through this, gain insights into combinations of epidrugs that would likely increase *Tbx1* expression. Although, these combinations could have been deduced on the basis of our general knowledge of activating histone marks and our specific knowledge of the role of *Tbx1* in promoting mono-methylation of H3K4, the volume of the genomics data handled by the algorithm used here greatly enhances the robustness of the results obtained. This was important for me, because I have recently initiated *in vivo* studies in the mouse in which I will test the

efficacy of GSK126-GSK2879552 combined treatment for alleviating the *Tbx1* haploinsufficiency phenotype.

In vivo validation of putative *Tbx1*-activating histone modifications

Unfortunately, this important part of my project, the *in vivo* validation of putative *Tbx1*-activating histone modifications, has been much delayed due to an outbreak of *Pasteurella* infection in the mouse colony of our collaborator Prof. Baldini in November 2023. Rederived *Tbx1* mutant mice have only recently reached sexual maturity. Matings between $Tbx1^{+/-}$ and wild-type mice have been set up and I expect to perform the first pilot experiments at the end of January or beginning of February 2025. The first experiments will be dedicated to learning how to collect embryos at the stage in which the *Tbx1* haploinsufficiency phenotype is evident (E10.5) and to practicing intracardiac ink injection, which is the method used to reveal the anatomy of the pharyngeal arch arteries, which are some of the most sensitive structures to *Tbx1* dosage (Jerome and Papaioannou, 2001; Lindsay, 2001; Lindsay et al., 2001; Merscher et al., 2001).

6. CONCLUSION

Twenty-five years have passed since genetic engineering techniques were employed to inactivate the murine *Tbx1* gene. The availability of *Tbx1* heterozygous and homozygous mutant mice and fish opened the door to the study of the molecular and developmental functions of TBX1, that were previously unknown. Analysis of the *Tbx1* mutant phenotype in model organisms revealed many of the same physical defects observed in 22q11.2DS patients, including cardiovascular anomalies and pharyngeal arch and arch artery defects, thereby validating its' status as a candidate disease gene. Later, the identification of rare cases of *TBX1* point mutations in humans established *TBX1* as the major gene involved in this disease.

Since then, much research effort has been dedicated to the discovery of the critical tissues and timing of TBX1 function during mouse and fish embryogenesis, and to the understanding of the cellular mechanisms that are disrupted when *Tbx1* is mutated. During this period, a limited number of interacting proteins were identified, an area of study that has been revolutionized by high throughput genomics, including RNA-seq, ChIP-seq, ATAC-seq and, more recently, by single cell versions of these methods. Much less, research attention has been dedicated to understanding how TBX1 is regulated, which is surprising given that 22q11.2DS is primarily a disease of *TBX1* haploinsufficiency. Only a few molecules are known to regulate TBX1 directly, and epigenetic mechanisms regulating its expression remain poorly understood.

My doctoral project used an innovative approach involving the use of epidrugs to modulate *Tbx1* expression and thereby identify potential *Tbx1*-activating histone marks. This lab-based approach was supported by a bioinformatics approach that enabled me to gather information about histone modifications at the TBX1 locus from genome-wide datasets deposited in public databases. The integration of the two approaches allowed me to identify an epidrug combination that led to increased *Tbx1* expression in C2C12 myoblasts. The combined treatment using GSK126 (an EZH2 inhibitor) and GSK2879552 (an LSD1 inhibitor) resulted in a significant increase in *Tbx1* expression, suggesting that simultaneous modulation of H3K4 and H3K27 methylation may be required to activate *Tbx1* or to increase its' expression above basal levels. In this context, the bioinformatics studies proved essential, as they enabled the identification of a potential synergistic effect between the two epigenetic modifications.

Future priorities are to test the effective epidrug combination *in vivo* through phenotypic rescue experiments using *Tbx1* mutant mice. I have initiated these studies only recently after a long delay due to the unavailability of the mouse lines.

FIGURE and TABLE INDEX

Figure 1. Clinical features associated with disorders related to mutations in TBX genes. 4
Figure 2. Domain structure and binding profile of human T-BOX transcription factors. 5
Figure 3. Domain structure of T-box proteins and crystal structure of T-domains bound to DNA. 6
Figure 4. TBX1 isoforms visualized using the UCSC Genome Browser. 8
Figure 5. Structure of the DNA-bound T-box domain of human TBX1 protein 9
Figure 6. Topography of the second heart field. 10
Figure 7. Reversible posttranslational lysine residues acetylation of histones is maintained by HATs and HDACs. 17
Figure 8. Structure of vorinostat (suberoylanilide hydroxamic acid, SAHA). 18
Figure 9. 3D structure of the enzyme with the SAHA compound bound in the active pocket to highlight the interaction mechanism between the inhibitor (SAHA) and the target enzyme (HDAC) 19
Figure 10. GSK126 structure 21
Figure 11. Images of C2C12 cells in culture at various seeding densities observed at 48 hours post-seeding (A-E) and after 48 hours (F-P) 39
Figure 12. Schematic representation of the SAHA treatment experiment conducted in 6-well plates. 40
Figure 13. Tbx1 expression in C2C12 myoblasts treated with SAHA at different concentrations (RTqPCR) 41
Figure 14. Effect of SAHA (2uM) on Tbx1 expression at different treatment times. 42
Figure 15. Lowering DMSO concentration did not improve Tbx1 expression in C2C12 cells treated with SAHA. 43
Figure 16. SAHA treatment (1uM- 5uM) did not induce cytotoxicity in C2C12 cells. 44
Figure 17. Treatment of C2C12 cells with GSK LSD1 reduces Tbx1 expression at high concentrations. 45
Figure 18. Treatment with GSK2879552 did not increase Tbx1 expression 46
Figure 19. Treatment with GSK126 did not increase *Tbx1* expression. 47
Figure 20. Evaluation of cytotoxicity in C2C12 cells treated with epidrugs. 47
Figure 21. Track of 14 putative enhancers at the Tbx1 locus. 48
Figure 22. Heatmap of normalized gene expression levels of *Gata2*, *Gapdh,* and *Tbx1* across 12 mouse tissues during different stages of embryonic development. 49
Figure 23. Bar charts showing the number of sequence overlaps obtained for each putative enhancer. 50
Figure 24. Distribution frequency of individual histone modifications (marks) across the 14 putative *Tbx1* enhancer sequences in tissues with high and low *Tbx1* expression. 51
Figure 25. Combined GSK126 – GSK2879552 treatment increases Tbx1 expression in C2C12 cells. 53
Figure 26. Combined GSK126 – GSK2879552 treatment increases Tbx1 expression in C2C12 cells. 54
Figure 27. Differentiation of cultured E14 mESCs. 55

Figure 28. Induction of differentiation in E14 mESC cells activates genes involved in mesodermal and endothelial differentiation. 56
Figure 29. Indian ink Injection 57

Table 1. Table of Epigenetic Modifications and Their Potential Effects in Different Genomic Regions. 22
Table 2. Effect of cell density on the growth of C2C12 cells in 6-well plates 38
Table 3. Histone modifications in embryonic tissues. 48
Table 4. Histone modifications at putative *Tbx1* enhancers. 52

Bibliography

Abraham, J., Nuñez-Álvarez, Y., Hettmer, S., Carrió, E., Chen, H.-I.H., Nishijo, K., Huang, E.T., Prajapati, S.I., Walker, R.L., Davis, S., Rebeles, J., Wiebush, H., McCleish, A.T., Hampton, S.T., Bjornson, C.R.R., Brack, A.S., Wagers, A.J., Rando, T.A., Capecchi, M.R., Marini, F.C., Ehler, B.R., Zarzabal, L.A., Goros, M.W., Michalek, J.E., Meltzer, P.S., Langenau, D.M., LeGallo, R.D., Mansoor, A., Chen, Y., Suelves, M., Rubin, B.P., Keller, C., 2014. Lineage of origin in rhabdomyosarcoma informs pharmacological response. Genes Dev. 28, 1578–1591. https://doi.org/10.1101/gad.238733.114

Airik, R., Bussen, M., Singh, M.K., Petry, M., Kispert, A., 2006. Tbx18 regulates the development of the ureteral mesenchyme. J. Clin. Invest. 116, 663–674. https://doi.org/10.1172/JCI26027

Al-Khindi, T., Sherman, M.B., Kodama, T., Gopal, P., Pan, Z., Kiraly, J.K., Zhang, H., Goff, L.A., du Lac, S., Kolodkin, A.L., 2022. The transcription factor Tbx5 regulates direction-selective retinal ganglion cell development and image stabilization. Curr. Biol. 32, 4286-4298.e5. https://doi.org/10.1016/j.cub.2022.07.064

Allis, C.D., Jenuwein, T., 2016. The molecular hallmarks of epigenetic control. Nat. Rev. Genet. 17, 487–500. https://doi.org/10.1038/nrg.2016.59

Andersen, P., Tampakakis, E., Jimenez, D.V., Kannan, S., Miyamoto, M., Shin, H.K., Saberi, A., Murphy, S., Sulistio, E., Chelko, S.P., Kwon, C., 2018. Precardiac organoids form two heart fields via Bmp/Wnt signaling. Nat. Commun. 9, 3140. https://doi.org/10.1038/s41467-018-05604-8

Antoniou, A.C., Easton, D.F., 2006. Models of genetic susceptibility to breast cancer. Oncogene 25, 5898–5905. https://doi.org/10.1038/sj.onc.1209879

Arnold, J.S., Werling, U., Braunstein, E.M., Liao, J., Nowotschin, S., Edelmann, W., Hebert, J.M., Morrow, B.E., 2006. Inactivation of Tbx1 in the pharyngeal endoderm results in 22q11DS malformations. Development 133, 977–987. https://doi.org/10.1242/dev.02264

Ataollahi, M., Sharifi, J., Paknahad, M., Paknahad, A., 2015. Breast cancer and associated factors: a review. J. Med. Life 8, 6–11.

Aurigemma, I., Lanzetta, O., Cirino, A., Allegretti, S., Lania, G., Ferrentino, R., Poondi Krishnan, V., Angelini, C., Illingworth, E., Baldini, A., 2024. Endothelial gene regulatory elements associated with cardiopharyngeal lineage differentiation. Commun. Biol. 7, 351. https://doi.org/10.1038/s42003-024-06017-8

Baldini, A., 2003. DiGeorge's syndrome: a gene at last. The Lancet 362, 1342–1343. https://doi.org/10.1016/S0140-6736(03)14671-5

Baldini, A., Fulcoli, F.G., Illingworth, E., 2017. Chapter Eight - Tbx1: Transcriptional and Developmental Functions, in: Frasch, M. (Ed.), Current Topics in Developmental Biology. Academic Press, pp. 223–243. https://doi.org/10.1016/bs.ctdb.2016.08.002

Bannister, A.J., Kouzarides, T., 2011. Regulation of chromatin by histone modifications. Cell Res. 21, 381–395. https://doi.org/10.1038/cr.2011.22

Barski, A., Cuddapah, S., Cui, K., Roh, T.Y., Schones, D.E., Wang, Z., Wei, G., Chepelev, I., Zhao, K., 2007. High-Resolution Profiling of Histone Methylations in the Human Genome. Cell 129, 823.

Bassett, A.S., Chow, E.W.C., 1999. 22q11 deletion syndrome: a genetic subtype of schizophrenia. Biol. Psychiatry 46, 882–891. https://doi.org/10.1016/S0006-3223(99)00114-6

Bassett, A.S., McDonald-McGinn, D.M., Devriendt, K., Digilio, M.C., Goldenberg, P., Habel, A., Marino, B., Oskarsdottir, S., Philip, N., Sullivan, K., Swillen, A., Vorstman, J., 2011. Practical Guidelines for Managing Patients with 22q11.2 Deletion Syndrome. J. Pediatr. 159, 332-339.e1. https://doi.org/10.1016/j.jpeds.2011.02.039

Beddington, R.S.P., Rashbass, P., Wilson, V., 1992. Brachyury - a gene affecting mouse gastrulation and early organogenesis. Development 116, 157–165. https://doi.org/10.1242/dev.116.Supplement.157

Bedford, M.T., Clarke, S.G., 2009. Protein Arginine Methylation in Mammals: Who, What, and Why. Mol. Cell 33, 1–13. https://doi.org/10.1016/j.molcel.2008.12.013

Bennett, R.L., Licht, J.D., 2018. Targeting Epigenetics in Cancer. Annu. Rev. Pharmacol. Toxicol. https://doi.org/10.1146/annurev-pharmtox-010716-105106

Berdasco, M., Esteller, M., 2019. Clinical epigenetics: seizing opportunities for translation. Nat. Rev. Genet. 20, 109–127. https://doi.org/10.1038/s41576-018-0074-2

Bernstein, B.E., Mikkelsen, T.S., Xie, X., Kamal, M., Huebert, D.J., Cuff, J., Fry, B., Meissner, A., Wernig, M., Plath, K., Jaenisch, R., Wagschal, A., Feil, R., Schreiber, S.L., Lander, E.S., 2006. A Bivalent Chromatin Structure Marks Key Developmental Genes in Embryonic Stem Cells. Cell 125, 315–326. https://doi.org/10.1016/j.cell.2006.02.041

Bird, A., 2007. Perceptions of epigenetics. Nature 447, 396–398. https://doi.org/10.1038/nature05913

Biswas, A.B., Furniss, F., 2016. Cognitive phenotype and psychiatric disorder in 22q11.2 deletion syndrome: A review. Res. Dev. Disabil. 53–54, 242–257. https://doi.org/10.1016/j.ridd.2016.02.010

Black, J.C., Van Rechem, C., Whetstine, J.R., 2012. Histone Lysine Methylation Dynamics: Establishment, Regulation, and Biological Impact. Mol. Cell 48, 491–507. https://doi.org/10.1016/j.molcel.2012.11.006

Blau, H.M., Chiu, C.-P., Webster, C., 1983. Cytoplasmic activation of human nuclear genes in stable heterocaryons. Cell 32, 1171–1180. https://doi.org/10.1016/0092-8674(83)90300-8

Bolden, J.E., Peart, M.J., Johnstone, R.W., 2006. Anticancer activities of histone deacetylase inhibitors. Nat. Rev. Drug Discov. 5, 769–784. https://doi.org/10.1038/nrd2133

Bollag, R.J., Siegfried, Z., Cebra-Thomas, J.A., Garvey, N., Davison, E.M., Silver, L.M., 1994. An ancient family of embryonically expressed mouse genes sharing a conserved protein motif with the T locus. Nat. Genet. 7, 383–389. https://doi.org/10.1038/ng0794-383

Bongers, E.M.H.F., Duijf, P.H.G., van Beersum, S.E.M., Schoots, J., van Kampen, A., Burckhardt, A., Hamel, B.C.J., Lošan, F., Hoefsloot, L.H., Yntema, H.G., Knoers, N.V.A.M., van Bokhoven, H., 2004. Mutations in the Human TBX4 Gene Cause Small Patella Syndrome. Am. J. Hum. Genet. 74, 1239–1248. https://doi.org/10.1086/421331

Bosada, F.M., van Duijvenboden, K., Giovou, A.E., Rivaud, M.R., Uhm, J.-S., Verkerk, A.O., Boukens, B.J., Christoffels, V.M., 2023. An atrial fibrillation-associated regulatory region modulates cardiac Tbx5 levels and arrhythmia susceptibility. eLife 12, e80317. https://doi.org/10.7554/eLife.80317

Braybrook, C., Doudney, K., Marçano, A.C.B., Arnason, A., Bjornsson, A., Patton, M.A., Goodfellow, P.J., Moore, G.E., Stanier, P., 2001. The T-box transcription factor gene TBX22 is mutated in X-linked cleft palate and ankyloglossia. Nat. Genet. 29, 179–183. https://doi.org/10.1038/ng730

Bubna, A.K., 2015. Vorinostat—An Overview. Indian J. Dermatol. 60.

Bussen, M., Petry, M., Schuster-Gossler, K., Leitges, M., Gossler, A., Kispert, A., 2004. The T-box transcription factor Tbx18 maintains the separation of anterior and posterior somite compartments. Genes Dev. 18, 1209-1221.

Butler, L.M., Zhou, X., Xu, W.-S., Scher, H.I., Rifkind, R.A., Marks, P.A., Richon, V.M., 2002. The histone deacetylase inhibitor SAHA arrests cancer cell growth, up-regulates thioredoxin-binding protein-2, and down-regulates thioredoxin. Proc. Natl. Acad. Sci. 99, 11700–11705. https://doi.org/10.1073/pnas.182372299

Caballero, R., Utrilla, R.G., Amorós, I., Matamoros, M., Pérez-Hernández, M., Tinaquero, D., Alfayate, S., Nieto-Marín, P., Guerrero-Serna, G., Liu, Q., Ramos-Mondragón, R., Ponce-Balbuena, D., Herron, T., Campbell, K.F., Filgueiras-Rama, D., Peinado, R., López-Sendón, J.L., Jalife, J., Delpón, E., Tamargo, J., 2017. Tbx20 controls the expression of the KCNH2 gene and of hERG channels. Proc. Natl. Acad. Sci. 114, E416–E425. https://doi.org/10.1073/pnas.1612383114

Cai, X., Zhang, W., Hu, J., Zhang, L., Sultana, N., Wu, B., Cai, W., Zhou, B., Cai, C.-L., 2013. Tbx20 acts upstream of Wnt signaling to regulate endocardial cushion formation and valve remodeling during mouse cardiogenesis. Development 140, 3176–3187. https://doi.org/10.1242/dev.092502

Cameron, E.E., Bachman, K.E., Myöhänen, S., Herman, J.G., Baylin, S.B., 1999. Synergy of demethylation and histone deacetylase inhibition in the re-expression of genes silenced in cancer. Nat. Genet. 21, 103–107. https://doi.org/10.1038/5047

Campbell, L.E., McCabe, K.L., Melville, J.L., Strutt, P.A., Schall, U., 2015. Social cognition dysfunction in adolescents with 22q11.2 deletion syndrome (velo-cardio-facial syndrome): relationship with executive functioning and social competence/functioning. J. Intellect. Disabil. Res. 59, 845–859. https://doi.org/10.1111/jir.12183

Cao, R., Wang, L., Wang, H., Xia, L., Erdjument-Bromage, H., Tempst, P., Jones, R.S., Zhang, Y., 2002. Role of Histone H3 Lysine 27 Methylation in Polycomb-Group Silencing. Science 298, 1039–1043. https://doi.org/10.1126/science.1076997

Caprio, C., Lania, G., Bilio, M., Ferrentino, R., Chen, L., Baldini, A., 2021. EZH2 is required for parathyroid and thymic development through differentiation of the third pharyngeal pouch endoderm. Dis. Model. Mech. 14, dmm.046789. https://doi.org/10.1242/dmm.046789

Cartron, P.-F., Cheray, M., Bretaudeau, L., 2019. Epigenetic protein complexes: the adequate candidates for the use of a new generation of epidrugs in personalized and precision medicine in cancer. Epigenomics.

Caterino, M., Paris, D., Torromino, G., Costanzo, M., Flore, G., Tramice, A., Golini, E., Mandillo, S., Cavezza, D., Angelini, C., Ruoppolo, M., Motta, A., De Leonibus, E., Baldini, A., Illingworth, E., Lania, G., 2025. Brain and behavioural anomalies caused by Tbx1 haploinsufficiency are corrected by vitamin B12. Life Sci. Alliance 8, e202403075. https://doi.org/10.26508/lsa.202403075

Chapman, D.L., Garvey, N., Hancock, S., Alexiou, M., Agulnik, S.I., Gibson-Brown, J.J., Cebra-Thomas, J., Bollag, R.J., Silver, L.M., Papaioannou, V.E., 1996. Expression of the T-box family genes, Tbx1–Tbx5, during early mouse development. Dev. Dyn. 206, 379–390. https://doi.org/10.1002/(SICI)1097-0177(199608)206:4<379::AID-AJA4>3.0.CO;2-F

Chen, L., Fulcoli, F.G., Ferrentino, R., Martucciello, S., Illingworth, E.A., Baldini, A., 2012. Transcriptional Control in Cardiac Progenitors: Tbx1 Interacts with the BAF Chromatin Remodeling Complex and Regulates Wnt5a. PLOS Genet. 8, e1002571. https://doi.org/10.1371/journal.pgen.1002571

Chen, L., Fulcoli, F.G., Tang, S., Baldini, A., 2009. Tbx1 Regulates Proliferation and Differentiation of Multipotent Heart Progenitors. Circ. Res. 105, 842–851. https://doi.org/10.1161/CIRCRESAHA.109.200295

Chen, L., Mupo, A., Huynh, T., Cioffi, S., Woods, M., Jin, C., McKeehan, W., Thompson-Snipes, L., Baldini, A., Illingworth, E., 2010. Tbx1 regulates Vegfr3 and is required for lymphatic vessel development. J. Cell Biol. 189, 417–424. https://doi.org/10.1083/jcb.200912037

Chen, Y., Xiao, D., Zhang, L., Cai, C.-L., Li, B.-Y., Liu, Y., 2021. The Role of Tbx20 in Cardiovascular Development and Function. Front. Cell Dev. Biol. 9.

Chieffo, C., Garvey, N., Gong, W., Roe, B., Zhang, G., Silver, L., Emanuel, B.S., Budarf, M.L., 1997. Isolation and Characterization of a Gene from the DiGeorge Chromosomal Region Homologous to the MouseTbx1Gene. Genomics 43, 267–277. https://doi.org/10.1006/geno.1997.4829

Chisholm, K.M., Wan, Y., Li, R., Montgomery, K.D., Chang, H.Y., West, R.B., 2012. Detection of Long Non-Coding RNA in Archival Tissue: Correlation with Polycomb Protein Expression in Primary and Metastatic Breast Carcinoma. PLOS ONE 7, e47998. https://doi.org/10.1371/journal.pone.0047998

Cillo, F., Coppola, E., Habetswallner, F., Cecere, F., Pignata, L., Toriello, E., De Rosa, A., Grilli, L., Ammendola, A., Salerno, P., Romano, R., Cirillo, E., Merla, G., Riccio, A., Pignata, C., Giardino, G., 2024. Understanding the Variability of 22q11.2 Deletion Syndrome: The Role of Epigenetic Factors. Genes 15. https://doi.org/10.3390/genes15030321

Cioffi, S., Martucciello, S., Fulcoli, F.G., Bilio, M., Ferrentino, R., Nusco, E., Illingworth, E., 2014. Tbx1 regulates brain vascularization. Hum. Mol. Genet. 23, 78–89. https://doi.org/10.1093/hmg/ddt400

Cirino, A., Aurigemma, I., Franzese, M., Lania, G., Righelli, D., Ferrentino, R., Illingworth, E., Angelini, C., Baldini, A., 2020. Chromatin and Transcriptional Response to Loss of TBX1 in Early Differentiation of Mouse Cells. Front. Cell Dev. Biol. 8.

Claerhout, S., Lim, J.Y., Choi, W., Park, Y.-Y., Kim, K., Kim, S.-B., Lee, J.-S., Mills, G.B., Cho, J.Y., 2011. Gene Expression Signature Analysis Identifies Vorinostat as a Candidate Therapy for Gastric Cancer. PLOS ONE 6, e24662. https://doi.org/10.1371/journal.pone.0024662

Co, M., Barnard, R.A., Jahncke, J.N., Grindstaff, S., Fedorov, L.M., Adey, A.C., Wright, K.M., O'Roak, B.J., 2022. Shared and Distinct Functional Effects of Patient-Specific Tbr1 Mutations on Cortical Development. J. Neurosci. 42, 7166. https://doi.org/10.1523/JNEUROSCI.0409-22.2022

Collinson, A., Collier, A.J., Morgan, N.P., Sienerth, A.R., Chandra, T., Andrews, S., Rugg-Gunn, P.J., 2016. Deletion of the Polycomb-Group Protein EZH2 Leads to Compromised Self-Renewal and Differentiation Defects in Human Embryonic Stem Cells. Cell Rep. 17, 2700–2714. https://doi.org/10.1016/j.celrep.2016.11.032

Conlon, F.L., Fairclough, L., Price, B.M.J., Casey, E.S., Smith, J.C., 2001. Determinants of T box protein specificity. Development 128, 3749–3758. https://doi.org/10.1242/dev.128.19.3749

Conti, E., Grifone, N., Sarkozy, A., Tandoi, C., Marino, B., Digilio, M.C., Mingarelli, R., Pizzuti, A., Dallapiccola, B., 2003. DiGeorge subtypes of nonsyndromic conotruncal defects: evidence against a major role of TBX1 Gene. Eur. J. Hum. Genet. 11, 349–351. https://doi.org/10.1038/sj.ejhg.5200956

Culhane, J.C., Cole, P.A., 2007. LSD1 and the chemistry of histone demethylation. Anal. Tech. Mech. 11, 561–568. https://doi.org/10.1016/j.cbpa.2007.07.014

de Ménorval, M.-A., Mir, L.M., Fernández, M.L., Reigada, R., 2012. Effects of Dimethyl Sulfoxide in Cholesterol-Containing Lipid Membranes: A Comparative Study of Experiments In Silico and with Cells. PLOS ONE 7, e41733. https://doi.org/10.1371/journal.pone.0041733

De Souza, C., Chatterji, B., 2015. HDAC inhibitors as Novel Anti-Cancer therapeutics. Recent Patents Anticancer Drug Discov. 10. https://doi.org/10.2174/1574892810666150317144511

Ding, Q., Wu, X., Li, X., Wang, H., 2022. Vorinostat Corrects Cognitive and Non-Cognitive Symptoms in a Mouse Model of Fragile X Syndrome. Int. J. Neuropsychopharmacol. 25, 147–159. https://doi.org/10.1093/ijnp/pyab081

Diokmetzidou, A., Tsikitis, M., Nikouli, S., Kloukina, I., Tsoupri, E., Papathanasiou, S., Psarras, S., Mavroidis, M., Capetanaki, Y., 2016. Chapter Fifteen - Strategies to Study Desmin in Cardiac Muscle and Culture Systems, in: Omary, M.B., Liem, R.K.H. (Eds.), Methods in Enzymology. Academic Press, pp. 427–459. https://doi.org/10.1016/bs.mie.2015.09.026

DOBROVOLSKAIA-ZAVADSKAIA, N., 1927. Sur la mortification spontanee de la queuw chez la spuris nouveau et sur l'existence d'un caractere (facteur) hereditaire non viable. Compr Soc Biol 97, 114–119.

Dong, L., Lyu, X., Faleti, O.D., He, M.-L., 2019. The special stemness functions of Tbx3 in stem cells and cancer development. Link. Metab. Epigenetic Reprogramming Stem Cells 57, 105–110. https://doi.org/10.1016/j.semcancer.2018.09.010

Eckschlager, T., Plch, J., Stiborova, M., Hrabeta, J., 2017. Histone Deacetylase Inhibitors as Anticancer Drugs. Int. J. Mol. Sci. 18. https://doi.org/10.3390/ijms18071414

El Omari, K., De Mesmaeker, J., Karia, D., Ginn, H., Bhattacharya, S., Mancini, E.J., 2012. Structure of the DNA-bound T-box domain of human TBX1, a transcription factor associated with the DiGeorge syndrome. Proteins Struct. Funct. Bioinforma. 80, 655–660. https://doi.org/10.1002/prot.23208

Eom, T.-Y., Schmitt, J.E., Li, Y., Davenport, C.M., Steinberg, J., Bonnan, A., Alam, S., Ryu, Y.S., Paul, L., Hansen, B.S., Khairy, K., Pelletier, S., Pruett-Miller, S.M., Roalf, D.R., Gur, R.E., Emanuel, B.S., McDonald-McGinn, D.M., Smith, J.N., Li, C., Christie, J.M., Northcott, P.A.,

Zakharenko, S.S., 2024. Tbx1 haploinsufficiency leads to local skull deformity, paraflocculus and flocculus dysplasia, and motor-learning deficit in 22q11.2 deletion syndrome. Nat. Commun. 15, 10510. https://doi.org/10.1038/s41467-024-54837-3

Esteller Manel, 2008. Epigenetics in Cancer. N. Engl. J. Med. 358, 1148–1159. https://doi.org/10.1056/NEJMra072067

Flore, G., Cioffi, S., Bilio, M., Illingworth, E., 2017. Cortical Development Requires Mesodermal Expression of Tbx1, a Gene Haploinsufficient in 22q11.2 Deletion Syndrome. Cereb. Cortex 27, 2210–2225. https://doi.org/10.1093/cercor/bhw076

Forneris, F., Binda, C., Dall'Aglio, A., Fraaije, M.W., Battaglioli, E., Mattevi, A., 2006. A Highly Specific Mechanism of Histone H3-K4 Recognition by Histone Demethylase LSD1 *. J. Biol. Chem. 281, 35289–35295. https://doi.org/10.1074/jbc.M607411200

Fulcoli, F.G., Franzese, M., Liu, X., Zhang, Z., Angelini, C., Baldini, A., 2016. Rebalancing gene haploinsufficiency in vivo by targeting chromatin. Nat. Commun. 7, 11688. https://doi.org/10.1038/ncomms11688

Fulcoli, F.G., Huynh, T., Scambler, P.J., Baldini, A., 2009. Tbx1 Regulates the BMP-Smad1 Pathway in a Transcription Independent Manner. PLOS ONE 4, e6049. https://doi.org/10.1371/journal.pone.0006049

Galvao, J., Davis, B., Tilley, M., Normando, E., Duchen, M.R., Cordeiro, M.F., 2014. Unexpected low-dose toxicity of the universal solvent DMSO. FASEB J. 28, 1317–1330. https://doi.org/10.1096/fj.13-235440

Ganesan, A., Arimondo, P.B., Rots, M.G., Jeronimo, C., Berdasco, M., 2019. The timeline of epigenetic drug discovery: from reality to dreams. Clin. Epigenetics 11, 174. https://doi.org/10.1186/s13148-019-0776-0

Gao, S., Li, X., Amendt, B.A., 2013. Understanding the Role of Tbx1 as a Candidate Gene for 22q11.2 Deletion Syndrome. Curr. Allergy Asthma Rep. 13, 613–621. https://doi.org/10.1007/s11882-013-0384-6

Garg, V., Yamagishi, C., Hu, T., Kathiriya, I.S., Yamagishi, H., Srivastava, D., 2001. Tbx1, a DiGeorge Syndrome Candidate Gene, Is Regulated by Sonic Hedgehog during Pharyngeal Arch Development. Dev. Biol. 235, 62–73. https://doi.org/10.1006/dbio.2001.0283

Ghosh, T.K., Brook, J.D., Wilsdon, A., 2017. Chapter Thirteen - T-Box Genes in Human Development and Disease, in: Frasch, M. (Ed.), Current Topics in Developmental Biology. Academic Press, pp. 383–415. https://doi.org/10.1016/bs.ctdb.2016.08.006

Gong, W., Gottlieb, S., Collins, J., Blescia, A., Dietz, H., Goldmuntz, E., McDonald-McGinn, D.M., Zackai, E.H., Emanuel, B.S., Driscoll, D.A., Budarf, M.L., 2001. Mutation analysis of TBX1 in non-deleted patients with features of DGS/VCFS or isolated cardiovascular defects. J. Med. Genet. 38, e45. https://doi.org/10.1136/jmg.38.12.e45

Gopalakrishnan, S., Van Emburgh, B.O., Robertson, K.D., 2008. DNA methylation in development and human disease. Epigenetics Dev. Hum. Dis. 647, 30–38. https://doi.org/10.1016/j.mrfmmm.2008.08.006

Goyal, R., Reinhardt, R., Jeltsch, A., 2006. Accuracy of DNA methylation pattern preservation by the Dnmt1 methyltransferase. Nucleic Acids Res. 34, 1182–1188. https://doi.org/10.1093/nar/gkl002

Guan, J.-S., Haggarty, S.J., Giacometti, E., Dannenberg, J.-H., Joseph, N., Gao, J., Nieland, T.J.F., Zhou, Y., Wang, X., Mazitschek, R., Bradner, J.E., DePinho, R.A., Jaenisch, R., Tsai, L.-H., 2009. HDAC2 negatively regulates memory formation and synaptic plasticity. Nature 459, 55–60. https://doi.org/10.1038/nature07925

Gui, C.-Y., Ngo, L., Xu, W.S., Richon, V.M., Marks, P.A., 2004. Histone deacetylase (HDAC) inhibitor activation of p21WAF1 involves changes in promoter-associated proteins, including HDAC1. Proc. Natl. Acad. Sci. 101, 1241–1246. https://doi.org/10.1073/pnas.0307708100

Habets, P.E., Moorman, A.F., Clout, D.E., van Roon, M.A., Lingbeek, M., van Lohuizen, M., Campione, M., Christoffels, V.M., 2002. Cooperative action of Tbx2 and Nkx2.5 inhibits ANF expression in the atrioventricular canal: implications for cardiac chamber formation. Genes Dev. 16, 1234–1246.

Hai, R., He, L., Shu, G., Yin, G., 2021. Characterization of Histone Deacetylase Mechanisms in Cancer Development. Front. Oncol. 11.

Hailu, G.S., Robaa, D., Forgione, M., Sippl, W., Rotili, D., Mai, A., 2017. Lysine Deacetylase Inhibitors in Parasites: Past, Present, and Future Perspectives. J. Med. Chem. 60, 4780–4804. https://doi.org/10.1021/acs.jmedchem.6b01595

Hayward, D., Cole, P.A., 2016. Chapter Eleven - LSD1 Histone Demethylase Assays and Inhibition, in: Marmorstein, R. (Ed.), Methods in Enzymology. Academic Press, pp. 261–278. https://doi.org/10.1016/bs.mie.2016.01.020

He, P., Du, L., Hao, P., Yang, H., Ren, Y., Kang, H., Ding, Y., Zhao, W., Xu, Y., Liu, H., 2023. Inhibition of lysine-specific demethylase 1 (LSD1) prevented tumor growth and metastasis by downregulating PD-L1 expression in lung adenocarcinoma. Genes Dis. 10, 1779–1782. https://doi.org/10.1016/j.gendis.2022.11.002

Herrmann, B.G., Labeit, S., Poustka, A., King, T.R., Lehrach, H., 1990. Cloning of the T gene required in mesoderm formation in the mouse. Nature 343, 617–622. https://doi.org/10.1038/343617a0

Hoffmann, I., Roatsch, M., Schmitt, M.L., Carlino, L., Pippel, M., Sippl, W., Jung, M., 2012. The role of histone demethylases in cancer therapy. Mol. Oncol. 6, 683–703. https://doi.org/10.1016/j.molonc.2012.07.004

Hon, G.C., Hawkins, R.D., Ren, B., 2009. Predictive chromatin signatures in the mammalian genome. Hum. Mol. Genet. 18, R195–R201. https://doi.org/10.1093/hmg/ddp409

Hooper, M., Hardy, K., Handyside, A., Hunter, S., Monk, M., 1987. HPRT-deficient (Lesch–Nyhan) mouse embryos derived from germline colonization by cultured cells. Nature 326, 292–295. https://doi.org/10.1038/326292a0

Huynh, T., Chen, L., Terrell, P., Baldini, A., 2007. A fate map of Tbx1 expressing cells reveals heterogeneity in the second cardiac field. genesis 45, 470–475. https://doi.org/10.1002/dvg.20317

Incarnato, D., Krepelova, A., Neri, F., 2014. High-throughput single nucleotide variant discovery in E14 mouse embryonic stem cells provides a new reference genome assembly. Genomics 104, 121–127. https://doi.org/10.1016/j.ygeno.2014.06.007

Jerome, L.A., Papaioannou, V.E., 2001. DiGeorge syndrome phenotype in mice mutant for the T-box gene, Tbx1. Nat. Genet. 27, 286–291. https://doi.org/10.1038/85845

Jin, B., Tao, Q., Peng, J., Soo, H.M., Wu, W., Ying, J., Fields, C.R., Delmas, A.L., Liu, X., Qiu, J., Robertson, K.D., 2008. DNA methyltransferase 3B (DNMT3B) mutations in ICF syndrome lead to altered epigenetic modifications and aberrant expression of genes regulating development, neurogenesis and immune function. Hum. Mol. Genet. 17, 690–709. https://doi.org/10.1093/hmg/ddm341

Jingjing, W., Zhikai, W., Xingyi, Z., Peixuan, L., Yiwu, F., Xia, W., Youpeng, S., Ershun, Z., Zhengtao, Y., 2021. Lysine-specific demethylase 1 (LSD1) serves as an potential epigenetic determinant to regulate inflammatory responses in mastitis. Int. Immunopharmacol. 91, 107324. https://doi.org/10.1016/j.intimp.2020.107324

Julien, C., Marcouiller, F., Bretteville, A., El Khoury, N.B., Baillargeon, J., Hébert, S.S., Planel, E., 2012. Dimethyl Sulfoxide Induces Both Direct and Indirect Tau Hyperphosphorylation. PLOS ONE 7, e40020. https://doi.org/10.1371/journal.pone.0040020

Kamminga, L.M., Bystrykh, L.V., de Boer, A., Houwer, S., Douma, J., Weersing, E., Dontje, B., de Haan, G., 2006. The Polycomb group gene Ezh2 prevents hematopoietic stem cell exhaustion. Blood 107, 2170–2179. https://doi.org/10.1182/blood-2005-09-3585

Kelly, R.G., 2012. Chapter two - The Second Heart Field, in: Bruneau, B.G. (Ed.), Current Topics in Developmental Biology. Academic Press, pp. 33–65. https://doi.org/10.1016/B978-0-12-387786-4.00002-6

Kelly, T.K., De Carvalho, D.D., Jones, P.A., 2010. Epigenetic modifications as therapeutic targets. Nat. Biotechnol. 28, 1069–1078. https://doi.org/10.1038/nbt.1678

Keppler, B.R., Archer, T.K., 2008a. Chromatin-modifying enzymes as therapeutic targets – Part 1. Expert Opin. Ther. Targets 12, 1301–1312. https://doi.org/10.1517/14728222.12.10.1301

Keppler, B.R., Archer, T.K., 2008b. Chromatin-modifying enzymes as therapeutic targets – Part 2. Expert Opin. Ther. Targets 12, 1457–1467. https://doi.org/10.1517/14728222.12.11.1457

Kerstjens-Frederikse, W.S., Bongers, E.M.H.F., Roofthooft, M.T.R., Leter, E.M., Douwes, J.M., Van Dijk, A., Vonk-Noordegraaf, A., Dijk-Bos, K.K., Hoefsloot, L.H., Hoendermis, E.S., Gille, J.J.P., Sikkema-Raddatz, B., Hofstra, R.M.W., Berger, R.M.F., 2013. TBX4 mutations (small patella syndrome) are associated with childhood-onset pulmonary arterial hypertension. J. Med. Genet. 50, 500. https://doi.org/10.1136/jmedgenet-2012-101152

Kispert, A., Herrmann, B.G., 1993. The Brachyury gene encodes a novel DNA binding protein. EMBO J. 12, 3211–3220. https://doi.org/10.1002/j.1460-2075.1993.tb05990.x

Kispert, A., Koschorz, B., Herrmann, B.G., 1995. The T protein encoded by Brachyury is a tissue-specific transcription factor. EMBO J. 14, 4763–4772. https://doi.org/10.1002/j.1460-2075.1995.tb00158.x

Lania, G., Zhang, Z., Huynh, T., Caprio, C., Moon, A.M., Vitelli, F., Baldini, A., 2009. Early thyroid development requires a Tbx1–Fgf8 pathway. Dev. Biol. 328, 109–117. https://doi.org/10.1016/j.ydbio.2009.01.014

Li, F.R., Gemayel, M., Lévesque, M., Wang, S., Suarez, C.F., Avoli, M., 2024. Low concentration dimethyl sulfoxide (DMSO) modulates epileptiform synchronization in the 4-aminopyridine in vitro model. J. Neurosci. Methods 411, 110255. https://doi.org/10.1016/j.jneumeth.2024.110255

Li, S., Luo, X., Sun, M., Wang, Yijun, Zhang, Z., Jiang, J., Hu, D., Zhang, J., Wu, Z., Wang, Yufei, Huang, W., Xia, L., 2024. Context-dependent T-BOX transcription factor family: from biology to targeted therapy. Cell Commun. Signal. 22, 350. https://doi.org/10.1186/s12964-024-01719-2

Liang, G., Chan, M.F., Tomigahara, Y., Tsai, Y.C., Gonzales, F.A., Li, E., Laird, P.W., Jones, P.A., 2002. Cooperativity between DNA Methyltransferases in the Maintenance Methylation of Repetitive Elements. Mol. Cell. Biol. 22, 480–491. https://doi.org/10.1128/MCB.22.2.480-491.2002

Liao, J., Aggarwal, V.S., Nowotschin, S., Bondarev, A., Lipner, S., Morrow, B.E., 2008. Identification of downstream genetic pathways of Tbx1 in the second heart field. Dev. Biol. 316, 524–537. https://doi.org/10.1016/j.ydbio.2008.01.037

Liao, J., Kochilas, L., Nowotschin, S., Arnold, J.S., Aggarwal, V.S., Epstein, J.A., Brown, M.C., Adams, J., Morrow, B.E., 2004. Full spectrum of malformations in velo-cardio-facial syndrome/DiGeorge syndrome mouse models by altering Tbx1 dosage. Hum. Mol. Genet. 13, 1577–1585. https://doi.org/10.1093/hmg/ddh176

Lillico, R., Lawrence, C.K., Lakowski, T.M., 2018. Selective DOT1L, LSD1, and HDAC Class I Inhibitors Reduce HOXA9 Expression in MLL-AF9 Rearranged Leukemia Cells, But Dysregulate the Expression of Many Histone-Modifying Enzymes. J. Proteome Res. 17, 2657–2667. https://doi.org/10.1021/acs.jproteome.8b00118

Lin, C.-C., Chen, Y.-P., Yang, W.-Z., Shen, J.C.K., Yuan, H.S., 2020. Structural insights into CpG-specific DNA methylation by human DNA methyltransferase 3B. Nucleic Acids Res. 48, 3949–3961. https://doi.org/10.1093/nar/gkaa111

Lindsay, E.A., 2001. Chromosomal microdeletions: dissecting del22q11 syndrome. Nat. Rev. Genet. 2, 858–868. https://doi.org/10.1038/35098574

Lindsay, E.A., Vitelli, F., Su, H., Morishima, M., Huynh, T., Pramparo, T., Jurecic, V., Ogunrinu, G., Sutherland, H.F., Scambler, P.J., Bradley, A., Baldini, A., 2001. Tbx1 haploinsufficiency in the DiGeorge syndrome region causes aortic arch defects in mice. Nature 410, 97–101. https://doi.org/10.1038/35065105

Lu, R., Yang, A., Jin, Y., 2011. Dual Functions of T-Box 3 (Tbx3) in the Control of Self-renewal and Extraembryonic Endoderm Differentiation in Mouse Embryonic Stem Cells *. J. Biol. Chem. 286, 8425–8436. https://doi.org/10.1074/jbc.M110.202150

Maiques-Diaz, A., Somervaille, T.C., 2016. LSD1: Biologic Roles and Therapeutic Targeting. Epigenomics 8, 1103–1116. https://doi.org/10.2217/epi-2016-0009

Manal, M., Chandrasekar, M.J.N., Gomathi Priya, J., Nanjan, M.J., 2016. Inhibitors of histone deacetylase as antitumor agents: A critical review. Bioorganic Chem. 67, 18–42. https://doi.org/10.1016/j.bioorg.2016.05.005

Mann, B.S., Johnson, J.R., Cohen, M.H., Justice, R., Pazdur, R., 2007. FDA Approval Summary: Vorinostat for Treatment of Advanced Primary Cutaneous T-Cell Lymphoma. The Oncologist 12, 1247–1252. https://doi.org/10.1634/theoncologist.12-10-1247

Marks, P.A., Breslow, R., 2007. Dimethyl sulfoxide to vorinostat: development of this histone deacetylase inhibitor as an anticancer drug. Nat. Biotechnol. 25, 84–90. https://doi.org/10.1038/nbt1272

Marks, P.A., Rifkind, R.A., Richon, V.M., Breslow, R., Miller, T., Kelly, W.K., 2001. Histone deacetylases and cancer: causes and therapies. Nat. Rev. Cancer 1, 194–202. https://doi.org/10.1038/35106079

Martucciello, S., Turturo, M.G., Bilio, M., Cioffi, S., Chen, L., Baldini, A., Illingworth, E., 2020. A dual role for Tbx1 in cardiac lymphangiogenesis through genetic interaction with Vegfr3. FASEB J. 34, 15062–15079. https://doi.org/10.1096/fj.201902202R

McCabe, M.T., Ott, H.M., Ganji, G., Korenchuk, S., Thompson, C., Van Aller, G.S., Liu, Y., Graves, A.P., Iii, A.D., Diaz, E., 2012. EZH2 Inhibition as A Therapeutic Strategy for Lymphoma with EZH2-Activating Mutations. Nature 492, 108.

McDonald-McGinn, D.M., Sullivan, K.E., Marino, B., Philip, N., Swillen, A., Vorstman, J.A.S., Zackai, E.H., Emanuel, B.S., Vermeesch, J.R., Morrow, B.E., Scambler, P.J., Bassett, A.S., 2015. 22q11.2 deletion syndrome. Nat. Rev. Dis. Primer 1, 15071. https://doi.org/10.1038/nrdp.2015.71

McMahon, K.W., Karunasena, E., Ahuja, N., 2017. The Roles of DNA Methylation in the Stages of Cancer. Cancer J. 23.

Merscher, S., Funke, B., Epstein, J.A., Heyer, J., Puech, A., Lu, M.M., Xavier, R.J., Demay, M.B., Russell, R.G., Factor, S., Tokooya, K., Jore, B.St., Lopez, M., Pandita, R.K., Lia, M., Carrion, D., Xu, H., Schorle, H., Kobler, J.B., Scambler, P., Wynshaw-Boris, A., Skoultchi, A.I., Morrow, B.E., Kucherlapati, R., 2001. TBX1 Is Responsible for Cardiovascular Defects in Velo-Cardio-Facial/DiGeorge Syndrome. Cell 104, 619–629. https://doi.org/10.1016/S0092-8674(01)00247-1

Metzger, E., Wissmann, M., Yin, N., Müller, J.M., Schneider, R., Peters, A.H.F.M., Günther, T., Buettner, R., Schüle, R., 2005. LSD1 demethylates repressive histone marks to promote androgen-receptor-dependent transcription. Nature 437, 436–439. https://doi.org/10.1038/nature04020

Mohammad, H.P., Smitheman, K.N., Kamat, C.D., Soong, D., Federowicz, K.E., Van Aller, G.S., Schneck, J.L., Carson, J.D., Liu, Y., Butticello, M., Bonnette, W.G., Gorman, S.A., Degenhardt, Y., Bai, Y., McCabe, M.T., Pappalardi, M.B., Kasparec, J., Tian, X., McNulty, K.C., Rouse, M., McDevitt, P., Ho, T., Crouthamel, M., Hart, T.K., Concha, N.O., McHugh, C.F., Miller, W.H., Dhanak, D., Tummino, P.J., Carpenter, C.L., Johnson, N.W., Hann, C.L., Kruger, R.G., 2015. A DNA Hypomethylation Signature Predicts Antitumor Activity of LSD1 Inhibitors in SCLC. Cancer Cell 28, 57.

Moore, L.D., Le, T., Fan, G., 2013. DNA Methylation and Its Basic Function. Neuropsychopharmacology 38, 23–38. https://doi.org/10.1038/npp.2012.112

Morel, D., Jeffery, D., Aspeslagh, S., Almouzni, G., Postel-Vinay, S., 2020. Combining epigenetic drugs with other therapies for solid tumours — past lessons and future promise. Nat. Rev. Clin. Oncol. 17, 91–107. https://doi.org/10.1038/s41571-019-0267-4

Morsheimer, M., Brown Whitehorn, T.F., Heimall, J., Sullivan, K.E., 2017. The immune deficiency of chromosome 22q11.2 deletion syndrome. Am. J. Med. Genet. A. 173, 2366–2372. https://doi.org/10.1002/ajmg.a.38319

Müller, C.W., Herrmann, B.G., 1997. Crystallographic structure of the T domain–DNA complex of the Brachyury transcription factor. Nature 389, 884–888. https://doi.org/10.1038/39929

Murphy, K.C., Jones, L.A., Owen, M.J., 1999. High Rates of Schizophrenia in Adults With Velo-Cardio-Facial Syndrome. Arch. Gen. Psychiatry 56, 940–945. https://doi.org/10.1001/archpsyc.56.10.940

Murry, C.E., Keller, G., 2008. Differentiation of Embryonic Stem Cells to Clinically Relevant Populations: Lessons from Embryonic Development. Cell 132, 661–680. https://doi.org/10.1016/j.cell.2008.02.008

Naiche, L.A., Arora, R., Kania, A., Lewandoski, M., Papaioannou, V.E., 2011. Identity and fate of Tbx4-expressing cells reveal developmental cell fate decisions in the allantois, limb, and external genitalia. Dev. Dyn. 240, 2290–2300. https://doi.org/10.1002/dvdy.22731

Naiche, L.A., Harrelson, Z., Kelly, R.G., Papaioannou, V.E., 2005. T-Box Genes in Vertebrate Development. Annu. Rev. Genet. https://doi.org/10.1146/annurev.genet.39.073003.105925

Naiche, L.A., Papaioannou, V.E., 2003. Loss of Tbx4 blocks hindlimb development and affects vascularization and fusion of the allantois. Development 130, 2681–2693. https://doi.org/10.1242/dev.00504

Nebbioso, A., Carafa, V., Benedetti, R., Altucci, L., 2012. Trials with 'epigenetic' drugs: an update. Mol Oncol 6, 657.

Niarchou, M., Martin, J., Thapar, A., Owen, M.J., van den Bree, M.B.M., 2015. The clinical presentation of attention deficit-hyperactivity disorder (ADHD) in children with 22q11.2 deletion syndrome. Am. J. Med. Genet. B Neuropsychiatr. Genet. 168, 730–738. https://doi.org/10.1002/ajmg.b.32378

Niklasson, L., Rasmussen, P., Óskarsdóttir, S., Gillberg, C., 2001. Neuropsychiatric disorders in the 22q11 deletion syndrome. Genet. Med. 3, 79–84. https://doi.org/10.1097/00125817-200101000-00017

Notman, R., Noro, M., O'Malley, B., Anwar, J., 2006. Molecular Basis for Dimethylsulfoxide (DMSO) Action on Lipid Membranes. J. Am. Chem. Soc. 128, 13982–13983. https://doi.org/10.1021/ja063363t

O. Moradei, C. R. Maroun, I. Paquin, A. Vaisburg, 2005. Histone Deacetylase Inhibitors: Latest Developments, Trends and Prospects. Contin. Anti-Cancer Agents Med. Chem. 5, 529–560. https://doi.org/10.2174/1568011054866946

Ogata, T., Niihori, T., Tanaka, N., Kawai, M., Nagashima, T., Funayama, R., Nakayama, K., Nakashima, S., Kato, F., Fukami, M., Aoki, Y., Matsubara, Y., 2014. TBX1 Mutation Identified by Exome Sequencing in a Japanese Family with 22q11.2 Deletion Syndrome-Like Craniofacial Features and Hypocalcemia. PLOS ONE 9, e91598. https://doi.org/10.1371/journal.pone.0091598

O'Meara, M.M., Simon, J.A., 2012. Inner Workings and Regulatory Inputs that Control Polycomb Repressive Complex 2. Chromosoma 121, 221.

Pane, L.S., Fulcoli, F., Cirino, A., Altomonte, A., Ferrentino, R., Bilio, M., Baldini, A., 2018. Tbx1 represses Mef2c gene expression and is correlated with histone 3 deacetylation of the anterior heart field enhancer. Dis. Model. Mech. 11, dmm029967. https://doi.org/10.1242/dmm.029967

Pane, L.S., Zhang, Z., Ferrentino, R., Huynh, T., Cutillo, L., Baldini, A., 2012. Tbx1 is a negative modulator of Mef2c. Hum. Mol. Genet. 21, 2485–2496. https://doi.org/10.1093/hmg/dds063

Papaioannou, V.E., 2014. The T-box gene family: emerging roles in development, stem cells and cancer. Development 141, 3819–3833. https://doi.org/10.1242/dev.104471

Papaioannou, V.E., 2001. T-box genes in development: From hydra to humans, in: International Review of Cytology. Academic Press, pp. 1–70. https://doi.org/10.1016/S0074-7696(01)07002-4

Papaioannou, V.E., Goldin, S.N., 2008. Introduction to the T-box genes and their roles in developmental signaling pathways., in: Epstein, C.J., Erickson, R.P., Wynshaw-Boris, A. (Eds.), In Inborn Errors of Development. The Molecular Basis of Clinical Disorders of Morphogenesis. Oxford: Oxford University Press., pp. 852–861.

Paylor, R., Glaser, B., Mupo, A., Ataliotis, P., Spencer, C., Sobotka, A., Sparks, C., Choi, C.-H., Oghalai, J., Curran, S., Murphy, K.C., Monks, S., Williams, N., O'Donovan, M.C., Owen, M.J., Scambler, P.J., Lindsay, E., 2006. Tbx1 haploinsufficiency is linked to behavioral disorders in mice and humans: Implications for 22q11 deletion syndrome. Proc. Natl. Acad. Sci. 103, 7729–7734. https://doi.org/10.1073/pnas.0600206103

Pepenella, S., Murphy, K.J., Hayes, J.J., 2014. Intra- and inter-nucleosome interactions of the core histone tail domains in higher-order chromatin structure. Chromosoma 123, 3–13. https://doi.org/10.1007/s00412-013-0435-8

Pradhan, S., Talbot, D., Sha, M., Benner, J., Hornstra, L., Li, E., Jaenisch, R., Roberts, R.J., 1997. Baculovirus-mediated expression and characterization of the full-length murine DNA methyltransferase. Nucleic Acids Res. 25, 4666–4673. https://doi.org/10.1093/nar/25.22.4666

Prapa, M., Lago-Docampo, M., Swietlik, E.M., Montani, D., Eyries, M., Humbert, M., Welch, C.L., Chung, W.K., Berger, R.M.F., Bogaard, H.J., Danhaive, O., Escribano-Subías, P., Gall, H., Girerd, B., Hernandez-Gonzalez, I., Holden, S., Hunt, D., Jansen, S.M.A., Kerstjens-Frederikse, W., Kiely, D.G., Lapunzina, P., McDermott, J., Moledina, S., Pepke-Zaba, J., Polwarth, G.J., Schotte, G., Tenorio-Castaño, J., Thompson, A.A.R., Wharton, J., Wort, S.J., Megy, K., Mapeta, R., Treacy, C.M., Martin, J.M., Li, W., Swift, A.J., Upton, P.D., Morrell, N.W., Gräf, S., Valverde, D., 2022. First Genotype–Phenotype Study in TBX4 Syndrome: Gain-of-Function Mutations Causative for Lung Disease. Am. J. Respir. Crit. Care Med. 206, 1522–1533. https://doi.org/10.1164/rccm.202203-0485OC

Prince, S., Carreira, S., Vance, K.W., Abrahams, A., Goding, C.R., 2004. Tbx2 Directly Represses the Expression of the p21WAF1 Cyclin-Dependent Kinase Inhibitor. Cancer Res. 64, 1669–1674. https://doi.org/10.1158/0008-5472.CAN-03-3286

Quina, A.S., Buschbeck, M., Di Croce, L., 2006. Chromatin structure and epigenetics. Spec. Issue Cell Signal. Transcr. Transl. Ther. Targets 72, 1563–1569. https://doi.org/10.1016/j.bcp.2006.06.016

Ramachandran, A., Omar, M., Cheslock, P., Schnitzler, G.R., 2003. Linker Histone H1 Modulates Nucleosome Remodeling by Human SWI/SNF*. J. Biol. Chem. 278, 48590–48601. https://doi.org/10.1074/jbc.M309033200

Rana, M.S., Sizarov, A., Christoffels, V.M., Moorman, A.F.M., 2014. Development of the human aortic arch system captured in an interactive three-dimensional reference model. Am. J. Med. Genet. A. 164, 1372–1383. https://doi.org/10.1002/ajmg.a.35881

Richon, V.M., Sandhoff, T.W., Rifkind, R.A., Marks, P.A., 2000. Histone deacetylase inhibitor selectively induces p21WAF1 expression and gene-associated histone acetylation. Proc. Natl. Acad. Sci. 97, 10014–10019. https://doi.org/10.1073/pnas.180316197

Robertson, K.D., 2005. DNA methylation and human disease. Nat. Rev. Genet. 6, 597–610. https://doi.org/10.1038/nrg1655

Rossetto, D., Avvakumov, N., Côté, J., 2012. Histone phosphorylation. Epigenetics 7, 1098–1108. https://doi.org/10.4161/epi.21975

Russ, A.P., Wattler, S., Colledge, W.H., Aparicio, S.A.J.R., Carlton, M.B.L., Pearce, J.J., Barton, S.C., Surani, M.A., Ryan, K., Nehls, M.C., Wilson, V., Evans, M.J., 2000. Eomesodermin is required for mouse trophoblast development and mesoderm formation. Nature 404, 95–99. https://doi.org/10.1038/35003601

Ryan, A.K., Goodship, J.A., Wilson, D.I., Philip, N., Levy, A., Seidel, H., Schuffenhauer, S., Oechsler, H., Belohradsky, B., Prieur, M., Aurias, A., Raymond, F.L., Clayton-Smith, J., Hatchwell, E., McKeown, C., Beemer, F.A., Dallapiccola, B., Novelli, G., Hurst, J.A., Ignatius, J., Green, A.J., Winter, R.M., Brueton, L., Brøndum-Nielsen, K., Scambler, P.J., 1997. Spectrum of clinical features associated with interstitial chromosome 22q11 deletions: a European collaborative study. J. Med. Genet. 34, 798. https://doi.org/10.1136/jmg.34.10.798

Sacilotto, N., Dessanti, P., Lufino, M.M.P., Ortega, A., Rodríguez-Gimeno, A., Salas, J., Maes, T., Buesa, C., Mascaró, C., Soliva, R., 2021. Comprehensive in Vitro Characterization of the LSD1 Small Molecule Inhibitor Class in Oncology. ACS Pharmacol. Transl. Sci. 4, 1818–1834. https://doi.org/10.1021/acsptsci.1c00223

Salarinia, R., A, S., Peyvandi, M., Mirzaei, H.R., Jaafari, mahmoud reza, Matbou Riahi, M., Ebrahimnejad, H., Sadri Nahand, J., Hadjati, J., MO, A., S, F., Salehi, R., H, M., 2016. Epi-Drugs and Epi-miRs: Moving Beyond Current Cancer Therapies. Curr. Cancer Drug Targets.

Sangwan, R., Rajan, R., Mandal, P.K., 2018. HDAC as onco target: Reviewing the synthetic approaches with SAR study of their inhibitors. Eur. J. Med. Chem. 158, 620–706. https://doi.org/10.1016/j.ejmech.2018.08.073

Sankpal, U.T., Abdelrahim, M., Connelly, S.F., Lee, C.M., Madero-Visbal, R., Colon, J., Smith, J., Safe, S., Maliakal, P., Basha, R., 2012. Small molecule tolfenamic acid inhibits PC-3 cell proliferation and invasion in vitro, and tumor growth in orthotopic mouse model for prostate cancer. The Prostate 72, 1648–1658. https://doi.org/10.1002/pros.22518

Sato, T., Kaneda, A., Tsuji, S., Isagawa, T., Yamamoto, S., Fujita, T., Yamanaka, R., Tanaka, Y., Nukiwa, T., Marquez, V.E., Ishikawa, Y., Ichinose, M., Aburatani, H., 2013. PRC2 overexpression and PRC2-target gene repression relating to poorer prognosis in small cell lung cancer. Sci. Rep. 3, 1911. https://doi.org/10.1038/srep01911

Saxonov, S., Berg, P., Brutlag, D.L., 2006. A genome-wide analysis of CpG dinucleotides in the human genome distinguishes two distinct classes of promoters. Proc. Natl. Acad. Sci. 103, 1412–1417. https://doi.org/10.1073/pnas.0510310103

Schneider, M., Debbané, M., Bassett, A.S., Chow, E.W.C., Fung, W.L.A., van den Bree, M.B.M., Owen, M., Murphy, K.C., Niarchou, M., Kates, W.R., Antshel, K.M., Fremont, W., McDonald-McGinn, D.M., Gur, R.E., Zackai, E.H., Vorstman, J., Duijff, S.N., Klaassen, P.W.J., Swillen, A., Gothelf, D., Green, T., Weizman, A., Van Amelsvoort, T., Evers, L., Boot, E., Shashi, V., Hooper, S.R., Bearden, C.E., Jalbrzikowski, M., Armando, M., Vicari, S., Murphy, D.G., Ousley, O., Campbell, L.E., Simon, T.J., Eliez, S., 2014. Psychiatric Disorders From Childhood to Adulthood in 22q11.2 Deletion Syndrome: Results From the International Consortium on Brain and Behavior in 22q11.2 Deletion Syndrome. Am. J. Psychiatry 171, 627–639. https://doi.org/10.1176/appi.ajp.2013.13070864

Scourzic, L., Mouly, E., Bernard, O.A., 2015. TET proteins and the control of cytosine demethylation in cancer. Genome Med. 7, 9. https://doi.org/10.1186/s13073-015-0134-6

Seifert, T., Stoelting, S., Wagner, T., Peters, S.O., 2008. Vasculogeneic maturation of E14 embryonic stem cells with evidence of early vascular endothelial growth factor independency. Differentiation 76, 857–867. https://doi.org/10.1111/j.1432-0436.2008.00271.x

Selvi, R.B., Kundu, T.K., 2009. Reversible acetylation of chromatin: Implication in regulation of gene expression, disease and therapeutics. Biotechnol. J. 4, 375–390. https://doi.org/10.1002/biot.200900032

Seto, E., Yoshida, M., 2014. Erasers of Histone Acetylation: The Histone Deacetylase Enzymes. Cold Spring Harb. Perspect. Biol. 6, a018713. https://doi.org/10.1101/cshperspect.a018713

Shi, X., Kachirskaia, I., Yamaguchi, H., West, L.E., Wen, H., Wang, E.W., Dutta, S., Appella, E., Gozani, O., 2007. Modulation of p53 Function by SET8-Mediated Methylation at Lysine 382. Mol Cell 27, 636.

Shi, Yujiang, Lan, F., Matson, C., Mulligan, P., Whetstine, J.R., Cole, P.A., Casero, R.A., Shi, Yang, 2004. Histone Demethylation Mediated by the Nuclear Amine Oxidase Homolog LSD1. Cell 119, 941–953. https://doi.org/10.1016/j.cell.2004.12.012

Smitheman, K.N., Severson, T.M., Rajapurkar, S.R., McCabe, M.T., Karpinich, N., Foley, J., Pappalardi, M.B., Hughes, A., Halsey, W., Thomas, E., Traini, C., Federowicz, K.E., Laraio, J., Mobegi, F., Ferron-Brady, G., Prinjha, R.K., Carpenter, C.L., Kruger, R.G., Wessels, L., Mohammad, H.P., 2019. Lysine specific demethylase 1 inactivation enhances differentiation and promotes cytotoxic response when combined with all-trans retinoic acid in acute myeloid leukemia across subtypes. Haematologica 104, 1156.

Stennard, F.A., Costa, M.W., Lai, D., Biben, C., Furtado, M.B., Solloway, M.J., McCulley, D.J., Leimena, C., Preis, J.I., Dunwoodie, S.L., Elliott, D.E., Prall, O.W.J., Black, B.L., Fatkin, D., Harvey, R.P., 2005. Murine T-box transcription factor Tbx20 acts as a repressor during heart development, and is essential for adult heart integrity, function and adaptation. Development 132, 2451–2462. https://doi.org/10.1242/dev.01799

Stirnimann, C.U., Ptchelkine, D., Grimm, C., Müller, C.W., 2010. Structural Basis of TBX5–DNA Recognition: The T-Box Domain in Its DNA-Bound and -Unbound Form. J. Mol. Biol. 400, 71–81. https://doi.org/10.1016/j.jmb.2010.04.052

Stoller, J.Z., Huang, L., Tan, C.C., Huang, F., Zhou, D.D., Yang, J., Gelb, B.D., Epstein, J.A., 2010. Ash2l interacts with Tbx1 and is required during early embryogenesis. Exp. Biol. Med. 235, 569–576. https://doi.org/10.1258/ebm.2010.009318

Sung, H., Ferlay, J., Siegel, R.L., Laversanne, M., Soerjomataram, I., Jemal, A., Bray, F., 2021. Global Cancer Statistics 2020: GLOBOCAN Estimates of Incidence and Mortality Worldwide for 36 Cancers in 185 Countries. CA. Cancer J. Clin. 71, 209–249. https://doi.org/10.3322/caac.21660

Szmant, H.H., 1975. PHYSICAL PROPERTIES OF DIMETHYL SULFOXIDE AND ITS FUNCTION IN BIOLOGICAL SYSTEMS. Ann. N. Y. Acad. Sci. 243, 20–23. https://doi.org/10.1111/j.1749-6632.1975.tb25340.x

Takai, N., Desmond, J.C., Kumagai, T., Gui, D., Said, J.W., Whittaker, S., Miyakawa, I., Koeffler, H.P., 2004a. Histone Deacetylase Inhibitors Have a Profound Antigrowth Activity in

Endometrial Cancer Cells. Clin. Cancer Res. 10, 1141–1149. https://doi.org/10.1158/1078-0432.CCR-03-0100

Takai, N., Kawamata, N., Gui, D., Said, J.W., Miyakawa, I., Koeffler, H.P., 2004b. Human ovarian carcinoma cells: Histone deacetylase inhibitors exhibit antiproliferative activity and potently induce apoptosis. Cancer 101, 2760–2770. https://doi.org/10.1002/cncr.20709

Tan, A.H.Y., Tu, W., McCuaig, R., Hardy, K., Donovan, T., Tsimbalyuk, S., Forwood, J.K., Rao, S., 2019. Lysine-Specific Histone Demethylase 1A Regulates Macrophage Polarization and Checkpoint Molecules in the Tumor Microenvironment of Triple-Negative Breast Cancer. Front. Immunol. 10.

Thinnes, C.C., England, K.S., Kawamura, A., Chowdhury, R., Schofield, C.J., Hopkinson, R.J., 2014. Targeting histone lysine demethylases — Progress, challenges, and the future. Methylation Multifaceted Modif. - Look. Transcr. Beyond 1839, 1416–1432. https://doi.org/10.1016/j.bbagrm.2014.05.009

Torres-Juan, L., Rosell, J., Morla, M., Vidal-Pou, C., García-Algas, F., de la Fuente, M.-A., Juan, M., Tubau, A., Bachiller, D., Bernues, M., Perez-Granero, A., Govea, N., Busquets, X., Heine-Suñer, D., 2007. Mutations in TBX1 genocopy the 22q11.2 deletion and duplication syndromes: a new susceptibility factor for mental retardation. Eur. J. Hum. Genet. 15, 658–663. https://doi.org/10.1038/sj.ejhg.5201819

Turner, B.M., 2000. Histone acetylation and an epigenetic code. BioEssays 22, 836–845. https://doi.org/10.1002/1521-1878(200009)22:9<836::AID-BIES9>3.0.CO;2-X

Ungerstedt, J.S., Sowa, Y., Xu, W.-S., Shao, Y., Dokmanovic, M., Perez, G., Ngo, L., Holmgren, A., Jiang, X., Marks, P.A., 2005. Role of thioredoxin in the response of normal and transformed cells to histone deacetylase inhibitors. Proc. Natl. Acad. Sci. 102, 673–678. https://doi.org/10.1073/pnas.0408732102

van Ouwerkerk, A.F., Bosada, F.M., van Duijvenboden, K., Houweling, A.C., Scholman, K.T., Wakker, V., Allaart, C.P., Uhm, J.-S., Mathijssen, I.B., Baartscheer, T., Postma, A.V., Barnett, P., Verkerk, A.O., Boukens, B.J., Christoffels, V.M., 2022. Patient-Specific TBX5-G125R Variant Induces Profound Transcriptional Deregulation and Atrial Dysfunction. Circulation 145, 606–619. https://doi.org/10.1161/CIRCULATIONAHA.121.054347

Vangkilde, A., Olsen, L., Hoeffding, L.K., Pedersen, C.B., Mortensen, P.B., Werge, T., Trabjerg, B., 2016. Schizophrenia Spectrum Disorders in a Danish 22q11.2 Deletion Syndrome Cohort Compared to the Total Danish Population—A Nationwide Register Study. Schizophr. Bull. 42, 824–831. https://doi.org/10.1093/schbul/sbv195

Vanyai, H.K., Thomas, T., Voss, A.K., 2015. Mesodermal expression of Moz is necessary for cardiac septum development. Dev. Biol. 403, 22–29. https://doi.org/10.1016/j.ydbio.2015.04.011

Verdelli, C., Avagliano, L., Guarnieri, V., Cetani, F., Ferrero, S., Vicentini, L., Beretta, E., Scillitani, A., Creo, P., Bulfamante, G.P., Vaira, V., Corbetta, S., 2017. Expression, function, and regulation of the embryonic transcription factor TBX1 in parathyroid tumors. Lab. Invest. 97, 1488–1499. https://doi.org/10.1038/labinvest.2017.88

Vermeulen, M., Eberl, H.C., Matarese, F., Marks, H., Denissov, S., Butter, F., Lee, K.K., Olsen, J.V., Hyman, A.A., Stunnenberg, H.G., Mann, M., 2010. Quantitative Interaction Proteomics and Genome-wide Profiling of Epigenetic Histone Marks and Their Readers. Cell 142, 967–980. https://doi.org/10.1016/j.cell.2010.08.020

Vorstman, J.A.S., Breetvelt, E.J., Duijff, S.N., Eliez, S., Schneider, M., Jalbrzikowski, M., Armando, M., Vicari, S., Shashi, V., Hooper, S.R., Chow, E.W.C., Fung, W.L.A., Butcher, N.J., Young, D.A., McDonald-McGinn, D.M., Vogels, A., van Amelsvoort, T., Gothelf, D., Weinberger, R., Weizman, A., Klaassen, P.W.J., Koops, S., Kates, W.R., Antshel, K.M., Simon, T.J., Ousley, O.Y., Swillen, A., Gur, R.E., Bearden, C.E., Kahn, R.S., Bassett, A.S., for the International Consortium on Brain and Behavior in 22q11.2 Deletion Syndrome, 2015. Cognitive Decline Preceding the Onset of Psychosis in Patients With 22q11.2 Deletion Syndrome. JAMA Psychiatry 72, 377–385. https://doi.org/10.1001/jamapsychiatry.2014.2671

Voss, A.K., Vanyai, H.K., Collin, C., Dixon, M.P., McLennan, T.J., Sheikh, B.N., Scambler, P., Thomas, T., 2012. MOZ regulates the Tbx1 locus, and Moz mutation partially phenocopies DiGeorge syndrome. Dev. Cell 23, 652–663. https://doi.org/10.1016/j.devcel.2012.07.010

Waddington, C.H., 1942. The epigenotype. Endeavour 1, 18–20.

Wang, W., Li, X., Ding, X., Xiong, S., Hu, Z., Lu, X., Zhang, K., Zhang, H., Hu, Q., Lai, K.S., Chen, Z., Yang, J., Song, H., Wang, Y., Wei, L., Xia, Z., Zhou, B., He, Y., Pu, J., Liu, X., Ke, R., Wu, T., Huang, C., Baldini, A., Zhang, M., Zhang, Z., 2023. Lymphatic endothelial transcription factor Tbx1 promotes an immunosuppressive microenvironment to facilitate post-myocardial infarction repair. Immunity 56, 2342-2357.e10. https://doi.org/10.1016/j.immuni.2023.07.019

Wawruszak, A., Borkiewicz, L., Okon, E., Kukula-Koch, W., Afshan, S., Halasa, M., 2021. Vorinostat (SAHA) and Breast Cancer: An Overview. Cancers 13. https://doi.org/10.3390/cancers13184700

Webster, A.L.H., Yan, M.S.-C., Marsden, P.A., 2013. Epigenetics and Cardiovascular Disease. Can. J. Cardiol. 29, 46–57. https://doi.org/10.1016/j.cjca.2012.10.023

Wehn, A.K., Farkas, D.R., Sedlock, C.E., Subedi, D., Chapman, D.L., 2020. Functionally distinct roles for T and Tbx6 during mouse development. Biol. Open 9, bio054692. https://doi.org/10.1242/bio.054692

Wei, J., Huang, K., Yang, C., Kan, C., 2017. Non-coding RNAs as regulators in epigenetics (Review). Oncol. Rep. 37, 3–9.

Weidgang, C.E., Russell, R., Tata, P.R., Kühl, S.J., Illing, A., Müller, M., Lin, Q., Brunner, C., Boeckers, T.M., Bauer, K., Kartikasari, A.E.R., Guo, Y., Radenz, M., Bernemann, C., Weiß, M., Seufferlein, T., Zenke, M., Iacovino, M., Kyba, M., Schöler, H.R., Kühl, M., Liebau, S., Kleger, A., 2013. TBX3 Directs Cell-Fate Decision toward Mesendoderm. Stem Cell Rep. 1, 248–265. https://doi.org/10.1016/j.stemcr.2013.08.002

Wiles, E.T., Selker, E.U., 2017. H3K27 methylation: a promiscuous repressive chromatin mark. Genome Archit. Expr. 43, 31–37. https://doi.org/10.1016/j.gde.2016.11.001

Willmer, T., Hare, S., Peres, J., Prince, S., 2016. The T-box transcription factor TBX3 drives proliferation by direct repression of the p21WAF1 cyclin-dependent kinase inhibitor. Cell Div. 11, 6. https://doi.org/10.1186/s13008-016-0019-0

Wilson, M.D., Benlekbir, S., Fradet-Turcotte, A., Sherker, A., Julien, J.-P., McEwan, A., Noordermeer, S.M., Sicheri, F., Rubinstein, J.L., Durocher, D., 2016. The structural basis of modified nucleosome recognition by 53BP1. Nature 536, 100–103. https://doi.org/10.1038/nature18951

Wilson, V., Conlon, F.L., 2002. The T-box family. Genome Biol. 3, reviews3008.1. https://doi.org/10.1186/gb-2002-3-6-reviews3008

Xu, H., Cerrato, F., Baldini, A., 2005. Timed mutation and cell-fate mapping reveal reiterated roles of Tbx1 during embryogenesis, and a crucial function during segmentation of the pharyngeal system via regulation of endoderm expansion. Development 132, 4387–4395. https://doi.org/10.1242/dev.02018

Xu, H., Morishima, M., Wylie, J.N., Schwartz, R.J., Bruneau, B.G., Lindsay, E.A., Baldini, A., 2004. Tbx1 has a dual role in the morphogenesis of the cardiac outflow tract. Development 131, 3217–3227. https://doi.org/10.1242/dev.01174

Xu, H., Viola, A., Zhang, Z., Gerken, C.P., Lindsay-Illingworth, E.A., Baldini, A., 2007. Tbx1 regulates population, proliferation and cell fate determination of otic epithelial cells. Dev. Biol. 302, 670–682. https://doi.org/10.1016/j.ydbio.2006.10.002

Xu, J., Nie, X., Cai, X., Cai, C.-L., Xu, P.-X., 2014. Tbx18 is essential for normal development of vasculature network and glomerular mesangium in the mammalian kidney. Dev. Biol. 391, 17–31. https://doi.org/10.1016/j.ydbio.2014.04.006

YAFFE, D., SAXEL, O., 1977. Serial passaging and differentiation of myogenic cells isolated from dystrophic mouse muscle. Nature 270, 725–727. https://doi.org/10.1038/270725a0

Yagi, H., Furutani, Y., Hamada, H., Sasaki, T., Asakawa, S., Minoshima, S., Ichida, F., Joo, K., Kimura, M., Imamura, S., Kamatani, N., Momma, K., Takao, A., Nakazawa, M., Shimizu, N., Matsuoka, R., 2003. Role of TBX1 in human del22q11.2 syndrome. The Lancet 362, 1366–1373. https://doi.org/10.1016/S0140-6736(03)14632-6

Yamagishi, H., Maeda, J., Hu, T., McAnally, J., Conway, S.J., Kume, T., Meyers, E.N., Yamagishi, C., Srivastava, D., 2003. Tbx1 is regulated by tissue-specific forkhead proteins through a common Sonic hedgehog-responsive enhancer. Genes Dev. 17, 269–281.

Yang, Y., Bedford, M.T., 2013. Protein arginine methyltransferases and cancer. Nat. Rev. Cancer 13, 37–50. https://doi.org/10.1038/nrc3409

Zaragoza, M.V., Lewis, L.E., Sun, G., Wang, E., Li, L., Said-Salman, I., Feucht, L., Huang, T., 2004. Identification of the TBX5 transactivating domain and the nuclear localization signal. Gene 330, 9–18. https://doi.org/10.1016/j.gene.2004.01.017

Zeng, D., Liu, M., Pan, J., 2016. Blocking EZH2 methylation transferase activity by GSK126 decreases stem cell-like myeloma cells. Oncotarget Vol 8 No 2.

Zhang, B., Feng, J., 2022. Mouse embryonic stem cells require multiple amino acids. Exp. Biol. Med. 247, 1379–1387. https://doi.org/10.1177/15353702221096059

Zhang, F., Rein, B., Zhong, P., Shwani, T., Conrow-Graham, M., Wang, Z.-J., Yan, Z., 2021. Synergistic inhibition of histone modifiers produces therapeutic effects in adult Shank3-deficient mice. Transl. Psychiatry 11, 99. https://doi.org/10.1038/s41398-021-01233-w

Zhang, L., Zhong, T., Wang, Y., Jiang, Q., Song, H., Gui, Y., 2006. TBX1, a DiGeorge syndrome candidate gene, is inhibited by retinoic acid. Int. J. Dev. Biol. 50, 55–61. https://doi.org/10.1387/ijdb.052036lz

Zhang, Z., Cerrato, F., Xu, H., Vitelli, F., Morishima, M., Vincentz, J., Furuta, Y., Ma, L., Martin, J.F., Baldini, A., Lindsay, E., 2005. Tbx1 expression in pharyngeal epithelia is necessary for

pharyngeal arch artery development. Development 132, 5307–5315. https://doi.org/10.1242/dev.02086

Zhao, Y., Wang, Y., Shi, L., McDonald-McGinn, D.M., Crowley, T.B., McGinn, D.E., Tran, O.T., Miller, D., Lin, J.-R., Zackai, E., Johnston, H.R., Chow, E.W.C., Vorstman, J.A.S., Vingerhoets, C., van Amelsvoort, T., Gothelf, D., Swillen, A., Breckpot, J., Vermeesch, J.R., Eliez, S., Schneider, M., van den Bree, M.B.M., Owen, M.J., Kates, W.R., Repetto, G.M., Shashi, V., Schoch, K., Bearden, C.E., Digilio, M.C., Unolt, M., Putotto, C., Marino, B., Pontillo, M., Armando, M., Vicari, S., Angkustsiri, K., Campbell, L., Busa, T., Heine-Suñer, D., Murphy, K.C., Murphy, D., García-Miñaúr, S., Fernández, L., Busa, T., Zhang, Z.D., Goldmuntz, E., Gur, R.E., Emanuel, B.S., Zheng, D., Marshall, C.R., Bassett, A.S., Wang, T., Morrow, B.E., International 22q11.2 Brain and Behavior Consortium (IBBC), 2023. Chromatin regulators in the TBX1 network confer risk for conotruncal heart defects in 22q11.2DS. Npj Genomic Med. 8, 17. https://doi.org/10.1038/s41525-023-00363-y

Zhu, Y., Gramolini, A.O., Walsh, M.A., Zhou, Y.-Q., Slorach, C., Friedberg, M.K., Takeuchi, J.K., Sun, H., Henkelman, R.M., Backx, P.H., Redington, A.N., MacLennan, D.H., Bruneau, B.G., 2008. Tbx5-dependent pathway regulating diastolic function in congenital heart disease. Proc. Natl. Acad. Sci. 105, 5519–5524. https://doi.org/10.1073/pnas.0801779105

Zirzow, S., Lüdtke, T.H.-W., Brons, J.F., Petry, M., Christoffels, V.M., Kispert, A., 2009. Expression and requirement of T-box transcription factors Tbx2 and Tbx3 during secondary palate development in the mouse. Dev. Biol. 336, 145–155. https://doi.org/10.1016/j.ydbio.2009.09.020